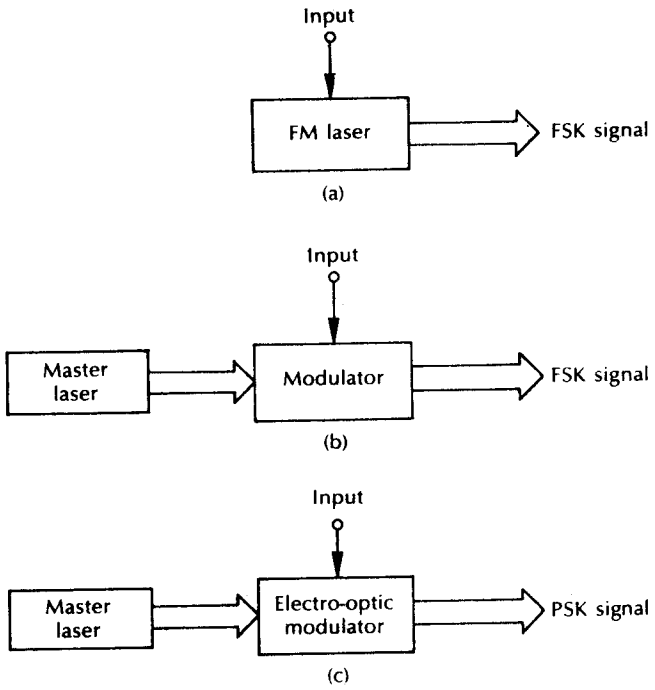

Figure 12.10 Transmitter configurations for FSK and PSK modulation: (a) FSK by direct modulation of an FM semiconductor laser injection current; (b) FSK using an external modulator; (c) PSK using an external electro-optic modulator.

[Ref. 18]. Although it has been observed that the use of a split electrode on the injection laser largely eliminates this effect [Ref. 58], alternative strategies have also been utilized. These include the use of bipolar optical FSK transmission [Ref. 59] and alternate mark inversion encoding [Ref. 60]. The former technique provided a transmission rate of 1 Gbit s^{-1} over 121 km whilst the latter operated at a rate of 565 Mbit s^{-1} using commercial DFB lasers.

When a single oscillator is switched between two frequencies, as is often the case with a semiconductor laser source, the phase of the signal is a continuous function of time and the modulation is known as continuous phase frequency shift keying (CPFSK) [Ref. 44]. This modulation scheme has been successfully demonstrated [Ref. 61] using integrated external cavity lasers (see Section 6.10.2). In this experiment transmission at 2 Gbit s^{-1} over 197 km of single-mode fiber was achieved. CPFSK is attractive because it allows direct current modulation of the injection laser whilst also providing high receiver sensitivity. Furthermore, it is suitable for high speed transmission since it creates no laser chirping degradation (see Section 6.7.3), as experienced in IM/DD systems. More recently the multichannel properties of CPFSK with a small frequency deviation have been

reported [Ref. 62] as a potential technique for optical frequency division multiplexing (OFDM).

External modulation techniques for FSK, shown schematically in Figure 12.10(b), include both acousto-optic and electro-optic approaches. Using bulk optic devices, FSK may be accomplished using a Bragg cell which employs travelling acoustic waves in a crystal to simultaneously diffract and frequency shift the optical signal. Alternatively, an equivalent effect can be obtained by using surface acoustic waves on an integrated optical waveguide device (see Section 10.6.2). FSK modulation can also be provided by a Mach–Zehnder interferometer with sinusoidal modulation applied to one of its branches. Such devices have been operated at modulation frequencies in excess of 1 GHz [Ref. 23].

Finally, multilevel frequency shift keying (MFSK) offers the potential for improving the coherent optical receiver sensitivity by increasing the choice of signalling frequencies [Ref. 63]. In principle this M'ary scheme provides the best receiver performance in the limit of large channel spacing [Ref. 23]. Thus eight-level FSK yields an equivalent sensitivity to binary PSK but at the expense of a greater receiver bandwidth requirement.

12.5.3 Phase shift keying

Although rarely employed, optical phase modulation can be achieved by direct current modulation of a semiconductor laser into which external coherent laser light is injected [Ref. 64]. When the injected laser frequency is exactly tuned to the modulating signal frequency, the output signal phase relative to the modulating signal phase is zero. A relative phase change of $\pi/2$ is obtained when the injected laser frequency is detuned away from the modulated light frequency to the injection locking limit. Hence the cutoff modulation frequency is determined by the injection locking bandwidth. Furthermore, this technique has the effect of reducing the linewidth of the injection locked laser to that of the injected signal device [Ref. 18].

External modulation for phase shift keying (PSK) is relatively straightforward and therefore normally utilized to provide the modulation format (see Figure 12.10(c)) which allows the most sensitive coherent detection mechanism within the binary modulation schemes (see Section 12.7). Simple integrated optical phase modulators fabricated from electro-optic materials such as lithium niobate or III–V compound semiconductors may be employed to give the appropriate shift with the application of an electric field (see Section 10.6.2). Such devices which exhibit a fiber to fiber insertion loss of 2 to 5 dB require around 5 V drive to produce a phase shift of π radians. Moreover, modulation bandwidths in excess of 10 GHz have been obtained from travelling-wave structures.

The phase detection process for PSK, however, necessitates synchronous detection with the requirement for corresponding narrow laser linewidths. These very narrow linewidth requirements for both PSK heterodyne and homodyne detection may be observed in Table 12.1 which presents the laser linewidths as a percentage of the transmission bit rate for the major modulation formats

Table 12.1 Laser linewidth requirements for various modulation formats as a percentage of the bit rate.

Modulation format	Homodyne	Heterodyne	
		Synchronous	Nonsynchronous
ASK	0.005–0.1%	0.05–0.1%	10–50%
FSK (wide deviation)	No	0.05–0.1%	10–50%
FSK (narrow deviation)	No		0.3–2.0%
PSK	0.005–0.01%	0.1–0.5%	No
DPSK	No	0.3–0.5%	No

considered in Section 12.5. Moreover, it may be noted that the most stringent laser linewidth requirement is for homodyne detection with binary PSK where for efficient detection linewidths of the order of 0.01% of the transmission rate are required [Ref. 65].

By contrast differential phase shift keying (DPSK) also indicated in Table 12.1 is a less demanding form of PSK since information is encoded as a change (or the absence of a change) in the optical phase on a bit by bit basis. The relationship between DPSK and PSK is illustrated in Figure 12.11 where it may be observed that with DPSK the incoming bit is delayed in order that its phase can be compared to the next received bit. Hence the technique does not require phase comparisons over more than two bit intervals. Moreover, the SNR performance of DPSK is only a fraction of a decibel less than that of heterodyne (synchronous) PSK [Ref. 2]. As

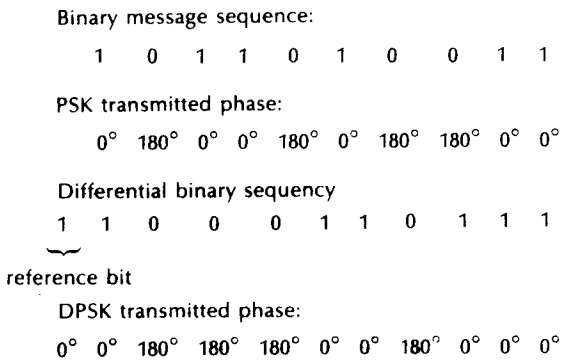

Figure 12.11 Comparison of a one-bit-at-a-time DPSK scheme with binary PSK. The differential binary sequence is obtained by repeating the preceding bit in the sequence if the message bit is a 1 or by changing to the opposite bit if the message bit is a 0.

laser linewidths of the order of 0.3 to 0.5% of the transmission rate can be tolerated with DPSK, experimental systems operating at 1.2 Gbit s^{-1} have been demonstrated using both an integrated external cavity DFB laser [Ref. 66] and an external fiber cavity DFB laser [Ref. 67]. In addition DPSK is technically straightforward to implement at high transmission rates because the phase fluctuation between the two signal bits is reduced [Ref. 20].

Unlike multilevel FSK which can provide improved receiver sensitivity by spectral expansion, M'ary PSK (and also, for that matter, M'ary ASK) could potentially provide spectral conservation through the use of multilevel signalling. Alternatively, M'ary PSK, M'ary ASK and their combinations such as quadrature amplitude modulation (QAM) [Ref. 3] can avoid noise degradation in the electronic preamplifier by increasing the utilization of the IF band frequency within optical heterodyne detection [Ref. 68]. The receiver sensitivities associated with these multilevel transmission techniques are discussed further in Section 12.7.

12.5.4 Polarization shift keying

An additional modulation format which has been investigated within coherent optical fiber communications involves use of the polarization characteristics of the transmitted optical signal. The digital transmission implementation of such polarization modulation is known as polarization shift keying (PolSK). A realization of coherent optical transmission using heterodyne detection with PolSK was obtained through external modulation by a lithium niobate phase modulator [Ref. 69]. This device produced a phase shift of π radians between the TE and TM modes, which rotated the signal polarization by 90°. These orthogonal polarization states were then maintained during transmission within a single-mode fiber. In this context a prerequisite for the fiber was that no coupling occurred between the two orthogonal polarization modes. The system was, however, successfully operated at a transmission rate of 560 Mbit s^{-1} and proved between 2 and 3 dB more sensitive than ASK modulation with heterodyne detection.

The differential variant of polarization shift keying (DPolSK) has also been demonstrated [Refs. 70, 71]. This modulation format eliminates the ambiguity involved in deciding whether a particular polarization represents a binary zero or a one. Furthermore, the DPolSK scheme can lead to the removal of the phase noise associated with both the laser source and the fluctuations from the transmission medium [Ref. 71]. This factor provides an improvement over PolSK where only the phase jitter of the laser may be cancelled.

The above binary schemes have been concerned with the two polarization modes of a single-mode fiber. Multilevel PolSK is also possible in which the transmitted symbols are each associated with different polarization states within the fiber [Refs. 72, 73]. Moreover, such a modulation format can provide a performance improvement over the more traditional multilevel systems outlined in Sections 12.5.2 and 12.5.3 [Ref. 73].

12.6 Demodulation schemes

Basic receiver configurations for optical heterodyne and homodyne detection are shown in Figure 12.12. In both cases it has been assumed that some form of polarization control is required to match the incoming signal SOP to that of the local oscillator signal (see Section 12.4.2). This factor therefore implies the use of conventional circularly symmetric single-mode fiber. For heterodyne detection (Figure 12.12(a)), a beat-note signal between the incoming optical signal and the local oscillator signal produces the IF signal which is obtained using the square law optical detector (see Section 12.3). The IF signal, which generally has a frequency of between three and four times the transmission rate, is then demodulated into the baseband using either a synchronous or nonsynchronous detection technique.* An

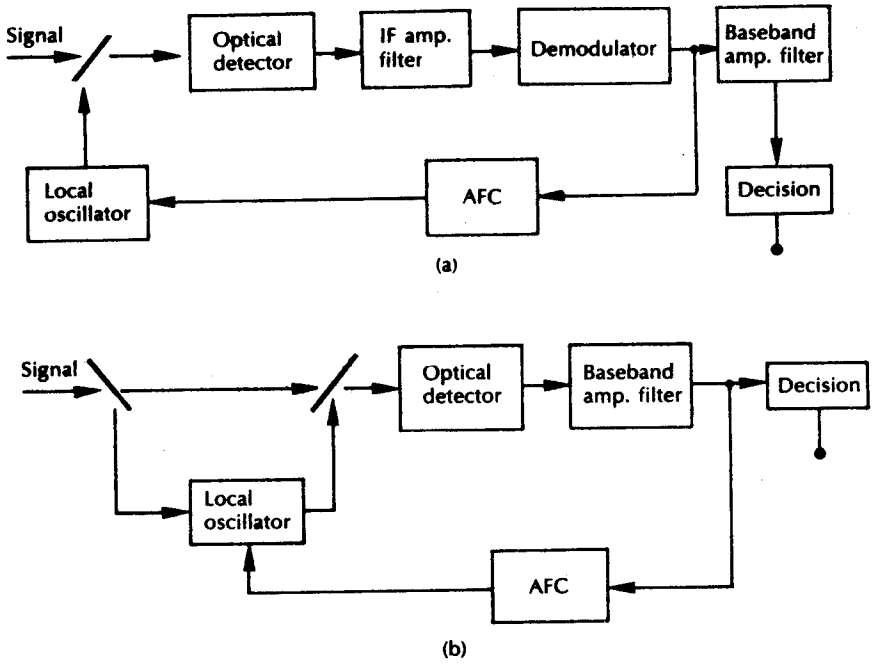

Figure 12.12 Basic coherent receiver configurations: (a) optical heterodyne receiver; (b) optical homodyne receiver illustrating the phase locking between the local oscillator and incoming signals.

* A brief explanation of the terminology was provided in Section 12.2. It should be noted that nonsynchronous heterodyne detection does not strictly require phase matching between the incoming signal and the local oscillator. Spatial coherence between the two signals is, however, required when they are combined so that nonsynchronous detection schemes do fall within the broad heading of coherent optical fiber systems.

optical receiver bandwidth several times greater than that of a direct detection receiver is therefore required for a specific transmission rate Moreover, as IF frequency fluctuation degrades the heterodyne receiver performance, then frequency stabilization may be achieved by feeding back from the demodulator through an automatic frequency control (AFC) circuit to the local oscillator drive circuit.

In the case of homodyne detection in which the phase of the local oscillator signal is locked to the incoming signal, then, by definition, a synchronous detection scheme must be employed. Moreover, the result of the mixing process in the optical detector produces an information signal which is in the baseband (see Section 12.3) and thus requires no further demodulation. An AFC loop is also shown within the homodyne receiver configuration of Figure 12.12(b) to provide the necessary frequency stabilization between the two signals. Hence any variant detection schemes based on homodyne detection, but in which the local oscillator laser is not phase locked to the incoming signal such as phase diversity or multiport detection, could be considered as a form of heterodyne rather than homodyne detection [Ref. 5]. However, this technique is dealt with separately in Section 12.6.4.

In both optical heterodyne and homodyne detection, where the incoming signal is demodulated using a local oscillator laser, FM noise in this device together with that resulting from the source laser causes SNR degradation in the receivers through FM to AM, or PM to AM conversion which generally determines the lower limit of bit error rate performance [Ref. 74]. FM noise which basically results from the spontaneous emission coupled to the lasing mode, is, in the semiconductor laser, enhanced by AM noise caused by photon number fluctuation which is generated through the same mechanism [Ref. 75]. Moreover, excess AM noise within the local oscillator laser due to its resonance characteristics also deteriorates the SNR performance and hence degrades the receiver sensitivity. To reduce the effect of local oscillator FM noise a semiconductor laser with a narrowed or suppressed spectral linewidth must be used [see Section 12.4.1]. The excess AM noise in the semiconductor laser decreases with an increase in the bias level so that high bias operation is effective in suppressing this mechanism [Ref. 75]. Furthermore, excess AM noise associated with the local oscillator can be suppressed by employing the balanced receiver configuration described in Section 12.4.3.

12.6.1 Heterodyne synchronous detection

Optical heterodyne synchronous detection necessitates an estimation of the phase of the IF signal in translating it to the baseband. Such an approach generally requires the use of phase locking techniques at the receiver in order to track phase fluctuations in the incoming and local oscillator signals. Since the information signal is to be processed on an IF carrier, then electrical phase estimation may be employed. Hence the phase locked loop (PLL) techniques and configurations appropriate to radiofrequency and microwave communications can be utilized

[Refs. 2, 23]. Such techniques have been investigated primarily for PSK demodulation where an estimation of the phase of the signal is required [Ref. 5]. Furthermore, synchronous PSK demodulation is the most sensitive of the heterodyne detection techniques (see Section 12.7). In order to achieve a measurement of the phase of a fully modulated PSK signal, it is necessary to obtain a phase reference from the phase of the average incoming optical signal within a particular time interval. Therefore the purpose of the PLL is to provide that reference where, in general, the time average is defined by the bandwidth of the loop.

An examination of the spectrum of a PSK signal reveals that no signal energy is present at the carrier frequency when the phase shift from the binary one to zero states is a full 180°.* The introduction of a nonlinear element within the PLL is therefore necessary to enable efficient carrier recovery. A squaring loop technique illustrated in Figure 12.13(a) is particularly applicable to binary PSK, phase noise-sensitive coherent optical fiber systems [Ref. 23]. By squaring the PSK signal frequency this method produces a carrier at twice the original frequency which can be filtered out and then used for phase estimation. A similar result may be obtained with the statistically equivalent Costas loop shown in Figure 12.13(b) [Ref. 76].

An alternative approach to carrier recovery is to reduce slightly the depth of the phase modulation so that a small component of the transmitted energy lies at the carrier frequency. This pilot carrier signal can then be amplified and recovered as a phase reference at the receiver. In this case of what is essentially a weak carrier, a much reduced loop bandwidth (i.e. reduced integration time) is required in order adequately to recover the carrier. Furthermore, whilst providing a stable reference, long integration times increase the sensitivity of the receiver to carrier phase noise. However, to detect the PSK signal adequately using a pilot carrier, a significant amount of signal power may be sacrificed [Ref. 23].

A variant on the pilot carrier technique for PSK synchronous demodulation is shown in Figure 12.14 in which carrier recovery takes place at the IF stage [Ref. 77]. In this case the detected IF signal is divided into two routes, one being the signal route and the other being the carrier recovery route. Following the carrier recovery route the signal is doubled by a frequency doubler (FD) to remove the $(0, \pi)$ phase modulation component. Twice the IF frequency of the resultant signal is then divided by a frequency halver (FH) to recover the reference carrier signal. Finally, the recovered carrier and signal are mixed to give the demodulator output. This technique which provides for suppression of phase noise has been demonstrated in an optical PSK system operating at 560 Mbit s^{-1} [Refs. 77, 78].

The above synchronous demodulation schemes can also be used within ASK and FSK heterodyne optical fiber systems but they do not provide the same potential receiver sensitivity performance as that of PSK. Moreover, alternative nonsynchronous techniques for ASK and FSK are often more reliable in the presence of phase noise and provide receiver sensitivities only slightly less than the

* This situation typifies a suppressed carrier modulation type [Ref. 3].

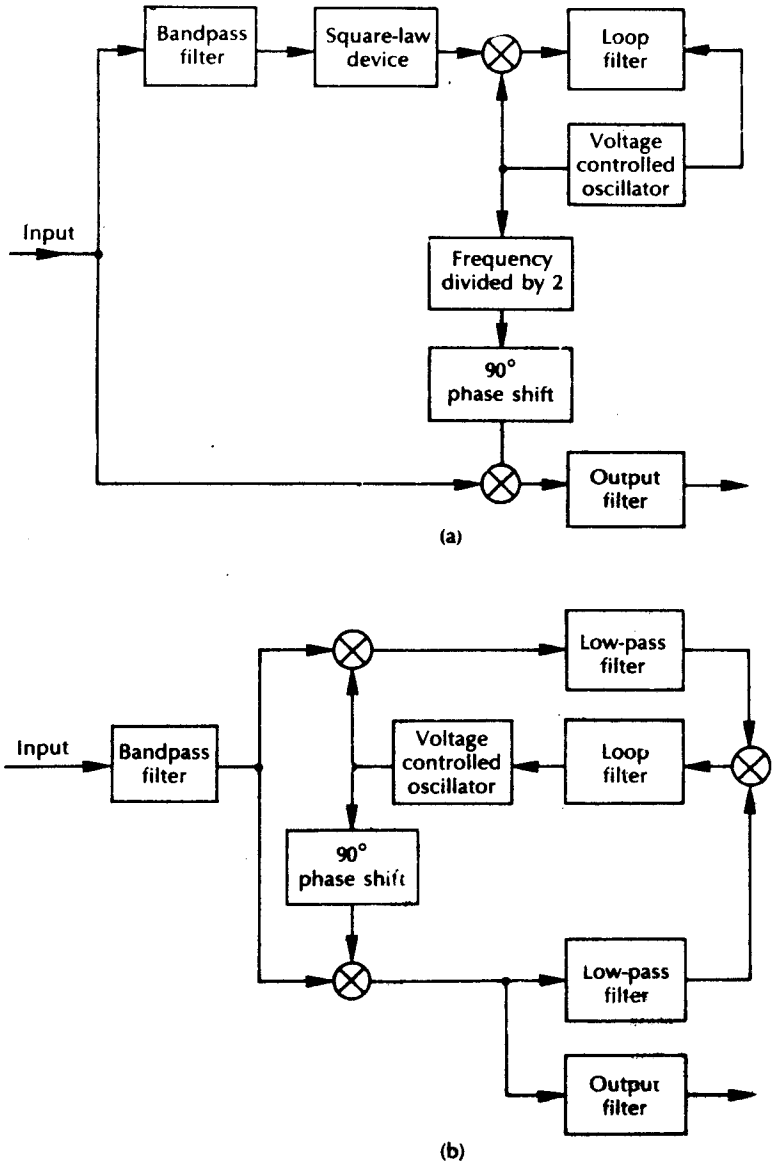

Figure 12.13 Techniques for carrier recovery used in coherent optical PSK receivers: (a) squaring loop; (b) Costas loop

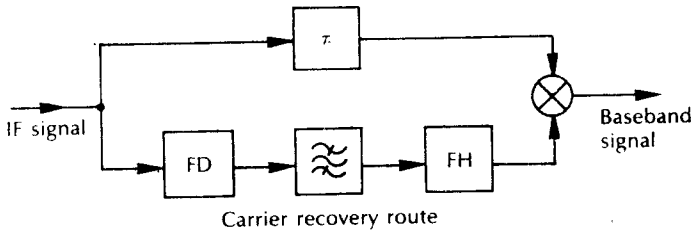

Figure 12.14 A carrier recovery synchronous demodulator [Ref. 77].

corresponding synchronous methods. These nonsynchronous demodulation schemes are therefore discussed in Section 12.6.2.

Although nonsynchronous demodulation of a PSK signal is strictly not possible because the message information resides in the phase of the carrier signal, the phase comparison detection associated with differential phase shift keying (DPSK) reduces the synchronization problems associated with PSK (see Figure 12.11). Therefore, as indicated in Section 12.5.3, a broader linewidth laser source and local oscillator laser may be utilized with DPSK and heterodyne detection than that necessary for binary PSK. In addition, optical DPSK reception is only a fraction of a decibel less sensitive than synchronous PSK.

In the optical heterodyne receiver the DPSK signal is first translated down to a suitable IF frequency prior to demodulation by a conventional DPSK, or phase comparison detector [Ref. 2]. Such a detection system is illustrated in Figure 12.15 where the incoming signal from the heterodyne process is band limited to reduce the phase noise. In the phase comparison system, the bandlimited version of the DPSK signal is delayed by a bit period T, and the product with the undelayed version is formed. This product is then integrated to eliminate residual noise, a positive voltage being obtained if the phases of the combined signals are the same. Alternatively, when the two phases differ by π radians, a negative voltage occurs at the output.

The use of a balanced heterodyne receiver (see Section 12.4.3) in an experimental DPSK system operating at 1.4 Gbit s^{-1} resulted in a receiver sensitivity of

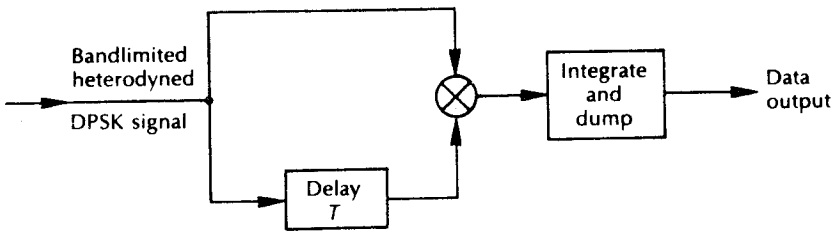

Figure 12.15 Heterodyne differential phase shifting keying demodulator.

−42.8 dBm (or 285 photons per bit) at a bit error rate of less than 10^{-9} [Ref. 79]. Furthermore, a local oscillator laser output power of only 0.5 mW was required.

12.6.2 Heterodyne nonsynchronous detection

It was indicated in Section 12.5 that both ASK and FSK may be demodulated using nonsynchronous detection techniques which puts the least demands on laser linewidth and phase stability. Such demodulation schemes, which include ASK envelope detection as well as FSK single and dual filter detection, do not therefore require the extremely narrow laser linewidths associated with synchronous binary PSK demodulation or even DPSK (see Section 12.5.3). Heterodyne envelope detection of an ASK signal may be achieved using an intermediate frequency bandpass filter followed by a peak detector to recover the baseband signal as shown in Figure 12.16(a). Such a scheme, however, incurs a receiver sensitivity penalty as a result of nonlinear filtering of the Gaussian distributed noise in the peak detection process combined with the phase noise broadening of the signal spectrum such that a significant proportion of the signal energy can be translated outside the IF signal band. An optimum receiver bandwidth balances these factors and, for combined

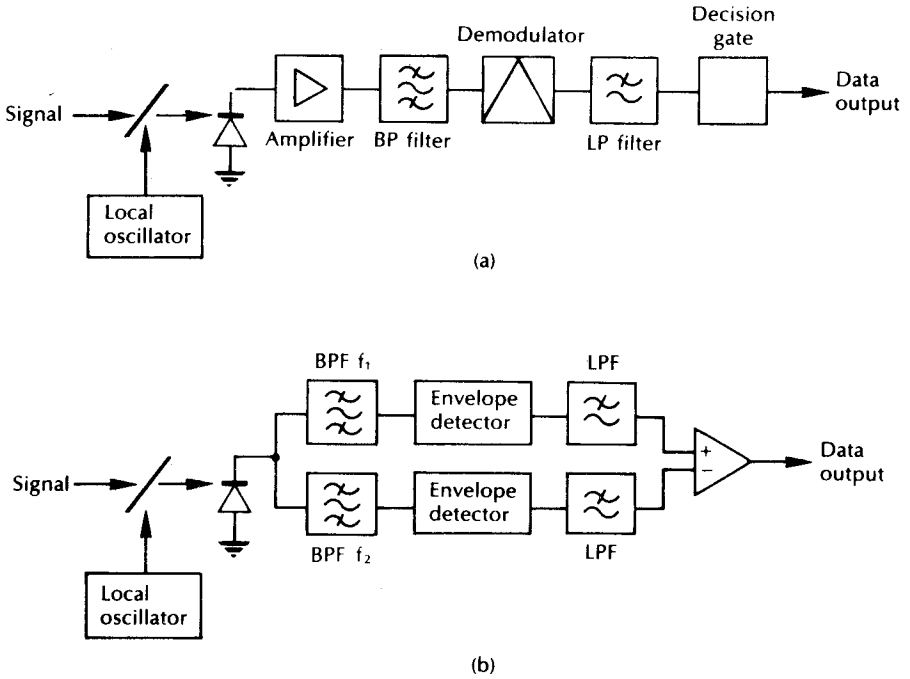

Figure 12.16 Nonsynchronous heterodyne detection: (a) ASK single envelope detector receiver; (b) FSK dual filter receiver.

source and local oscillator linewidths of 10% of the transmitted data rate, the receiver penalty is around 3 dB [Ref. 42].

By employing parallel filters with channels centred on the two transmitted frequencies it is possible to use envelope detection on each channel of a binary FSK signal. The configuration for this dual filter demodulation technique is provided in Figure 12.16(b) [Ref. 44]. At the output it produces a differential ASK signal with a receiver sensitivity which is slightly better than nonsynchronous ASK demodulation in the presence of phase noise (i.e. a 2 dB penalty when source and local oscillator laser linewidths are 10% of the transmitted data rate [Ref. 42]). This improvement results from the complementary behaviour of the dual filter approach where, for large spacing between the two FSK signal channels, it is possible to have a significant spectral broadening of the signal but with insufficient energy in the complementary channel to register an error [Ref. 23].

12.6.3 Homodyne detection

The attraction of optical homodyne detection is not just the potential 3 dB improvement in receiver sensitivity (see Section 12.3) but also that it can ease the receiver bandwidth requirement considerably. This factor is illustrated in Figure 12.17 which compares the spectra at the output of the detector for PSK homodyne and PSK heterodyne detection. It may be observed that homodyne detection requires only the normal direct detection receiver bandwidth whereas heterodyne detection requires at least twice this bandwidth and often a factor of three or four times it. Unfortunately, optical homodyne detection using independent source and local oscillator lasers (i.e. not self homodyne) has proved extremely difficult to achieve because of the problems associated with remotely optical locking a local oscillator laser to a low level modulated signal [Ref. 45]. Such phase locking is essential because the phase difference ϕ in Eq. (12.12) must be held near zero for high sensitivity reception. Furthermore, if ϕ drifts to $\pi/2$, then the output signal current I_S will become zero and the detection process will cease.

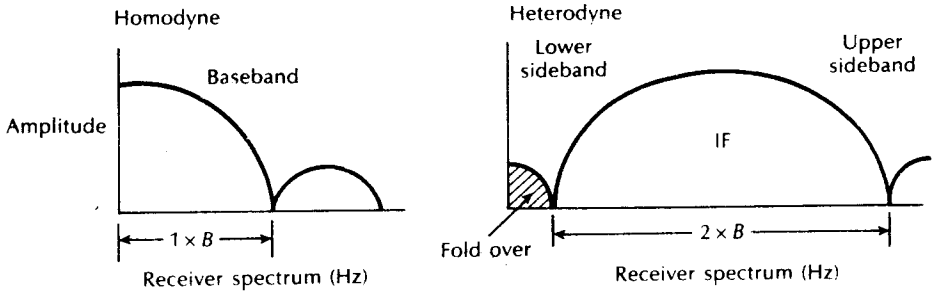

Figure 12.17 Comparison of the electrical spectra at the optical detector output for homodyne and heterodyne detection of a PSK signal.

Two homodyne demodulation strategies have, however, proved successful in demonstration at optical frequencies. They are the use of an optical phase lock loop and the selective amplification of the carrier [Refs. 2, 18, 23, 45]. Unlike the electrical PLL techniques described in Section 12.6.1 which comprised an electrical phase detector, loop filter and voltage controlled oscillator (VCO), in the optical PLL, the photodetector and laser local oscillator act as the phase detector and VCO respectively. Hence the optical phase difference between the incoming signal and the local oscillator signal, or the phase error signal, is detected by the photodetector prior to being fed back to correct the local oscillator frequency and phase. Although homodyne detection using an optical PLL has been demonstrated [Ref. 80], it is somewhat difficult to realize and puts stringent demands on the laser linewidths [Ref. 65].

The optical PPL configuration shown in Figure 12.18 [Ref. 80] employs a pilot carrier strategy for PSK homodyne detection. In common with other pilot carrier techniques (see Section 12.6.1) this carrier is generated by using incomplete (less than 180°) phase modulation. The pilot carrier signal, together with the incoming signal, are combined in a 3 dB fiber directional coupler and then detected using a balanced receiver. The output signal from difference amplifier (Figure 12.18) is therefore a function of the phase error which may be used for phase locking through the loop filter to the optical local oscillator which performs as the VCO. It should be noted, however, that any carrier power used in this phase locking process directly reduces the receiver sensitivity by an equivalent amount. Furthermore, the signal power required to track the phase of the incoming carrier to a specified accuracy (i.e. the tracking error relates directly to a degradation in the bit error rate performance) is dependent upon the combined phase noise of the source and local oscillator lasers as well as the PLL bandwidth. Hence, extending the optical PLL bandwidth improves the tracking performance until a point is reached where the increased shot noise significantly degrades the loop SNR. There is, therefore, an optimum loop bandwidth to provide a minimum phase error and

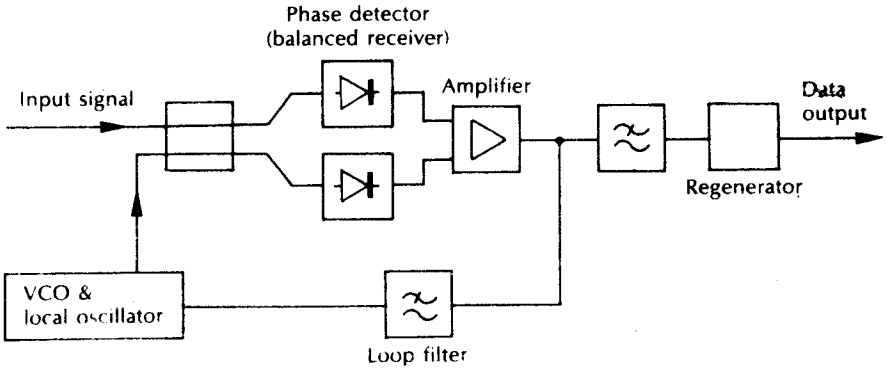

Figure 12.18 Pilot carrier optical phase locked loop receiver [Ref. 80].

it is possible to improve the performance of the optical homodyne receiver when the local oscillator laser has substantial phase noise by simply increasing the PLL bandwidth.

The basic principle of an optical Costas PLL has also been demonstrated at a wavelength of 10.6 μm using carbon dioxide lasers to provide the source and local oscillator signals [Ref. 81]. A hypothetical optical Costas PLL homodyne receiver for antipodal PSK modulation is illustrated in Figure 12.19 [Ref. 45]. In this case the incoming and local oscillator signals are combined in an optical hybrid which ensures a 90° phase difference between the output signals from the two detectors.

The 90° hybrid device can be realized using the phase shift properties of polarized light [Ref. 82]. A 90° phase shift can be obtained by combining a circularly polarized local oscillator signal with a linearly polarized incoming signal and then by resolving the combined signal into two orthogonal components with a polarization beam splitter. The linearly polarized incoming signal must, however, be aligned at 45° to the beam splitter plane.

The two outputs from the optical hybrid are detected, amplified prior to multiplication in the mixer shown in Figure 12.19. The phase of the suppressed carrier is then determined by the low pass filtering of this product. Moreover, the control signal is also filtered and then used to adjust the local oscillator frequency in a similar manner to that employed in the pilot carrier optical PLL. Using the optical Costas PLL, however, provides the advantage that all the low level circuits, prior to the mixer, can be a.c. coupled and there is no wastage of transmitted power in a pilot carrier component.

It is possible to achieve optical homodyne detection without the use of an optical PLL if a residual carrier component of the incoming signal is selectively amplified (i.e. the modulation sidebands are not amplified) and then recombined with the sidebands before photodetection. In this way the amplified carrier functions as the

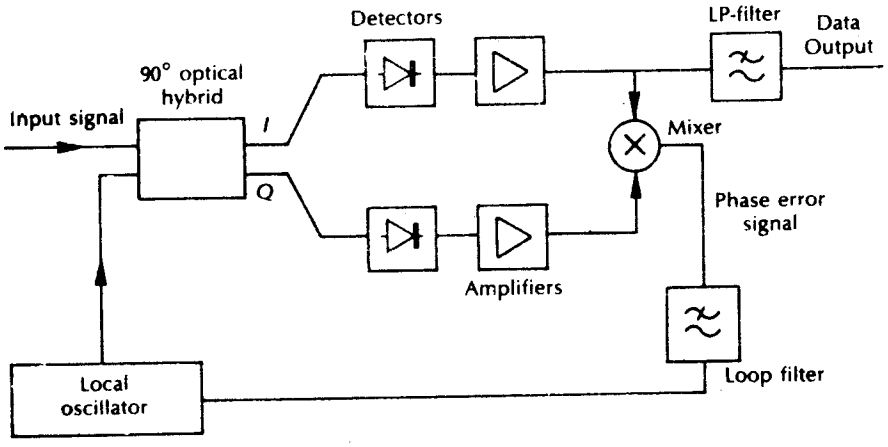

Figure 12.19 Hypothetical optical Costas loop receiver [Ref. 45].

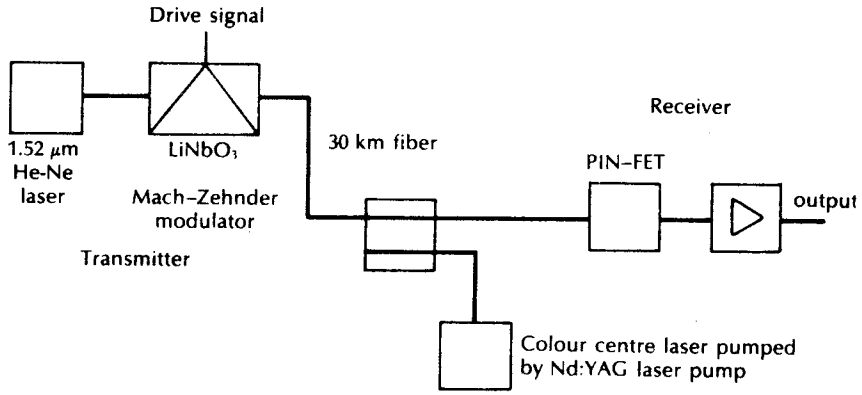

Figure 12.20 Brillouin amplification of the carrier signal providing homodyne detection [Ref. 84].

local oscillator signal. The principle was first demonstrated with a resonant gas laser amplifier [Ref. 83] but a more recent strategy for such self homodyne detection utilized the Brillouin gain process (see Section 3.14) which has a bandwidth of about 20 MHz in silica fiber. The experimental arrangement for this homodyne receiver is shown in Figure 12.20 [Ref. 84]. The fiber was pumped with a colour centre laser* in a direction back towards the transmission fiber at a frequency of 11 GHz (the Stokes shift) higher than the incoming carrier signal. Pump powers of between 3 and 5 mW were typically required to obtain carrier gains of around 50 dB. The homodyne gain, however, was equal to one half of the carrier gain and hence a homodyne gain of 26 dB was reported [Ref. 83]. This Brillouin homodyne technique can be used directly for ASK demodulation, but for PSK demodulation it would be necessary to form a pilot carrier at the optical transmitter.

12.6.4 Phase diversity reception

An additional demodulation scheme employed in microwave systems which has been applied to coherent optical systems is phase diversity reception, or multiport detection [Refs. 85, 86]. In these techniques the local oscillator laser is operated at a frequency comparable to the frequency of the incoming signal but the two signals are not phase locked. The phase diversity receiver does, however, convert the incoming signal directly to the baseband and therefore has the bandwidth advantage of homodyne detection. As the optical mixing is not phase synchronized, the demodulation strategy avoids this major problem associated with homodyne detection, but at best the receiver sensitivity is equivalent to that of heterodyne detection. Hence, from the viewpoint of receiver bandwidth requirements, phase

* The colour centre laser was itself pumped by an Nd : YAG laser.

diversity reception behaves like an optical homodyne receiver but it is essentially nonsynchronous with the sensitivity performance of, or worse than, a heterodyne receiver. It cannot therefore be regarded strictly as a homodyne technique* and certain authors suggest it is more appropriate to classify such multiport detection schemes with heterodyne receivers [Ref. 5].

A number of optical phase diversity reception schemes have been investigated operating with two or more ports and two or more matched receivers. The technique utilizes a fixed phase relationship between the ports of a multiport coupler to provide the direct demodulation to the baseband without the requirement for an optical PLL. One variant of the optical phase diversity receiver known as the in-phase and quadrature (I & Q) receiver is shown in Figure 12.21. In this two phase [Refs. 86 to 90] scheme the incoming and local oscillator signals are combined in a 90° optical hybrid similar to the one described in Section 12.6.3. The optical hybrid is connected to two detectors, the outputs of which are amplified and then passed through square law devices prior to electrical recombination. The output signals from each receiver path prior to recombination can be written in terms of their voltages V_1 and V_2 as:

$$V_1^2 = k_1^2 m^2(t) \sin^2 \delta\phi \tag{12.21}$$

$$V_2^2 = k_2^2 m^2(t) \cos^2 \delta\phi \tag{12.22}$$

where k_1 and k_2 are constants, $m(t)$ is the modulation and $\delta\phi$ is the phase error.

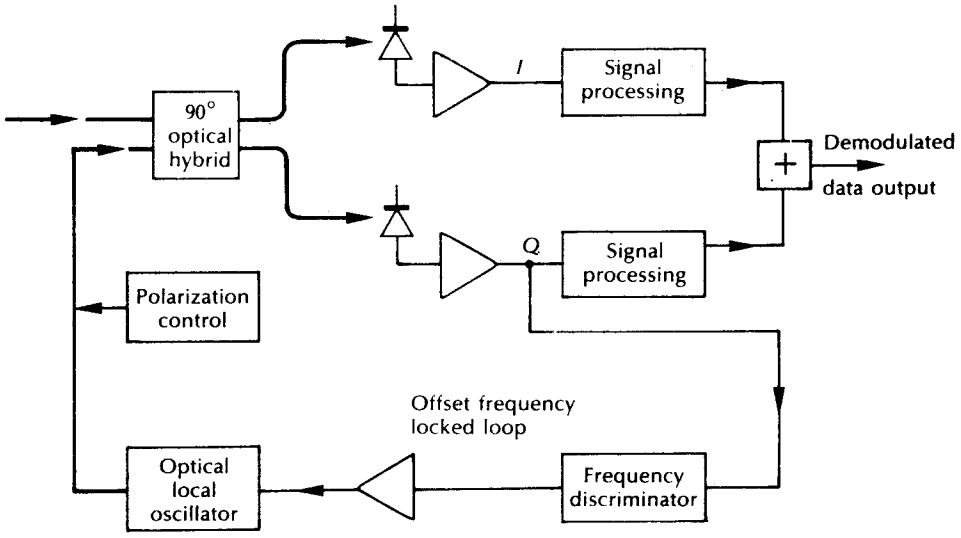

Figure 12.21 In-phase and quadrature phase diversity (two phase) receiver.

*Many authors do, however, refer to it as a homodyne strategy [Refs. 87 – 89].

Hence the output signal from the receiver is:

$$V_1^2 + V_2^2 = k^2[m(t)]^2 \tag{12.23}$$

where we assume $k = k_1 = k_2$. It may be observed from Eq. (12.23) that for ASK the demodulated signal is constant irrespective of the relative phase between the incoming and local oscillator signals. Therefore, with ASK modulation the laser linewidth requirements are comparable to heterodyne detection with nonsynchronous IF demodulation (see Section 12.5.1). For example, the experimental demonstration of such two phase ASK demodulation has been achieved at a transmission rate of 150 Mbit s^{-1} [Ref. 89]. The system utilized commercial 1.5 μm DFB laser with linewidths of 38 MHz and achieved a sensitivity of -55 dBm.

For PSK modulation, however, the signal may be differentially demodulated by the inclusion of a one bit delay in one of the inputs to the square law mixer. Hence the change in phase during a single bit period only is of concern and any longer term phase drift is removed. This DPSK I & Q demodulation is expected to have similar laser linewidth requirements to DPSK heterodyne detection (see Section 12.5.3) [Ref. 45]. The I & Q phase diversity receiver is more sensitive to fluctuations of the incoming SOP than a conventional optical heterodyne receiver [Ref. 90]. Polarization control should, however, be more straightforward in the I & Q case because it is possible to obtain electrical signals directly from the two receiver arms which provide exact information on the received polarization state. Nevertheless, problems do exist with two port phase diversity reception, as in practice the electrical square law demodulation is imperfect and produces additional terms which tend to appear in the baseband along with the demodulated signal. Moreover, the two detected currents must be 90° out of phase which may only be achieved at the expense of additional signal processing [Ref. 82], and also the two arms of the receiver must be well matched.

Other phase diversity techniques can be used as alternatives to I & Q detection. In particular, the phase diversity receiver using three phase reception has proved successful [Refs. 86, 87, 91, 92]. A schematic diagram of the generalised three phase receiver is shown in Figure 12.22. It may be observed that in this phase diversity scheme a 120° hybrid is required which can be conveniently realized from the intrinsic symmetry associated with the construction of a three fiber fused biconical coupler [Ref. 93]. Furthermore, this strategy avoids the polarization sensitivity of the two phase arrangement. However, the receiver sensitivity of this approach is poorer than the conventional optical heterodyne strategy as the additional port for the third detector introduces an extra 1.8 dB degradation [Ref. 85].

Demonstrations of three phase schemes have taken place using helium–neon lasers operating at 650 Mbit s^{-1} [Ref. 91] and DFB lasers at 140 Mbit s^{-1} [Ref. 92]. Furthermore, demodulation of direct FSK signals generated from a DFB laser operating at 5 Gbit s^{-1} has recently been demonstrated using a three port single filter phase diversity receiver [Ref. 88]. The single filter detection was achieved by setting the local oscillator frequency equal to the centre frequency of the stronger

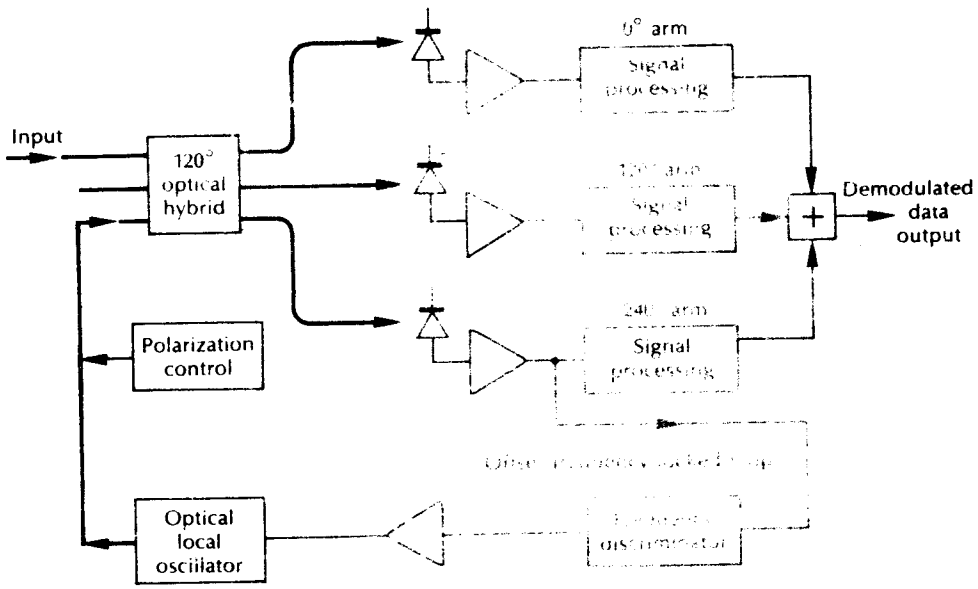

Figure 12.22 Phase diversity receiver using three phase detection.

FSK sideband [Ref. 93]. Receiver sensitivities for a bit error rate of 10^{-9} of -30.5 dBm and -27.0 dBm were obtained at transmission rates of 4 and 5 Gbit s^{-1} respectively [Ref. 88].

In the longer term, it is suggested [Ref. 45] that multiport detection will be extended to provide both phase and polarization diversity reception (see Section 12.4.2.2). Furthermore, greater numbers of ports than three for phase diversity receivers are envisaged (i.e. four, six or eight) combined with a balanced receiver approach (see Section 12.4.3) in order to reduce excess noise from the local oscillator laser [Refs. 23, 45, 85, 94].

12.7 Receiver sensitivities

The basic detection principles for the ASK coherent optical receiver were discussed in Section 12.3. In addition, the 3 dB SNR improvement for the ASK homodyne receiver in comparison with the corresponding heterodyne receiver in the shot noise limit was demonstrated (Eqs. (12.16) and (12.17)). Although a synchronous detection process was assumed in Section 12.3 for ASK with heterodyne detection, ASK with nonsynchronous detection can achieve approximately the same SNR limit [Ref. 95]. It is now important to consider the receiver sensitivities for the other

major modulation schemes and detection processes so that the choices regarding the implementation of coherent optical fiber systems can be understood.

In Section 12.3 comparison between ASK heterodyne and homodyne reception was undertaken from determination of their respective shot or quantum noise limited SNRs. As in this section we propose to extend this comparison to receiver sensitivities of other digital modulation schemes, it is useful to transfer from considerations of SNR to those of bit error rate (BER). In addition we will continue to consider minimum receiver sensitivities in the presence of quantum noise only, neglecting thermal and other noise sources in the electronic preamplifier discussed in Section 9.3, as well as excess noise sources in the local oscillator laser. Although these other noise sources are normally present, comparison of the modulation formats under quantum noise limited detection assists in the deliberations regarding the desirability of specific schemes. Furthermore, near-quantum noise limited reception is more readily achieved using heterodyne or homodyne detection than by employing direct detection. We concentrate on synchronous demodulation for the major modulation formats (i.e. ASK, FSK, PSK) prior to consideration of homodyne detection for the ASK and PSK modulation schemes.

12.7.1 ASK heterodyne detection

The ASK or OOK modulation format has similarities to digital transmission in a IM/DD optical fiber system, a BER analysis for the latter system being provided in Section 11.6.3. In a heterodyne receiver, however, the analyses of signal and noise phenomena are more complicated than in the IM–DD case because the optical detector output appears as an IF signal and not as a baseband signal. Hence the IF output current from the photodetector $I_S(t)$ which corresponds to the input current to the preamplifier from Eq. (12.9) can be written as:

$$I_S(t) = \begin{cases} I_{SH} \cos(\omega_{IF} t + \phi), & \text{for a 1 bit} \\ 0, & \text{for a 0 bit} \end{cases} \tag{12.24}$$

where

$$I_{SH} = \frac{2\eta e}{hf} \sqrt{P_S P_L} \tag{12.25}$$

To obtain the IF noise current, two assumptions can be made. Firstly, it is assumed that the local oscillator signal power is much larger than the incoming signal power so that the total noise current is approximately equal to $\overline{i_{SL}^2}$, given by Eq. (12.14) and this applies for both the 1 and the 0 bit. Secondly, it is assumed that this IF noise current $N(t)$ can be considered as narrowband noise which can be expressed as [Ref. 3]:

$$N(t) = x(t) \cos \omega_{IF} t + y(t) \sin \omega_{IF} t \tag{12.26}$$

where $x(t)$ and $y(t)$ are functions of time which vary at a much slower rate than the IF signal. It should be noted that the first and second terms in Eq. (12.26)

represent the in-phase and quadrature components respectively. Hence the mean square values of $x(t)$ and $y(t)$ may be written as:

$$\overline{x^2}(t) = \overline{y^2}(t) = \overline{i_{SL}^2} \tag{12.27}$$

For heterodyne synchronous detection, the IF amplifier is followed by a demodulation circuit which has a phase synchronised reference signal proportional to cos $\omega_{IF}t$. Therefore, the detector output $V_d(t)$ is given by:

$$V_d(t) = k[I_S(t) + x(t)] \tag{12.28}$$

The probability density functions of $V_d(t)$ for the ASK signal $I_S(t)$ represented by Eq. (12.24) are illustrated in Figure 12.23. Moreover, it may be observed that these probability density functions are similar to those for digital IM–DD reception shown in Figure 11.35. Assuming this to be the case, the optimum decision threshold level D is set midway between the zero current (0 state) and the peak signal current (1 state) such that:

$$I_D \simeq \frac{I_{SH}}{2} = \frac{\eta e}{hf}\sqrt{\overline{P_S}\,\overline{P_L}} \tag{12.29}$$

The optical detector output given by Eq. (12.28) can now be considered as a baseband signal and noise contribution. Hence the analysis for BER can follow the method utilized for IM/DD in Section 11.6.3. We are therefore in a position to move straight to Eq. (11.21) and to substitute in the appropriate values from this

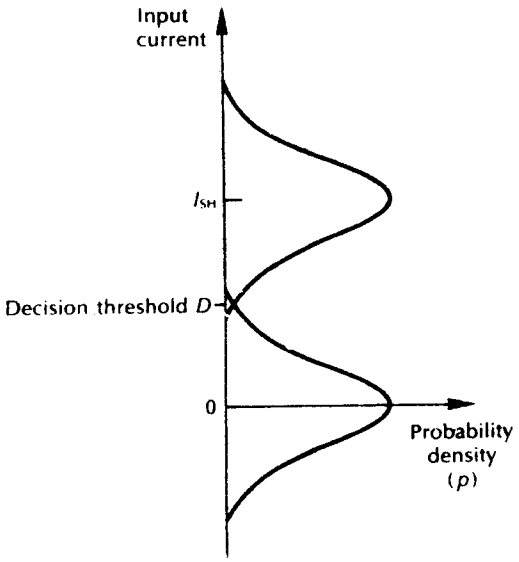

Figure 12.23 Probability density functions for ASK heterodyne synchronous detection.

derivation. Thus the probability of error $P(e)$ for ASK heterodyne synchronous detection can be written as:

$$P(e) = \tfrac{1}{2}\left[\tfrac{1}{2}\operatorname{erfc}\left(\frac{|I_{SH} - I_D|}{(\overline{i_{SL}^2})^{\frac{1}{2}}\sqrt{2}}\right) + \tfrac{1}{2}\operatorname{erfc}\left(\frac{|-I_D|}{(\overline{i_{SL}^2})^{\frac{1}{2}}\sqrt{2}}\right)\right] \tag{12.30}$$

Substituting for I_D from Eq. (12.29) gives:

$$P(e) = \tfrac{1}{2}\left[\tfrac{1}{2}\operatorname{erfc}\left(\frac{|I_{SH}/2|}{(\overline{i_{SL}^2})^{\frac{1}{2}}\sqrt{2}}\right) + \tfrac{1}{2}\operatorname{erfc}\left(\frac{|-I_{SH}/2}{(\overline{i_{SL}^2})^{\frac{1}{2}}\sqrt{2}}\right)\right]$$

$$= \tfrac{1}{2}\operatorname{erfc}\left(\frac{I_{SH}}{2(\overline{i_{SL}^2})^{\frac{1}{2}}\sqrt{2}}\right) \tag{12.31}$$

Finally substituting for I_{SH} using Eq. (12.25) and for $\overline{i_{SL}^2}$ from Eq. (12.14), where we replace B with the IF signal bandwidth B_{IF} because $I_S(t)$ was originally an IF signal exhibiting this bandwidth, then Eq. (12.31) can be written as:

$$P(e) = \tfrac{1}{2}\operatorname{erfc}\frac{2\eta e\sqrt{P_S P_L}}{hf}\Big/2\sqrt{2}\left(\frac{2e^2\eta P_L B_{IF}}{hf}\right)^{\frac{1}{2}}$$

$$= \tfrac{1}{2}\operatorname{erfc}\left(\frac{\eta P_S}{4hf\,B_{IF}}\right)^{\frac{1}{2}} \tag{12.32}$$

It is more appropriate to specify the probability of error in terms of the transmission bit rate B_T rather than the receiver bandwidth and, therefore, assuming transmission at a rate equivalent to twice the baseband bandwidth (see Eq. (3.12)), then $B_T = 2B \simeq B_{IF}$. Hence Eq. (12.32) becomes:

$$P(e) = \tfrac{1}{2}\operatorname{erfc}\left(\frac{\eta P_S}{4hf\,B_T}\right)^{\frac{1}{2}} \tag{12.33}$$

This expression allows the shot noise limited performance of ASK heterodyne synchronous detection to be compared with alternative detection schemes.

For ASK heterodyne nonsynchronous or envelope detection it can be shown that the probability of error in the shot noise limit, under similar assumptions to those used above for synchronous detection, is given by the approximate expression [Refs. 95, 96]:

$$P(e) \simeq \tfrac{1}{2}\exp - \left(\frac{I_{SH}^2}{8(\overline{i_{SL}^2})}\right) \tag{12.34}$$

Again substituting for I_{SH} and $\overline{i_{SL}^2}$ from Eqs. (12.25) and (12.14), respectively, gives:

$$P(e) \simeq \tfrac{1}{2}\exp - \left(\frac{\eta P_S}{4hf\,B_T}\right) \tag{12.35}$$

Moreover, as indicated in Section 12.7.5, these formulae give approximately equivalent BER results to those provided by Eqs. (12.31) and (12.33) for ASK

heterodyne synchronous detection. The reason for this situation is that the approximation erfc $(u) \simeq \exp -(u)^2$ holds for large u and hence for a low BER [Ref. 96].

12.7.2 FSK heterodyne detection

We commence by considering FSK heterodyne synchronous detection in the shot or quantum noise limit. The two angular frequencies for the transmitted 1 and 0 bits are assumed to be ω_1 and ω_2 so that:

$$I_S(t) = \begin{cases} I_{SH} \cos(\omega_1 + \phi), & \text{for a 1 bit} \\ I_{SH} \cos(\omega_2 + \phi), & \text{for a 0 bit} \end{cases} \tag{12.36}$$

where I_{SH} is defined in Eq. (12.25) and ϕ, which is a function of time, represents the phase noise associated with the semiconductor laser. This is neglected, as before in Section 12.7.1, because we are concerned with shot noise limited detection.

It is assumed that the signal $I_S(t)$ is received using two receivers tuned to ω_1 and ω_2 and that the output voltages from receivers 1 and 2 are V_1 and V_2 respectively. Furthermore it is assumed that the two receivers exhibit ideal frequency selectivity such that there is no crosstalk between ω_1 and ω_2 and therefore any additional voltages are generated by shot noise effects only. It is possible to just consider the time slot when a 1 bit (ω_1) is transmitted without losing generality. Hence the PDF of the output from receiver 1 is given by [Ref. 95]:

$$p_1(V) = \frac{1}{(\overline{i_{SL}^2})^{\frac{1}{2}}\sqrt{2\pi}} \exp - \left[\frac{(I_{SH} - V_1)^2}{2(\overline{i_{SL}^2})}\right] \tag{12.37}$$

Again we assume the local oscillator output power to be much higher than that of the incoming signal so that the total noise current is approximately equal to $\overline{i_{SL}^2}$ provided by Eq. (12.14). The noise output from receiver 2 can therefore be written as:

$$p_2(V) = \frac{1}{(\overline{i_{SL}^2})^{\frac{1}{2}}\sqrt{2\pi}} \exp - \left[\frac{V_2^2}{2(\overline{i_{SL}^2})}\right] \tag{12.38}$$

As an error occurs when $V_2 > V_1$, then the probability of error $P(e)$ is equivalent to the probability that $V_1 - V_2 < 0$. Hence:

$$P(e) = \int_{-\infty}^{0} \frac{1}{[2\pi 2(\overline{i_{SL}^2})]^{\frac{1}{2}}} \exp - \left[\frac{(w - I_{SH})^2}{4(\overline{i_{SL}^2})}\right] dw \tag{12.39}$$

Changing the limits of the integration gives:

$$P(e) = \int_{I_{SH}/(\overline{i_{SL}^2})}^{\infty} \frac{1}{\sqrt{\pi}} \exp(-z^2)\, dz \tag{12.40}$$

Comparison with the definition for the complementary error function given in

Eq. (11.17) allows Eq. (12.40) to be written as:

$$P(\mathrm{e}) = \tfrac{1}{2}\,\mathrm{erfc}\left(\frac{I_{\mathrm{SH}}}{2(\overline{i_{\mathrm{SL}}^2})^{\frac{1}{2}}}\right) \tag{12.41}$$

Finally, substituting from Eq. (12.25) for I_{SH} and from Eq. (12.13) for $\overline{i_{\mathrm{SL}}^2}$ where the bandwidth, which in this heterodyne detection case is B_{IF}, is again (see Section 12.7.1) written in terms of the transmission bit rate B_{T}; then the probability of error becomes:

$$P(\mathrm{e}) = \tfrac{1}{2}\,\mathrm{erfc}\left(\frac{\eta P_{\mathrm{S}}}{2hf B_{\mathrm{T}}}\right)^{\frac{1}{2}} \tag{12.42}$$

The comparison of Eq. (12.42) with Eq. (12.33) indicates that FSK heterodyne synchronous detection has a receiver sensitivity which in the shot noise limit is 3 dB higher than that of ASK heterodyne synchronous detection. This improvement in sensitivity for FSK modulation may be attributed to the use of two frequencies (and hence dimensions) rather than only the one in the case of ASK. It should be noted, however, that a similar BER is obtained with the two modulation schemes when the same average power is transmitted. Whereas with ASK, zero signal power is transmitted for a binary 0 bit, in FSK a similar signal power is continuously transmitted [Ref. 97]. Nevertheless, there are advantages associated with the use of FSK over ASK, even when two systems with the same average signal power are considered. In particular, the optimization of the decision level proves easier and the spectrum broadening as a result of switching between a one and a zero state in practice is much reduced on that obtained with ASK.

Considering FSK heterodyne nonsynchronous or envelope detection, it can be shown that the probability of error in the shot noise limit under similar assumptions to those above for synchronous detection is given by the expression [Refs. 95, 96]:

$$P(\mathrm{e}) = \tfrac{1}{2}\exp - \left(\frac{I_{\mathrm{SH}}^2}{4(\overline{i_{\mathrm{SL}}^2})}\right) \tag{12.43}$$

Substituting for I_{SH} and $\overline{i_{\mathrm{SL}}^2}$ from Eqs. (12.25) and (12.14), respectively, gives:

$$P(\mathrm{e}) = \tfrac{1}{2}\exp - \left(\frac{\eta P_{\mathrm{S}}}{2hf B_{\mathrm{T}}}\right) \tag{12.44}$$

This result for FSK nonsynchronous detection is approximately equivalent to the one obtained for synchronous detection (Eq. (12.42)) and shows a 3 dB improvement over ASK nonsynchronous detection (Eq. (12.35)).

12.7.3 PSK heterodyne detection

In this modulation format the information is transmitted by a carrier of one phase for a binary 1 and a different phase for a binary 0. The phase shift employed is

normally π radians so that:

$$I_S(t) = \begin{cases} I_{SH} \cos(\omega_{IF} t + \phi), & \text{for a 1 bit} \\ I_{SH} \cos(\omega_{IF} t + \pi + \phi), & \\ \text{or} & \text{for a 0 bit} \\ -I_{SH} \cos(\omega_{IF} t + \phi), & \end{cases} \tag{12.45}$$

Therefore the synchronously detected signal $I_S(t)$ is positive for the 1 bits and negative for the 0 bits. In this case the optimum decision level current is given as $I_D = 0$ instead of that obtained in Eq. (12.29) for ASK synchronous detection. Nevertheless, a similar method to obtain the probability of error $P(e)$ for the PSK heterodyne synchronous detection to that used in Section 12.7.1 for ASK detection may be employed. Hence assuming that the output voltage from the receiver for a binary one is V_1 and for a binary zero it is V_2 then:

$$\begin{aligned} P(e) &= \frac{1}{2} \int_{-\infty}^{0} \frac{1}{(\overline{i_{SL}^2})^{\frac{1}{2}}\sqrt{2\pi}} \exp - \left(\frac{(I_{SH} - V_1)^2}{2(\overline{i_{SL}^2})} \right) dV_1 \\ &\quad + \frac{1}{2} \int_{0}^{\infty} \frac{1}{(\overline{i_{SL}^2})^{\frac{1}{2}}\sqrt{2\pi}} \exp - \left(\frac{(-I_{SH} - V_2)^2}{2(\overline{i_{SL}^2})} \right) dV_2 \\ &= \frac{1}{2} \operatorname{erfc}\left(\frac{I_{SH}}{(\overline{i_{SL}^2})^{\frac{1}{2}}\sqrt{2}} \right) \end{aligned} \tag{12.46}$$

Substituting from Eq. (12.25) for I_{SH} and from Eq. (12.13) for $\overline{i_{SL}^2}$ where the bandwidth, which in this heterodyne detection case is B_{IF}, and following Section 12.7.1, it is written in terms of the transmission bit rate B_T; then the probability of error becomes:

$$P(e) = \tfrac{1}{2} \operatorname{erfc}\left(\frac{\eta P_S}{h f B_T} \right)^{\frac{1}{2}} \tag{12.47}$$

It may be noted that in the shot noise limit PSK heterodyne synchronous detection exhibits 3 dB and 6 dB more sensitivity than the FSK and ASK heterodyne synchronous detection schemes respectively (Eqs. (12.42) and (12.33)). In practice, however, very small levels of phase fluctuation at the transmitter can significantly deteriorate the potential low BER of the PSK system.

Although nonsynchronous PSK detection is not strictly realizable, a more relaxed synchronous detection process is afforded by differential PSK (DPSK) in which the transmitted information is contained by the phase difference between two consecutive bit periods (see Sections 12.5.3 and 12.7.1). The probability of error in the detection of this modulation format at the shot noise limit and under the previous assumption is given by [Refs. 95, 96]:

$$P(e) = \tfrac{1}{2} \exp - \left(\frac{I_{SH}^2}{2(\overline{i_{SL}^2})} \right) \tag{12.48}$$

Furthermore, substituting for I_{SH} and $\overline{i_{SL}^2}$ from Eqs. (12.25) and (12.14) gives:

$$P(e) = \tfrac{1}{2} \exp - \left(\frac{\eta P_S}{hf B_T}\right) \tag{12.49}$$

This expression for DPSK indicates a roughly equivalent probability of error for this scheme to that obtained with PSK synchronous detection (Eq. (12.47)). Moreover, it demonstrates a potential 3 dB and 6 dB improvement over the FSK and ASK nonsynchronous detection schemes respectively.

12.7.4 ASK and PSK homodyne detection

From the three basic modulation formats, ASK and PSK signals can be demodulated using a homodyne detection scheme, provided that both the frequency and the phase of the local oscillator output signal can be synchronized to the incoming carrier signal (see Section 12.6.3). It should be noted that FSK modulation can only be detected using a homodyne type receiver when the device has two phase controlled local oscillators. The only exception to this occurs when phase diversity reception (see Section 12.6.4) is employed, but these techniques cannot be regarded as true homodyne detection schemes.

It was shown in Section 12.3 that the reduction in the bandwidth requirement for homodyne detection produced a sensitivity improvement of 3 dB over the corresponding ASK heterodyne detection scheme. The probability of error for ASK homodyne detection can be derived from a slight modification to the result obtained in Eq. (12.31) for ASK heterodyne synchronous detection. This modification involves the noise power term ($\overline{i_{SL}^2}$) which in the homodyne case is reduced by a half because of the factor of two bandwidth reduction. Hence the probability of error for ASK homodyne detection is given by [Ref. 96]:

$$\begin{aligned} P(e) &= \tfrac{1}{2} \operatorname{erfc}\left(\frac{I_{SH}}{2(\overline{i_{SL}^2}/2)^{\frac{1}{2}}\sqrt{2}}\right) \\ &= \tfrac{1}{2} \operatorname{erfc}\left(\frac{I_{SH}}{2(\overline{i_{SL}^2})^{\frac{1}{2}}}\right) \end{aligned} \tag{12.50}$$

It should be noted, however, that the signal power in Eq. (12.50) remains the same as in the heterodyne case which may be observed to be correct by comparing Eqs. (12.10) and (12.11). Substitution from Eq. (12.25) for I_{SH} and from Eq. (12.14) for $\overline{i_{SL}^2}$ where in this case the bit rate B_T is set equal to the baseband bandwidth B gives:

$$P(e) = \tfrac{1}{2} \operatorname{erfc}\left(\frac{\eta P_S}{2hf B_T}\right)^{\frac{1}{2}} \tag{12.51}$$

Considering now the PSK homodyne detection scheme, Eq. (12.46) for PSK synchronous detection can be modified in a similar manner to the above so that the

probability of error is given by:

$$P(e) = \tfrac{1}{2}\,\mathrm{erfc}\left(\frac{I_{SH}}{(\overline{i_{SL}^2})^{\frac{1}{2}}}\right) \tag{12.52}$$

Again substituting from Eqs. (12.25) and (12.14) gives the probability of error for PSK homodyne detection in the shot noise limit as.

$$P(e) = \tfrac{1}{2}\,\mathrm{erfc}\left(\frac{2\eta P_S}{hf B_T}\right)^{\frac{1}{2}} \tag{12.53}$$

The result obtained in Eq. (12.53) represents the lowest error probability and hence the highest receiver sensitivity of all the coherent detection schemes. As anticipated, it displays a 3 dB improvement over PSK heterodyne synchronous detection.

12.7.5 Comparison of sensitivities

A comparison of the analytical results for the major modulation formats and detection schemes obtained in Section 12.7.1 to 12.7.4 is provided in Table 12.2. Moreover, to allow a comparison to be made with direct detection, an additional column records the details determined from Eq. (9.7) and Example 9.1. It should be noted, however, that the average number of photons per bit required to maintain a BER of 10^{-9} assumes in the case of ASK that photons arrive over two bit periods because no light is transmitted for a binary zero. Hence the values shown must be doubled if the actual number of photons required to register a binary one with a BER of 10^{-9} is to be recorded (i.e. not the average over the two bit periods). This factor can lead to some confusion in the approaches adopted by different authors (e.g. Refs. 3, 23, 96, 98, 99]. However, no such difficulties occur with the FSK and PSK modulation formats as a constant amplitude carrier signal is transmitted for both the binary one and zero bits.

The average number of received photons per bit at a particular BER as given in Table 12.2 may be determined from the expressions which are provided for the respective error probabilities in the table. An analytical definition for the number of received photons per bit, however, is needed. This may be written down by considering Eq. (8.7) which simply provides the generation rate for electrons from incident photons in an optical detector. This equation therefore represents the received photon rate. To convert this into the photon number per bit N_p the expression must be simply multiplied by the signalling interval τ so that:

$$N_p = \frac{\eta P_S \tau}{hf} = \frac{\eta P_S}{hf B_T} \tag{12.54}$$

where we have written the peak signal power P_S in place of P_o in Eq. (8.7) for consistency with the notation in this chapter, and B_T is the transmission bit rate. Furthermore, it is useful to note that Eqs. (12.16) and (12.17) which provide the SNRs for heterodyne and homodyne detection, respectively, in their shot noise

Table 12.2 Comparison of optical receiver sensitivities in the quantum or shot noise limit. The upper entry in each detection technique provides the possibility of error determined for the different schemes, whilst the lower entry represents the average number of photons per bit required by an ideal binary receiver ($\eta = 1$) to achieve a BER of 10^{-9}

Modulation \ Receiver	Homodyne detection	Heterodyne: Synchronous detection	Heterodyne: Nonsynchronous detection	Direct detection
ASK or OOK	$\frac{1}{2}\text{erfc}\left(\frac{\eta P_s}{2hfB_T}\right)^{1/2}$	$\frac{1}{2}\text{erfc}\left(\frac{\eta P_s}{4hfB_T}\right)^{1/2}$	$\frac{1}{2}\exp-\left(\frac{\eta P_s}{4hfB_T}\right)$	$\frac{1}{2}\exp-\left(\frac{\eta P_s}{hfB_T}\right)$
Av. no. photons per bit*	18	36	40	10.4
FSK	No (only very special receiver)	$\frac{1}{2}\text{erfc}\left(\frac{\eta P_s}{2hfB_T}\right)^{1/2}$	$\frac{1}{2}\exp-\left(\frac{\eta P_s}{2hfB_T}\right)$	No
Av. no. photons per bit	—	36	40	—
PSK	$\frac{1}{2}\text{erfc}\left(\frac{2\eta P_s}{hfB_T}\right)^{1/2}$	$\frac{1}{2}\text{erfc}\left(\frac{\eta P_s}{hfB_T}\right)^{1/2}$	DPSK† $\frac{1}{2}\exp-\left(\frac{\eta P_s}{hfB_T}\right)$	No
Av. no. photons per bit	9	18	20	—

* Values provided assume that the photons arrive over two bit periods.
† Strictly speaking, there is not a heterodyne nonsynchronous demodulation scheme for PSK. Differential PSK (DPSK), however, exhibits a less stringent synchronous detection technique than conventional PSK and is therefore included in the nonsynchronous column for convenience.

limits can also be expressed in terms of the number of received photons per bit by taking $B_T = 2B$ as [Ref. 96]:

$$\left(\frac{S}{N}\right)_{\text{het-lim}} = \frac{\eta P_S}{hf B_T} = \eta N_p \tag{12.55}$$

and

$$\left(\frac{S}{N}\right)_{\text{hom-lim}} = \frac{\eta P_S}{hf B_T/2} = 2\eta N_p \tag{12.56}$$

At this stage, however, we are concerned with the determination of the average numbers of photons per bit for the various digital modulation schemes listed in Table 12.2. An explanation of how these values are obtained is provided in the following example.

Example 12.3

Calculate the number of received photons per bit in order to maintain a BER of 10^{-9} for:

(a) ASK heterodyne synchronous detection;
(b) ASK heterodyne nonsynchronous detection;
(c) PSK homodyne detection.

An ideal binary receiver may be assumed in all cases.

Solution: (a) Substituting N_p from Eq. (12.54) in Eq. (12.33) gives the probability of error for ASK heterodyne detection as:

$$P(e) = \tfrac{1}{2}\,\mathrm{erfc}\left(\frac{\eta N_p}{4}\right)^{\frac{1}{2}}$$

To maintain a BER of 10^{-9} and with an ideal binary receiver ($\eta = 1$):

$$10^{-9} = \tfrac{1}{2}\,\mathrm{erfc}\left(\frac{N_p}{4}\right)^{\frac{1}{2}}$$

and

$$\left(\frac{N_p}{4}\right)^{\frac{1}{2}} = 4.24$$

Hence:

$$\frac{N_p}{4} \simeq 18 \qquad \text{and} \qquad N_p = 72$$

However, for ASK the 72 photons can arrive over two bit periods, assuming an equal number of ones and zeros. Hence the average number of photons per bit required is 36.

(b) Substituting N_p from Eq. (12.54) into Eq. (12.35) gives:

$$P(e) = \tfrac{1}{2}\exp -\left(\frac{\eta N_p}{4}\right)$$

In this case:

$$\exp -\left(\frac{N_p}{4}\right) = 2 \times 10^{-9}$$

and therefore

$$\frac{N_p}{4} \simeq 20 \qquad \text{and} \qquad N_p = 80$$

Again we are considering ASK modulation so that the average number of received photons per bit is 40. It may be noted that this result is very approximately equal to the number obtained in (a).

(c) For PSK homodyne detection, N_p from Eq. (12.54) may be substituted in Eq. (12.47) to give:

$$P(e) = \tfrac{1}{2} \operatorname{erfc} (2N_p)^{\frac{1}{2}}$$

Hence

$$(2N_p)^{\frac{1}{2}} = 4.24$$

and

$$N_p \simeq \frac{18}{2} = 9$$

In this case N_p is equal to the average number of photons per bit as 9 photons must be received for zero bit as well as the one bit in order to achieve a BER of 10^{-9}.

As mentioned in Section 12.7.1, the approximation $\operatorname{erfc}(u) \simeq \exp -(u)^2$ is used by some authors [Refs. 95, 96] to indicate the rough equivalence between the error probabilities for the synchronous and nonsynchronous detection cases. However, it may be observed from Table 12.2 and Example 12.3 that the nonsynchronous detection in reality requires slightly more photons per bit (slightly higher incoming optical power) than does synchronous detection in the shot noise limit. It should be noted that a more accurate approximation relating the complementary error function to the negative exponential of $\operatorname{erfc}(u) \simeq \exp -(u)^2/x\sqrt{\pi}$ for $x > 3$ is used by some authors [Refs. 3, 99].

Nevertheless, aside from these approximations it is possible to write down a generalized expression for the error probabilities of the various modulation formats with synchronous detection schemes recorded in Table 12.2. For fully synchronous heterodyne and homodyne detection the generalized expression therefore takes the form:*

$$P(e) = \tfrac{1}{2} \operatorname{erfc}\left(\frac{KZ\eta P_S}{4hf B_T}\right)^{\frac{1}{2}} \tag{12.57}$$

where K is a constant which is equal to 1 for heterodyne detection and 2 for homodyne detection. The constant Z is determined by the modulation scheme as follows: for ASK and FSK, $Z = 1$ and for PSK, $Z = 4$. As with the expressions recorded in Table 12.2, the generalized relationship of Eq. (12.57) can also be used to determine the minimum detectable power level to maintain a particular BER with a specific modulation scheme and synchronous receiver.

* The exception to this is DPSK which, although in reality is synchronous, does not fulfil the necessary continuous phase matching condition.

Example 12.4

Determine the minimum incoming optical power level required to detect a 400 Mbit s^{-1} FSK signal at a BER of 10^{-9} using an ideal heterodyne synchronous receiver operating at a wavelength of 1.55 μm.

Solution: For FSK heterodyne synchronous detection, $K = 1$ and $Z = 1$ in Eq. (12.57); therefore:

$$10^{-9} = \tfrac{1}{2}\,\mathrm{erfc}\left(\frac{\eta P_S}{2hf B_T}\right)^{\frac{1}{2}}$$

Hence for the ideal receiver:

$$\frac{P_S}{2hf B_T} = 18$$

and

$$P_S \simeq \frac{36hc\,B_T}{\lambda} = \frac{36 \times 6.63 \times 10^{-34} \times 3 \times 10^8 \times 400 \times 10^6}{1.55 \times 10^{-6}}$$

$$= 1.8\ \text{nW or } -57.4\ \text{dBm}$$

Therefore, the minimum incoming peak power level to maintain a BER of 10^{-9} is -57.4 dBm. Although this level may appear at first sight rather high, it must be remembered that the bit rate is also relatively high at 400 Mbit s^{-1}, a factor which directly contributes to the lowering of the sensitivity for the receiver.

The relative sensitivities of the different modulation formats and detection schemes can be readily deduced from consideration of the average numbers of photons per bit indicated for each detection technique in Table 12.2. However, a more immediate comparison of the relative receiver performances may be obtained from Figure 12.24 [Ref. 4]. It may be observed that the sensitivity improvement of ASK heterodyne coherent detection over IM/DD is 10 to 25 dB in Figure 12.24, whereas in Table 12.2 direct detection would appear to be around 6 dB more sensitive than ASK heterodyne detection. This second statement is true in theory but in practice practical direct detection receivers require in the order of 400 to 4000 photons per bit to maintain a BER of 10^{-9} [Ref. 23]. By contrast, practical ASK heterodyne coherent receivers are far more likely to be operated near the quantum or shot noise limit and thus provide the sensitivity indicated in Table 12.2.

To further illustrate the point concerning the relative receiver sensitivities of IM/DD and coherent systems, ASK heterodyne detection using both synchronous and nonsynchronous detection is compared with direct detection in the theoretical characteristics shown in Figure 12.25 [Ref. 95]. The substantial improvement in receiver sensitivity offered by the coherent detection schemes may be observed even when compared with direct detection with very low photodetector dark current (I_d). Moreover, the reduction in receiver sensitivity with increases in the

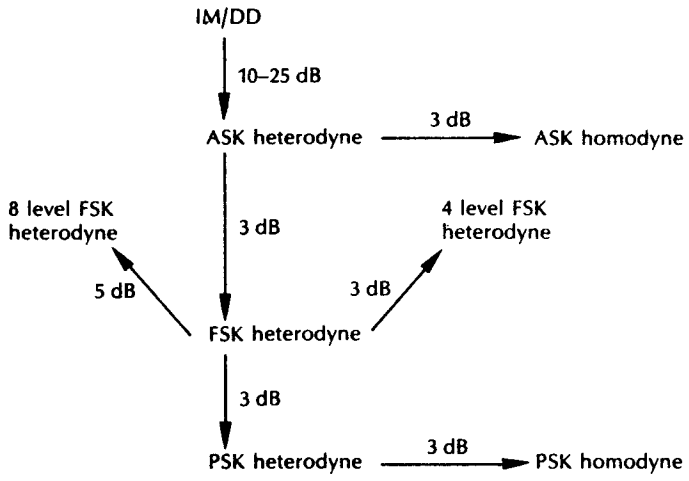

Figure 12.24 Receiver sensitivity improvements using various coherent modulation and demodulation schemes.

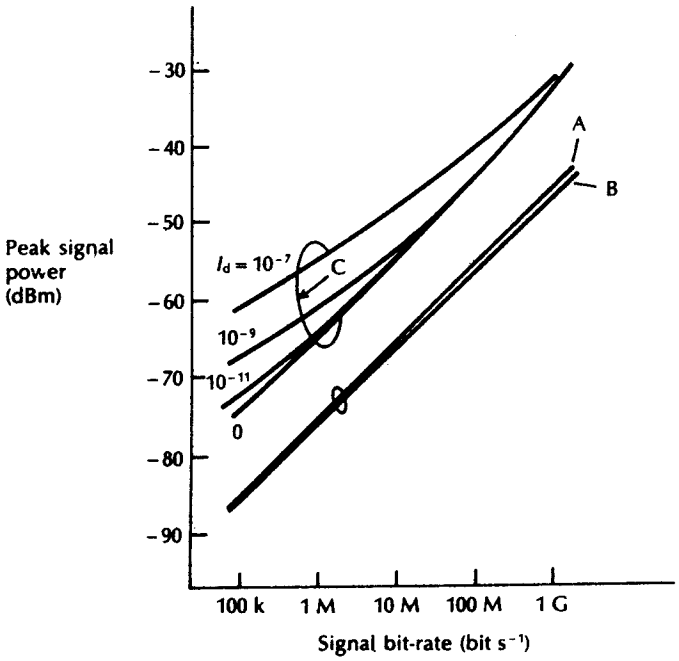

Figure 12.25 Comparison of ASK heterodyne nonsynchronous and synchronous receiver sensitivities with IM/DD for a BER of 10^{-9} using an APD with excess noise factor of 1.0, curve A; ASK heterodyne nonsynchronous detection, curve B: ASK heterodyne synchronous detection; curves C; IM/DD, in which the photodetector dark current (I_d) is a parameter. Reproduced with permission from T. Okoshi, K. Emura, K. K. Kikuchi and R. Th. Kersten, *J. Opt. Commun.*, **2**, p. 89, 1981 [Ref. 95].

transmission bit rate can be noted, as mentioned in Example 12.3. The aforementioned factors are of particular interest when we consider the potential or ultimate repeater spacings that may be afforded by coherent optical fiber transmission [Ref. 20].

Example 12.5

Calculate the absolute maximum repeater spacing that could be provided to maintain a BER of 10^{-9} within a coherent optical fiber system operating at a wavelength of 1.55 μm when the fiber and splice/connector losses average out at 0.2 dB km^{-1}, the optical power launched into the fiber link is 2.5 mW and the transmission rates are 50 Mbit s^{-1} and 1 Gbit s^{-1}. For both bit rates consider the following ideal receiver types:

(a) ASK heterodyne synchronous detection;
(b) PSK homodyne detection.

Solution: (a) Considering the 50 Mbit s^{-1} transmission rate and using the result obtained for ideal ASK heterodyne synchronous detection in Example 12.3 (average photons per bit required 36) from Eq. (12.54)

$$N_p = \frac{P_S}{hf\,B_T} = \frac{P_S}{hf\,B_T} \simeq 36$$

Hence

$$P_S \simeq 36hc\,B_T = \frac{36 \times 6.63 \times 10^{-34} \times 3 \times 10^8 \times 50 \times 10^6}{1.55 \times 10^{-6}}$$

$$= 0.23 \text{ nW or } -66.4 \text{ dBm}$$

The maximum system margin with no overheads is therefore:

$$\textit{Max. system margin} = 4 \text{ dBm} - (-66.4) \text{ dBm} = 70.4 \text{ dB}$$

Moreover, the absolute maximum repeater spacing is:

$$\textit{Max. repeater spacing} = \frac{70.4}{0.2} = 352 \text{ km}$$

For 1 Gbit s^{-1} we have:

$$P_S \simeq \frac{36 \times 6.63 \times 10^{-34} \times 3 \times 10^8 \times 10^9}{1.55 \times 10^{-6}}$$

$$= 4.6 \text{ nW or } -53.4 \text{ dBm}$$

Therefore the maximum system margin is 57.4 dB and

$$\textit{Max. repeater spacing} = \frac{57.4}{0.2} = 287 \text{ km}$$

Again using the result for PSK homodyne detection obtained in example 12.3 and considering first the 50 Mbit s^{-1} rate, then from Eq. (12.54):

$$N_p = \frac{P_S}{hf\,B_T} = \frac{P_S}{hf\,B_I} \simeq 9$$

and

$$P_S \simeq {}^{9}hc\,B_I = \frac{9 \times 6.63 \times 10^{-34} \times 3 \times 10^{8} \times 50 \times 10^{6}}{1.55 \times 10^{-6}}$$

$$= 58 \text{ pW or } 72.4 \text{ dBm}$$

The maximum system margin is now 76.4 dB so that,

$$\textit{Max. repeater spacing} = \frac{76.4}{0.2} = 382 \text{ km}$$

For 1 Gbit s^{-1}:

$$P_S \simeq \frac{9 \times 6.63 \times 10^{-34} \times 3 \times 10^{8} \times 10^{9}}{1.55 \times 10^{-6}}$$

$$= 1.15 \text{ nW or } -59.4 \text{ dBm}$$

Hence the maximum system margin is 63.4 dB and

$$\textit{Max. repeater spacing} = \frac{63.4}{0.2} = 317 \text{ km}$$

Thus the range of repeater spacings indicated by this example is between 287 and 392 km.

The relative receiver sensitivities of two multilevel FSK modulation schemes are also indicated in Figure 12.24. Hence, as anticipated, these four and eight level FSK heterodyne detection schemes display a reduction in sensitivity of 3 dB and 5 dB, respectively, over binary FSK heterodyne detection. Receiver sensitivity characteristics for other M'ary modulation schemes are shown in Figure 12.26(a) [Ref. 68]. The receiver sensitivities for binary PSK (BPSK), quaternary or four level PSK (QPSK) and sixteen level quadrature amplitude modulation (QAM) against their information transmission capacities are displayed. Furthermore, these characteristics are a function of the receiver thermal noise parameters which are also shown in Figure 12.26(a). It may be observed that at higher transmission rates the receiver sensitivities are degraded by increases in thermal noise, as demonstrated by the corresponding characteristics given in Figure 12.26(b) [Ref. 68].

However, QPSK may provide an M'ary modulation format which will enable the achievement of high capacity coherent optical transmission with no sensitivity penalty in comparison with binary PSK. It may be noted that in Figure 12.26(a) the

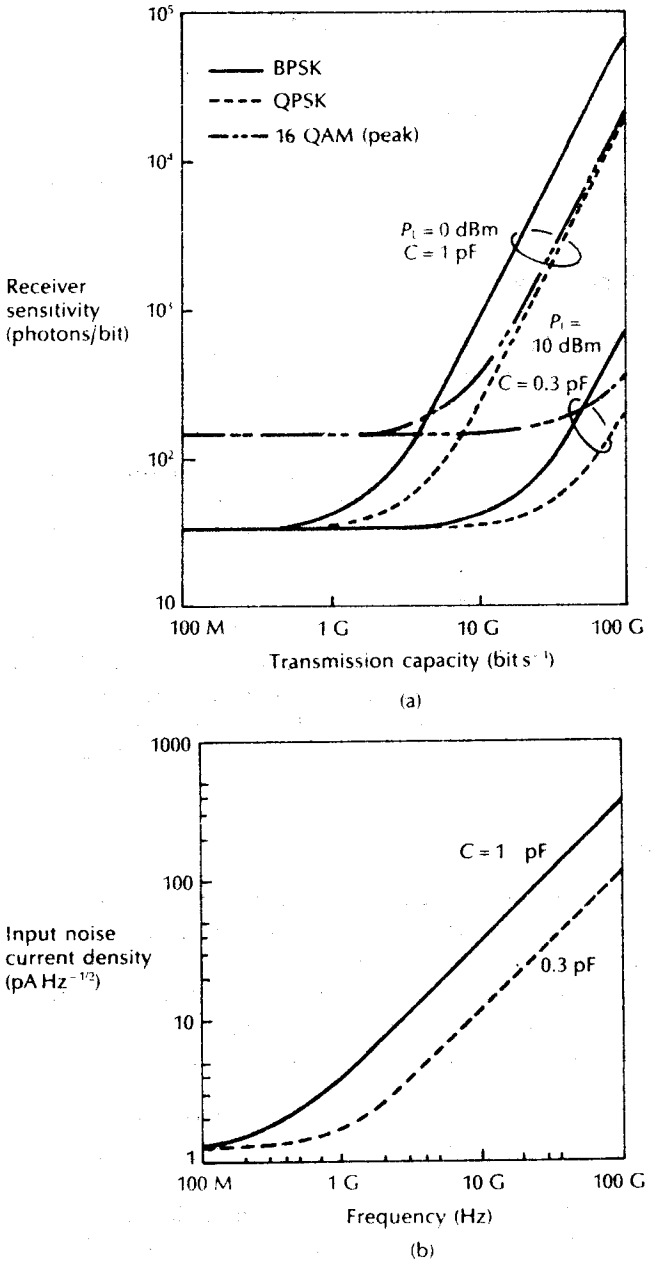

Figure 12.26 (a) Receiver sensitivities for M'ary modulation schemes; (b) Equivalent input noise current density of preamplifier used to determine characteristics provided in (a) where C is the total input capacitance, the transconductance is 50 mS and the numerical factor is 1.1. Reproduced with permission from K. Nosu and K. Iwashita, 'A consideration of factors affecting future coherent lightwave communication systems', *J. Lightwave Technol.*, **6**, p. 686, 1988. Copyright © 1988 IEEE.

sensitivity of QPSK is at least equivalent to (or marginally better than) that of BPSK. Moreover, a recent feasibility study concerned with coherent optical QPSK transmission also supports this observation [Ref. 99]. With higher numbers of levels using PSK or QAM, however, the receiver sensitivity degrades and hence narrower linewidth lasers will be required.

12.8 Single and multicarrier systems

Since the initial measurements of bit error rate on experimental coherent optical fiber systems were reported in 1981, many experimental systems have been developed in the laboratory with research workers' concern shifting from heterodyne ASK to the more sophisticated FSK, CPSK, PSK and DPSK heterodyne demodulation schemes [Refs. 4, 18, 44, 45, 101]. In addition, more recently, interest has grown in ASK using phase diversity reception [Ref. 86] as well as ASK heterodyne detection employing polarization diversity receivers [Ref. 40]. Various of these experimental systems were outlined in Sections 12.4.2.2, 12.5 and 12.6, where their performance characteristics were also indicated. Therefore, in this section we consider the next stage of these developments which is the deployment of coherent optical fiber systems within the telecommunication network. This is approached through a description of the first demonstration of a coherent optical transmission system in an operational network, followed by a brief discussion of potential developments in multicarrier coherent fiber optical system and network strategies.

12.8.1 DPSK field demonstration system

The first demonstration of the deployment of a coherent optical fiber communication system in an operational environment was reported in October 1988 [Ref. 102]. The system configuration for this DPSK demonstrator system is provided in Figure 12.27. Miniaturized LEC lasers were employed as the optical sources at the transmitter and local oscillator, each of which provided a spectral linewidth less than 100 kHz and a launch power of 0 dBm [Ref. 26]. Mechanical adjustment also allowed the output wavelength to be preset with a range of around 50 nm with continuous wavelength tuning over a range of 50 GHz provided by electronic control about the preset wavelength. For the demonstration the operational wavelength was set to 1.534 μm.

A lithium niobate phase modulator was used to apply DPSK modulation at a rate of 565 Mbit s^{-1} to the transmitter laser output. The optical isolator shown in Figure 12.27 was a fiber-coupled 30 dB commercial device [Ref. 103] which when inserted between the LEC laser and the modulator proved sufficient for the suppression of reflection induced linewidth broadening as LEC lasers are relatively insensitive to reflected optical power. The output from the modulator was boosted by a semiconductor laser optical amplifier prior to launching into the installed conventional single-mode fiber cable. This amplifier was introduced to overcome the loss through

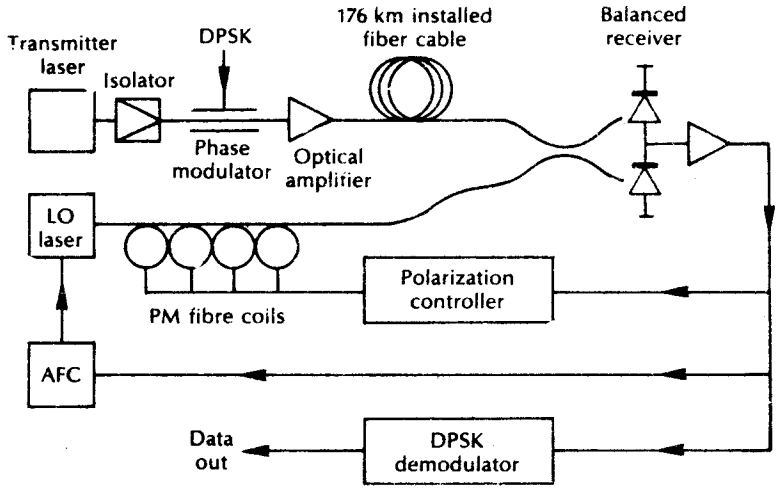

Figure 12.27 Configuration for the DPSK field demonstration system [Ref. 102].

the optical isolator and the modulator, and therefore to increase the launch power from -10 to $+1$ dBm when transmission over 176 km of installed fiber was required.

At the receive terminal an automated polarization control system was applied to the local oscillator laser output. The device consisted of four transducers formed by winding polarization maintaining fiber onto piezoelectric cylinders, and provided a limitless range of polarization control as described in Section 12.4.2.1. A dual detector balanced optical input was provided at the receiver to minimize the thermal noise penalty. It was also designed to give a low return loss to the local oscillator laser and therefore remove the requirement for an optical isolator. Automatic frequency control applied to the piezoelectric movements in the grating mount of the local oscillator laser allowed the IF between the received carrier and the local oscillator to be stabilized at 847 ± 10 MHz (i.e. $1.5 \times$ bit rate). Finally, the transmitted data were recovered using a delay line demodulator with IF bandpass filtering.

The system which was installed using an eighteen fiber cable in an underground duct between Cambridge and Bedford in the United Kingdom demonstrated a long term measured BER of 5×10^{-9} with a receiver sensitivity of -47.6 dBm (276 photons per bit) over the 176 km route. Error-free operation with no error floor at BER levels above 10^{-13} was also observed using the same system arrangement but operating over 150 km of installed fiber cable. Moreover, subsequent improvements to the system included a hybrid integrated balanced receiver using a GaAs–FET IC preamplifier to improve the sensitivity to -52 dBm as well as the incorporation of an injection laser pumped erbium doped fiber amplifier repeater [Ref. 104].

12.8.2 Multicarrier system and network concepts

It was mentioned in Section 12.1 that a major attribute of coherent optical transmission was its ability to provide wavelength/frequency selectivity with narrow channel spacings for future multicarrier systems and networks. Wavelength division multiplexing technology and techniques have been discussed in relation to IM/DD optical fiber systems (see Sections 5.6.3 and 11.8.3) but it is apparent that far more optical carriers could be employed using coherent optical receivers which may be tuned to specific incoming carrier signals. For such coherent systems, because the channel widths are very narrow (often of the order of the data transmission rate) in comparison with conventional WDM, then the channel spacings are measured in frequency rather than wavelength units. Consequently, multicarrier coherent optical systems and networks are often referred to as frequency division multiplexed (FDM) [Refs. 6, 7, 105 to 108].

It is clear that coherent optical FDM systems provide a powerful strategy for the utilization of the enormous optical bandwidth potential of fibers (over 50 000 GHz between 1.3 and 1.6 μm) whilst avoiding the potential bottleneck created by the speed of the electronics within single carrier systems. Although 10 Gbit s^{-1} may finally be achieved within single channel installed systems, moving to higher rates with electronic TDM looks increasingly doubtful [Ref. 1]. However, far greater capacity could be achieved at more modest transmission rates using coherent optical FDM techniques. For example, even at spacings of 10 GHz several thousand frequency/wavelength channels could be accommodated over the 1.3 to 1.6 μm wavelength band.

At present a favoured technique within coherent multicarrier systems is to use a passive star coupler to distribute or broadcast the optical signals over the network [Refs. 105 to 107]. A block schematic for such an FDM coherent star network is illustrated in Figure 12.28. All the optical carriers (shown as λ_i, λ_j, λ_k, etc.) are generated and modulated individually for transmission over the network. At the network output, tunable, highly selective optical heterodyne receiver local oscillators provide multiple channel access. Alternatively, fixed wavelengths/frequencies could be assigned to the receivers and tunable lasers could be employed at the transmitters. The former strategy has been demonstrated for a small number of channels [Refs. 7, 107]. In the latter demonstration four FSK modulated channels operating at 200 Mbit s^{-1} and spaced 2.45 GHz apart were combined in a 16×16 passive star coupler. Demultiplexing was achieved using a heterodyne FM receiver with an IF of 850 MHz. Moreover, the minimum received optical power required to maintain a BER of 10^{-9} was -55.5 dBm (109 photons per bit) and the degradation due to adjacent channel interference was found to be negligible.

Considering an $N \times N$ coherent passive star network of the form shown in Figure 12.28. The minimum power required at each receiver P_S can be obtained from Eq. (12.55) or Eq. (12.56) as:

$$P_S \geq N_p \, hf \, B_T \tag{12.58}$$

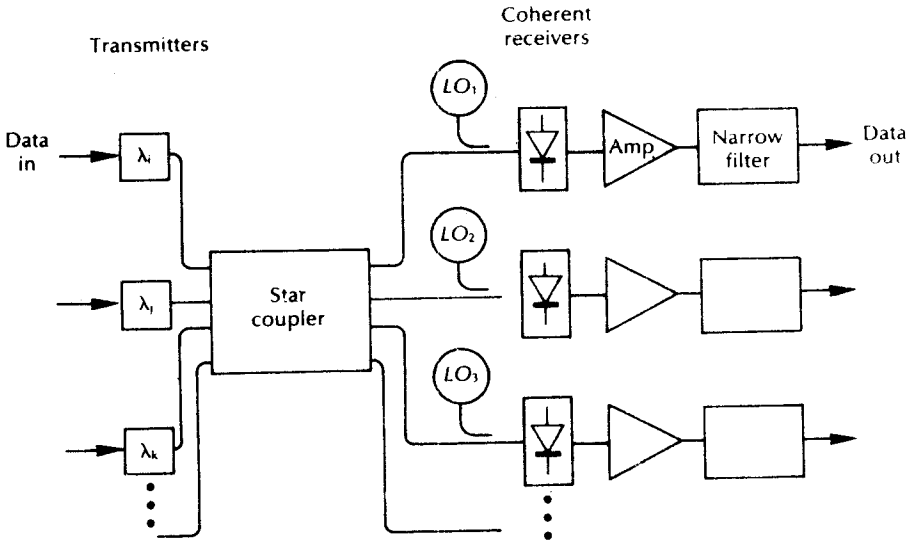

Figure 12.28 Frequency division multiplexed coherent star network.

Then taking account of the star coupler distribution loss and assuming no excess loss through the device, the power required to be launched from each transmitter P_{tx} is:

$$P_{tx} \geqslant N_p \, hf \, B_T \, N \tag{12.59}$$

where N is the number of ports on the coupler.

The relationship given in Eq. (12.59) may be seen to be correct because the division of power on the network is inversely related to N (see Section 5.6.2), as is the portion of the total fiber optical bandwidth available to each terminal. However, since for an optical FDM network the total information throughput capacity $N \times B_T$ is limited by the fiber bandwidth B_{fib} then the transmission capacity (bit rate) available to each terminal is:

$$B_T \leqslant \frac{B_{fib}}{N} \tag{12.60}$$

Substituting Eq. (12.60) into (12.59) gives:

$$P_{tx} \geqslant N_p \, hf \, B_{fib} \tag{12.61}$$

This is an interesting result which indicates that the transmitter power requirement is independent of the number of terminals on the network [Ref. 44].

Example 12.6

Estimate the minimum transmitter power requirement for an optical coherent FDM passive star network using heterodyne synchronous receivers which need an average of 150 photons per bit for reception at the desired BER. It may be assumed that the network is operating from a shortest wavelength of 1.3 μm with an optical bandwidth of 20 THz.

Solution: The minimum required transmitter power P_{tx} may be obtained directly from Eq. (12.61) as the worst case occurs at the shortest wavelength. Hence:

$$P_{tx} \simeq N_p\, hf\, B_{fib} = \frac{N_p\, hc\, B_{fib}}{\lambda}$$

$$= \frac{150 \times 6.63 \times 10^{-34} \times 3 \times 10^{8} \times 20 \times 10^{12}}{1.3 \times 10^{-6}}$$

$$= 0.5 \text{ mW or } -3 \text{ dBm}$$

The result obtained in Example 12.6 indicates that relatively modest transmitter power will, in principle, facilitate the operation of optical coherent FDM star networks with arbitrarily large numbers of terminals. It must be emphasized, however, that significant losses on the network (coupler excess loss, fiber losses, etc.) have not been taken into account and that the restriction on the number of channels will generally be substantially greater than that dictated by Eq. (12.60) in which the channel bandwidth requirement was taken to be approximately equal to the transmission bit rate. In many cases the modulated spectrum can be much wider than this amount (e.g. for wide deviation FSK) and, in addition, guard bands are necessary between channels.

A coherent optical FDM experimental system for cable television (CATV) distribution has recently been demonstrated [Ref. 108]. The experimental ten channel system, which again operated as a broadcast network using a 16×16 passive star coupler, is shown in Figure 12.29. The ten optical FDM transmitters, each incorporating wavelength tunable DBR lasers (see Section 6.6.2), are located on the left of Figure 12.29, together with a channel spacing controller. This latter device provided a channel space locking system based on a reference pulse technique in order to stabilize the channel spacings and therefore suppress the crosstalk penalties [Ref. 110]. The DBR lasers were FSK modulated using a 400 Mbit s^{-1} NRZ format for the TV signal.* The transmitted optical signals were then multiplexed through the star coupler.

At the receive terminals (block on the right of Figure 12.29) balanced polarization diversity receivers were employed with random access channel selection circuits.

* It was assumed that this signal would be high definition TV (HDTV) with its higher bandwidth requirement than conventional TV.

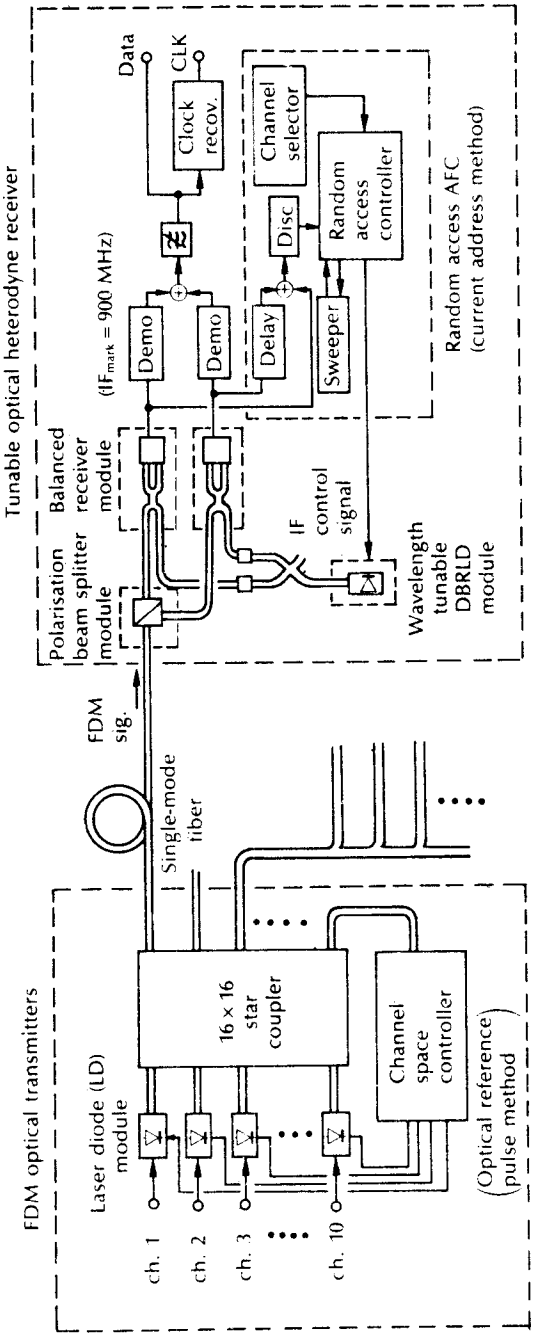

Figure 12.29 Experimental ten channel coherent optical frequency division multiplexed CATV system [Ref. 108].

Hence the receiver could select a particular channel through the control of the frequency of a local oscillator laser which again was a wavelength tunable DBR laser of the same design as the transmitter laser. A single filter detection scheme was used to demodulate the FSK signals which necessitated a large modulation index of between 3 and 4. Although a minimum theoretical channel spacing of 5 GHz was required, the developed system utilized an 8 GHz channel spacing. Receiver sensitivities of -45 dBm at 400 Mbit s^{-1} were obtained for all ten channels. Furthermore, the feasibility of the use of a travelling wave optical amplifier together with a wideband tunable local oscillator laser indicated the potential to distribute over eighty HDTV channels to some 16 000 subscriber terminals [Ref. 108].

Furthermore, coherent optical wavelength/frequency division switching systems are also under investigation for incorporation in future coherent optical networks [Ref. 111]. Such a switching system has been demonstrated for two channels which were wavelength synchronized using 8 GHz spaced optical FSK signals transmitted at a rate of 180 Mbit s^{-1}. The wavelength switch comprised coherent balanced optical receivers using FSK single filter detection connected to wavelength/frequency tunable DBR lasers which provided the wavelength converted output signals. Similar tunable devices were employed for the local oscillator lasers within the coherent receivers and the tuning ranges indicated that thirty-two wavelength channels could be obtained [Ref. 111].

Finally, both single wavelength and multiwavelength coherent carriers have been transmitted through optical amplifiers (see Sections 10.2 to 10.4). In the former case semiconductor laser amplifiers [Ref 112, 113] and erbium doped fiber amplifiers [Ref. 114] have been cascaded within experimental coherent optical fiber systems. However, fiber amplifier devices may prove more successful for use with coherent transmission systems as they have been shown to be polarization insensitive [Ref. 115].

Multicarrier coherent transmission through an erbium doped fiber amplifier has also been demonstrated in the field. For example, British Telecom have reported [Ref. 116] on the operation of a two channel coherent WDM system with 10 GHz channel spacing incorporating an erbium doped fiber amplifier repeater. This system was operated over a distance of 200 km between Edinburgh and Newcastle in the United Kingdom at a rate of 622 Mbit s^{-1} on each channel. Therefore the use of coherent multicarrier systems to provide for very long-haul transmission also appears likely in the future.

Problems

12.1 (a) Outline the rationale behind the pursuit of coherent optical systems. Indicate the major problems encountered in the realization of coherent optical transmission and briefly describe the ways in which they have been overcome.

(b) Discuss, with the aid of a suitable block diagram, a coherent optical fiber

communication system. Comment on the differing system requirements to facilitate heterodyne detection in comparison with homodyne detection.

12.2 The frequency stability requirement for a local oscillator laser in an ASK optical heterodyne detection system is 10 MHz. When the laser is emitting at a centre frequency of 1.55 μm and exhibits an output frequency change with temperature of 14 GHz $^{\circ}C^{-1}$, estimate:

(a) the fractional stability necessary for the device;
(b) the maximum temperature change that could be permitted for the device when there is no other form of laser frequency control;
(c) the maximum transmission bandwidth that would be allowed by the laser frequency stability.

12.3 (a) Obtain from first principles the theoretical SNR improvement in the shot noise limit for optical homodyne detection over heterodyne detection. Indicate the primary reason for this improvement.
(b) Briefly discuss the strategies which have been adopted to provide optical homodyne detection.

12.4 A homodyne OOK receiver has a bandwidth of 250 MHz and utilizes a photodiode with a responsivity of 0.6 AW^{-1} at the operating wavelength. The device is shot noise limited and a received SNR of 11 dB is required to provide an acceptable BER. Compute the receiver sensitivity and the photocurrent obtained when the local oscillator laser output power is -3 dBm and the phase difference between this signal and the incoming one is 12°.

12.5 The incoming signal power to an ASK optical heterodyne receiver operating at its shot noise limit is 1.28 nW for a received SNR of 9 dB. Determine the transmission wavelength of the ASK system if the quantum efficiency of the photodetector is 75% at this wavelength and the transmission bandwidth is 400 MHz.

12.6 Outline the major practical constraints associated with coherent optical transmission and discuss the techniques which have been adopted to overcome them.

12.7 To allow nonsynchronous ASK heterodyne detection the linewidths of the signal and local oscillator lasers should be less than 50% of the transmitted bit rate. Estimate the maximum permitted linewidths in nanometres for such ASK system sources:

(a) emitting at a wavelength around 1.30 μm when the transmission rate is 140 Mbit s^{-1};
(b) emitting at a wavelength around 1.55 μm when the transmission rate is 2.4 Gbit s^{-1}.

12.8 Compare and contrast the attributes and drawbacks associated with direct modulation of the laser signal source and indirect modulation of the source in both ASK and FSK coherent optical fiber communication systems.

12.9 (a) Describe what is understood by continuous phase shift keying (CPFSK) modulation within coherent optical transmission. Indicate the benefits of this modulation technique in comparison with FSK.
(b) Discuss the advantages and suggest a drawback associated with coherent optical differential phase shift keying (DPSK) in comparison with synchronous PSK heterodyne detection.

12.10 A coherent PSK optical fiber communication system employing synchronous heterodyne detection requires a minimum input optical power level of -58.2 dBm in

order to receive with a BER of 10^{-9}. The system is operated at a transmission rate of 600 Mbit s^{-1} and the quantum efficiency of the receiver photodetector is 80%. Assuming shot noise limited operation at the receiver, obtain the transmission wavelength for the system.

12.11 Outline the major techniques employed to achieve nonsynchronous optical ASK and FSK heterodyne detection. Indicate the benefits of these schemes over the corresponding synchronous demodulation schemes.

12.12 Describe what is meant by phase diversity reception for coherent optical fiber communication systems. Discuss with the aid of a suitable block diagram the salient features of the in-phase and quadrature receiver when used for optical ASK demodulation.

12.13 Verify that in order to obtain a BER of 10^{-9}:

(a) an average of eighteen photons per bit is required within an ideal ASK homodyne detection system;

(b) an average of forty photons per bit is necessary for ideal nonsynchronous FSK heterodyne detection.

12.14 Determine the minimum detectable peak optical power levels for both of the detection schemes in problem 12.13 when the transmission wavelength and bit rate are 1.31 μm and 100 Mbit s^{-1} respectively.

12.15 A coherent DPSK system operating at a wavelength of 1.54 μm uses a photodetector with a quantum efficiency of 83% at this wavelength. In shot noise limited performance a BER of 0.94×10^{-12} is obtained at the coherent optical receiver for a minimum detectable optical power level of 2.1 nW. Calculate both the average number of photons per bit required to maintain the BER and the transmission bit rate of the system under these circumstances.

12.16 An OOK coherent optical fiber system using nonsynchronous heterodyne detection has a transmission wavelength of 1.55 μm. Estimate the number of photons required for a one bit to provide a BER of 10^{-10} when there is shot noise limited detection and the responsitivity of the system photodetector at the operating wavelength is 0.7.

12.17 An FSK coherent optical fiber system employing synchronous heterodyne detection has a transmission wavelength of 1.3 μm where the fiber and splice/connector losses average out at 0.4 dB km^{-1}. If 2 mW of optical power is launched into the system link and an ideal photodetector is assumed, determine the absolute maximum repeater spacing to maintain a BER of 10^{-9} at transmission rates of: (a) 140 Mbit s^{-1}; (b) 2.4 Gbit s^{-1}.

12.18 A DPSK coherent optical fiber system operating at a transmission wavelength and bit rate of 1.55 μm and 250 Mbit s^{-1} respectively, has a repeater spacing of 300 km. Assuming a launch power of 0 dBm with shot noise limited detection and average overall transmission losses of 0.2 dB km^{-1} at the operation wavelength, compute the minimum quantum efficiency required for the photodetector to enable the system to function with a BER of 10^{-10}.

12.19 Indicate what is understood by FDM in relation to coherent optical transmission. Describe, with the aid of a suitable diagram, the possible implementation of a coherent multicarrier distribution system based on a passive star coupler.

Estimate the number of photons per bit obtained with an optical coherent FDM passive star network, which is operating from the shortest wavelength of 1.50 μm with an optical bandwidth of 100 nm, when the transmitter powers are 0 dBm. Comment on the result.

12.20 The two spectral transmission regions for coherent multicarrier systems may be considered to be 1.27 μm to 1.35 μm and 1.48 μm to 1.60 μm. Determine the number of FDM channels that could be accommodated in each region when coherent optical PSK transmission at 2 Gbit s^{-1} is to be utilized on each channel. A 25% guard band frequency for filter roll-off should be assumed.

Answers to numerical problems

12.2 (a) 1.93 in 10^7
(b) 7×10^{-4} °C
(c) 50 MHz
12.4 −60.8 dBm; 0.76 μA
12.5 1.32 μm
12.7 (a) 4×10^{-4} nm
(b) 1×10^{-2} nm
12.10 1.57 μm
12.14 (a) 273 pW
(b) 607 pW
12.15 27, 500 MHz
12.16 164
12.17 (a) 160.3 km
(b) 129.5 km
12.18 71.4%
12.19 603
12.20 5590; 6068

References

[1] J. C. Campbell, A. G. Dentai, W. S. Holden and B. L. Casper, 'High performance avalanche photodiode with separate absorption, grading and multiplication regions', *Electron. Lett.*, **19**, pp. 818–819, 1983.

[2] J. Saltz, 'Modulation and detection for coherent lightwave communications', *IEEE Commun. Mag.*, **24**(6), pp. 38–49, 1986.

[3] M. Schwatz, *Information Transmission, Modulation and Noise:* 4th edn, McGraw-Hill, 1990.

[4] T. Okoshi, 'Recent advances in coherent optical fiber communication systems, *J. of Lightwave Technol.*, **LT-5**(1), pp. 44–51, 1987.

[5] T. G. Hodgkinson, D. W. Smith, R. Wyatt and D. J. Malyon, 'Coherent optical fiber transmission systems', *Br. Telecom Technol. J.*, **3**(3), pp. 5–18, 1985.

[6] B. S. Glance, J. Stone, K. J. Pollock, P. J. Fitzgerald, C. A. Burrus Jr, B. L. Kasper and L. W. Stulz, 'Densely spaced FDM coherent star network with optical signals confined to equally spaced frequencies', *J. of Lightwave Technol.*, **6**(11), pp. 1170–1181, 1988.

[7] K. Nosu, H. Toba and K. Iwashita, 'Optical FDM transmission technique', *J. of Lightwave Technol.*, **LT-5**(9), pp. 1301–1308, 1987.

[8] M. C. Brain, 'Coherent optical networks', *Br. Telecom Technol. J.*, **7**(1), pp. 50–57, 1989.

[9] F. E. Goodwin, 'A 3.39 μm infrared optical heterodyne communication system', *IEEE J. Quantum Electron.*, **QE-3**(11), pp. 524–531, 1967.

[10] M. C. Teich, 'Homodyne detection of infrared radiation from a moving diffuse target', *Proc. IEEE*, **57**(5), pp. 789–792, 1969.

[11] O. E. DeLange, 'Wide-band optical communication systems: part II – frequency division multiplexing', *Proc. IRE*, **58**(10), pp. 1683–1690, 1970.

[12] S. Machida, A. Kawana, K. Ishihara and H. Tsuchiya, 'Interference of a AlGaAs

laser diode using 4.15 km single-mode fiber cable', *IEEE J. Quantum Electron.*, **QE-15**(7), pp. 535–537, 1979.

[13] T. Kimura and Y. Yamamoto, 'Progress of coherent optical fibre communication systems', *Opt. Quantum Electron.*, **15**, pp. 1–39, 1983.

[14] F. Favre, L. Jeunhomme, I. Joindot, M. Monerie and J. C. Simon, 'Progress towards heterodyne-type single-mode fibre communication systems', *IEEE J. Quantum Electron.*, **QE-17**(6), pp. 897–905, 1981.

[15] S. Saito, Y. Yamamoto and T. Kimura, 'Optical heterodyne detection of directly frequency modulated semiconductor laser signals', *Electron. Lett.*, **16**, pp. 826–827, 1980.

[16] D. W. Smith, R. A. Harmon and T. G. Hodgkinson, 'Polarisation stability requirements for coherent optical fibre transmission systems', *Br. Telecom Technol. J.*, **1**(2), pp. 12–16, 1983.

[17] I. W. Stanley, 'A tutorial review of techniques for coherent optical fibre transmission systems', *IEEE Commun. Mag.*, **23**(8), pp. 37–53, 1985.

[18] T. Kimura, 'Coherent optical fiber transmission', *J. of Lightwave Technol.*, **LT-5**(4), pp. 414–428, 1987.

[19] D. W. Smith, 'Coherent fiberoptic communications', *Laser Focus*, pp. 92–106, November 1985.

[20] T. Okoshi, 'Ultimate performance of heterodyne/coherent optical fiber communications', *J. of Lightwave Technol.*, **LT-4**(10), pp. 1556–1562, 1986.

[21] R. Lang, 'Injection locking properties of a semiconductor laser', *IEEE J. Quantum Electron.*, **QE-18**(6), pp. 976–983, 1982.

[22] R. Wyatt, D. W. Smith and K. H. Cameron, 'Megahertz linewidth from a 1.5 μm semiconductor laser with HeNe laser injection', *Electron. Lett.*, **18**, pp. 292–293, 1982.

[23] E. Basch and T. Brown, 'Introduction to coherent fiber-optic communication', in E. E. Basch (Ed.)., *Optical-Fiber Transmission*, H. W. Sams & Co., pp. 503–542, 1987.

[24] F. G. Walker and J. E. Kaufman, 'Characterization of GaAlAs laser diode frequency noise', *Sixth Top. Mtg. Opt. Fib. Commun.*, New Orleans, USA, paper TUJ5, February 1983.

[25] M. Osinski and J. Buus, 'Linewidth broadening factor in semiconductor lasers – an overview', *IEEE J. Quantum Electron.*, **QE-23**(1), pp. 9–29, 1987.

[26] J. Mellor, S. Al-Chalabi, K. H. Cameron, R. Wyatt, J. C. Regnault, V. W. Devlin and M. C. Brain, 'Performance characteristics of miniature external cavity semiconductor lasers', *Proc. CLEO'89*, Baltimore, USA, paper FP1, April 1989.

[27] T. Myogadani, S. Tanaka and Y. Suetsugu, Polarization fluctuation in single mode fiber cables', *IOOC–ECOC'85*, **1**, pp. 151–154, 1985.

[28] R. Ulrich, 'Polarization stabilization on single-mode fiber', *Appl. Phys. Lett.*, **35**(11), pp. 840–842, 1979.

[29] M. Kubota, T. Oohara, K. Furuya and Y. Suematsu, 'Electrooptical polarization control on single-mode fibres', *Electron. Lett.*, **16**(15), p. 573, 1980.

[30] H. C. Lefevre, 'Single-mode fiber fractional wave devices and polarization controllers', *Electron. Lett.*, **16**(20), pp. 778–780, 1980.

[31] T. Imai, K. Nosu and H. Yamaguchi, 'Optical polarization control utilising an optical heterodyne detection scheme', *Electron. Lett.*, **21**(2), pp. 52–53, 1985.

[32] T. Okoshi, N. Fukaya and K. Kikuchi, 'A new polarization-state control device: rotatable fibre cranks', *Electron. Lett.*, **21**(20), pp. 895–896, 1985.

[33] T. Okoshi, Y. Cheng and K. Kikuchi, 'A new polarization-control scheme for optical heterodyne receivers', *Electron. Lett.*, **21**(18), pp. 787–788, 1985.

[34] N. G. Walker and G. R. Walker, 'Polarization control for coherent optical fibre systems', *Br. Telecom Technol. J.*, **5**(2), pp. 63–76, 1987.

[35] M. J. Creaner, R. C. Steele, G. R. Walker and N. G. Walker, '565 Mbit/s optical PSK transmission system with endless polarization control', *Electron. Lett.*, **24**(5), pp. 270–271, 1988.

[36] N. G. Walker and G. R. Walker, 'Polarization control for coherent communications', *J. of Lightwave Technol.*, **8**(3), pp. 438–458, 1990.

[37] N. G. Walker, G. R. Walker and J. Davidson, 'Endless polarization control using an integrated optic lithium niobate device', *Electron. Lett.*, **24**(5), pp. 266–268, 1988.

[38] T. Okoshi, S. Ryu and K. Kikuchi, 'Polarization diversity receiver for heterodyne/coherent optical-fiber communications', *4th Internat. Conf. Integrated Opt. and Opt. Fiber Commun.*, Tokyo, Japan, paper 30C3-2, June 1983.

[39] T. E. Darcie, B. Glance, K. Gayliard, J. R. Talman, B. L. Kasper and C. A. Burrus, 'Polarization-insensitive operation of coherent FSK transmission system using polarisation diversity', *Electron Lett.*, **23**(25), pp. 1382–1384, 1987.

[40] T. G. Hodgkinson, R. A. Harmon and D. W. Smith, 'Performance comparison of ASK polarization diversity and standard coherent heterodyne receivers', *Electron. Lett.*, **24**(1), pp. 58–59, 1988.

[41] A. D. Kersey, M. J. Marrone and A. Dandridge, 'Adaptive polarisation diversity receiver configuration for coherent optical fibre communications', *Electron. Lett.*, **25**(4), pp. 275–277, 1989.

[42] I. Garrett and G. Jacobsen, 'Theoretical analysis of heterodyne optical receivers for transmission systems using (semiconductor) lasers with non-negligible linewidth', *J. of Lightwave Technol.*, **LT-4**(3), pp. 323–334, 1986.

[43] T. G. Hodgkinson, R. A. Harmon and D. W. Smith, 'Polarisation insensitive heterodyne detection using polarisation scrambling', *Electron. Lett.*, **23**(10), pp. 513–514, 1987.

[44] R. A. Linke and A. H. Gnauck, 'High capacity coherent lightwave systems', *J. of Lightwave Technol.*, **6**(11), pp. 1750–1769, 1988.

[45] D. W. Smith, 'Techniques for multigigabit coherent optical transmission', *J. of Lightwave Technol.*, **LT-5**(10), pp. 1466–1478, 1987.

[46] T. G. Hodgkinson, R. Wyatt and D. W. Smith, 'Experimental assessment of a 140 Mbit/s coherent optical receiver at 1.52 microns', *Electron. Lett.*, **18**, pp. 523–525, 1982.

[47] J. L. Gimlett, 'Low noise 8 GHz *p–i–n*/FET optical receiver', *Electron. Lett.*, **23**, pp. 281–283, 1987.

[48] S. B. Alexander, 'Design of wide-band optical heterodyne balanced mixer receivers', *J. of Lightwave Technol.*, **LT-5**(4), pp. 523–537, 1987.

[49] H. P. Yuen and V. W. S. Chan, 'Noise in homodyne and heterodyne detection', *Opt. Lett.*, **8**(3), pp. 177–179, 1983.

[50] G. L. Abbas, V. W. Chan and T. K. Yee, 'Dual detector optical heterodyne receiver for local oscillator noise suppression', *J. of Lightwave Technol.*, **LT-3**(5), pp. 1110–1122, 1985.

[51] B. L. Kasper, C. A. Burrus, J. R. Talman and K. L. Hall, 'Balanced dual detector receiver for optical heterodyne communication at Gbit/s rates', *Electron. Lett.*, **22**, pp. 413–414, 1986.

[52] A. H. Gnauck, R. A. Linke, B. L. Kasper, K. J. Pollock, K. C. Reichmann, R. Valenzula and R. C. Alferness, 'Coherent lightwave transmission at 2 Gbit/s over 170 km of optical fibre using phase modulation', *Electron. Lett.*, **23**, pp. 286–287, 1987.

[53] A. F. Elrefaie, R. E. Wagner, D. A. Atlas and D. G. Daut, 'Chromatic dispersion limitations in coherent lightwave transmission systems', *J. of Lightwave Technol.*, **6**(5), pp. 704–709, 1988.

[54] K. Iwashita and N. Takachio, 'Chromatic dispersion compensation in coherent optical communications', *J. of Lightwave Technol.*, **8**(3), pp. 367–375, 1990.

[55] A. R. Chraplyvy, 'Limitations on lightwave communications imposed by optical fiber nonlinearities', *Opt. Fiber Commun. Conf. (OFC'88)*, New Orleans, USA, paper TUD3, January 1988.

[56] I. Garrett and G. Jacobson, 'The effect of laser linewidth on coherent optical receivers', *J. of Lightwave Technol.*, **LT-5**(4), pp. 551–560, 1987.

[57] K. Emura, S. Yamazaki, S. Fujita, M. Shikada, I. Mito and K. Minemura, 'Over 300 km transmission experiment on an optical FSK heterodyne dual filter detection system', *Electron. Lett.*, **22**(21), pp. 1096–1097, 1986.

[58] K. Emura, S. Yamazaki, M. Shikada, S. Fujita, M. Yamaguchi, I. Mito and K. Minemura, 'System design and long-span transmission experiments on an optical FSK heterodyne single filter detection system', *J. of Lightwave Technol.*, **LT-5**(4), pp. 469–477, 1987.

[59] R. S. Vodhanel, '1 Gbit/s bipolar optical FSK transmission experiment over 121 km of fibre', *Electron. Lett.*, **24**(3), pp. 163–164, 1988.

[60] R. C. Steele and M. Creaner, '565 Mbit/s AMI FSK coherent system using commercial DFB lasers', *Electron. Lett.*, **25**(11), pp. 732–734, 1989.

[61] K. Iwashita and N. Takachio, '2 Gbit/s optical CPFSK heterodyne transmission through 200 km single-mode fibre', *Electron. Lett.*, **23**(7), pp. 341–342, 1987.

[62] L. G. Kazovsky and G. Jacobsen, 'Multichannel CPFSK coherent optical communications system', *J. of Lightwave Technol.*, **7**(6), pp. 972–982, 1989.

[63] L. L. Jeromin and V. W. S. Chan, 'M'ary FSK performance for coherent optical communication systems using semiconductor lasers', *IEEE Trans. Commun.*, **COM-34**(4), pp. 375–381, 1986.

[64] S. Kobayashi and T. Kimura, 'Optical phase modulation in an injection locked AlGaAs semiconductor laser', *IEEE J. Quantum Electron.*, **QE-18**(10), pp. 1662–1669, 1982.

[65] B. Glance, 'Performance of homodyne detection of binary PSK optical signals', *J. of Lightwave Technol.*, **LT-4**(2), pp. 228–235, 1986.

[66] S. Yamazaki, S Murata, K. Komatsu, Y. Koizumi, S. Fujita and K. Emura, '1.2 Gbit/s optical DPSK heterodyne detection transmission system using monolithic external-cavity DFB LDs', *Electron. Lett.*, **23**(16), pp. 860–862, 1987.

[67] T. Chikama, T. Naitou, H. Onaka, T. Kiyonaga, S. Watanabe, M. Suyama, M. Seino and H. Kuwahara, '1.2 Gbit/s, 201 km optical DPSK heterodyne transmission experiment using a compact, stable external fibre DFB laser module', *Electron. Lett.*, **24**(10), pp. 636–637, 1988.

[68] K. Nosu and K. Iwashita, 'A consideration of factors affecting future coherent

lightwave communication systems', *J. of Lightwave Technol.*, **6**(5), pp. 686–694, 1988.

[69] E. Dietrich, B. Enning, R. Gross and H. Knupke, 'Heterodyne transmission of a 560 Mbit/s optical signal by means of polarization shift keying', *Electron. Lett.*, **23**(8), pp. 421–422, 1987.

[70] R. Calvani, R. Caponi and R. Cisternino, 'Polarization phase-shift keying: a coherent transmission technique with differential heterodyne detection', *Electron. Lett.*, **24**(10), pp. 642–643, 1988.

[71] Y. Imai, K. Iizuka and R. T. B. James, 'Phase-noise-free coherent optical communication system utilizing differential polarization shift keying (DPolSK), *J. of Lightwave Technol.*, **8**(5), pp. 691–698, 1990.

[72] S. Betti, F. Curti, G. De Marchis and E. Iannone, 'Multilevel coherent optical system based on Stokes parameters modulation', *IEEE J. of Lightwave Technol.*, **8**(7), pp. 1127–1136, 1990.

[73] P. Benedelta and P. Poggliolini, 'Performance evaluation of multilevel polarization shift keying modulation schemes, *Electron. Lett.*, **26**(4), pp. 244–246, 1990.

[74] S. Saito, Y. Yamamoto and T. Kimura, 'S/N and error rate evaluation for an optical FSK–heterodyne detection system using semiconductor lasers', *IEEE J. Quantum Electron.*, **QE-19**(2), pp. 180–193, 1983.

[75] Y. Yamamoto, 'AM and FM quantum noise in semiconductor lasers – Part I and II', *IEEE J Quantum Electron.*, **QE-19**(1), pp. 34–58, 1983.

[76] T. G. Hodgkinson, 'Costas loop analysis for coherent optical receivers'. *Electron. Lett.*, **22**(7), pp. 394–396, 1986.

[77] S. Watanabe, T. Chikama, T. Naito and H. Kuwahara, '560 Mb/s optical PSK heterodyne detection using carrier recovery', *Electron. Lett.*, **25**, pp. 588–590, 1989.

[78] T. Chirkawa, S. Watanabe, T. Naito, H. Onaka, T. Kiyonaga, Y. Onoda, H. Miyata, M. Suyama, M. Seino and H. Kuwahara, 'Modulation and demodulation techniques in optical heterodyne PSK transmission systems', *J. of Lightwave Technol.*, **8**(3), pp. 309–322, 1990.

[79] J. M. P. Delavaux, L. D. Tzeng, M. Dixon and R. E. Tench, '1.4 Gbit/s optical DPSK heterodyne transmission system experiment', *Fourteenth European Conf. on Opt. Commun., (ECOC'88)*, UK, pp. 475–477, September 1988.

[80] D. J. Malyon, D. W. Smith and R. Wyatt, 'Semiconductor laser homodyne optical phase lock loop', *Electron. Lett.*, **22**, pp. 421–422, 1986.

[81] H. K. Phillip, A. L. Scholtz, E. Bonek and W. Leeb, 'Costas loop experiments for a 10.6 μm communications receiver'. *IEEE Trans. Commun.*, **COM-31**(8), pp 1000–1002, 1983.

[82] L. Kazovsky, L. Curtis, W. Young and N. Cheung, 'All fiber 90° optical hybrid for coherent communications', *Appl. Opt.*, **26**(3), pp. 437–439, 1987.

[83] J. A. Arnaud, 'Enhancement of optical receiver sensitivities by amplification of the carrier', *IEEE J. Quantum Electron.*, **QE-4**, pp. 893–899, 1968.

[84] C. G. Atkins, D. Cotter, D. W. Smith and R. Wyatt, 'Application of Brillouin amplification in coherent optical transmission', *Electron. Lett.*, **22**, pp. 556–558, 1986.

[85] N. G. Walker and J. E. Carroll, 'Simultaneous phase and amplitude measurements on optical signals using a multiport junction', *Electron. Lett.*, **20**, pp. 981–983, 1984.

[86] A. Davis, M. Pettitt, J. King and S. Wright, 'Phase diversity techniques for coherent optical receivers', *J. of Lightwave Technol.*, **LT-5**(4), pp. 561–572, 1987.

[87] L. Kazovsky, P. Meissner and E. Patzak, 'ASK multiport optical homodyne receiver', *J. of Lightwave Technol.*, **LT-5**(6), pp. 770–791, 1987.

[88] K. Emura, R. S. Vodhanel, R. Welter and W. B. Sessa, '5 Gbit/s optical phase diversity homodyne detection experiment', *Electron. Lett.*, **25**(6), pp. 400–401, 1989.

[89] R. Welter and L. G. Kazovsky, '150 Mbit s^{-1} phase diversity ASK homodyne receiver with a DFB laser', *Optical Fiber Commun. Conf. (OFC'88)*, New Orleans, USA, paper TU1, January 1988.

[90] T. G. Hodgkinson, R. A. Harmon and D. W. Smith, 'Demodulation of optical DPSK using in-phase and quadrature detection', *Electron. Lett.*, **21**, pp. 867–868, 1985.

[91] A. W. Davis, S. Wright, M. J. Pettitt, J. P. King and K. Richards, 'Coherent optical receiver for 680 Mbit/s using phase diversity', *Electron. Lett.*, **22**, pp. 9–11, 1986.

[92] M. J. Pettitt, D. Remodios, A. W. Davies, A. Hadjifotiou and S. Wright, 'A coherent transmission system using DFB lasers and phase diversity', *Proc. IEE Colloq.* (UK), pp. 9/1–9/5, 1987.

[93] E. Gottwald and J. Pietzsch, 'Measurement method for determination of optical phase shifts in 3×3 fibre couplers', *Electron. Lett.*, **24**, pp. 265–266, 1988.

[94] J. Siuzdak and W. van Etten, 'BER evaluation for phase and polarization diversity optical homodyne receivers using non-coherent ASK and DPSK demodulation', *J. of Lightwave Technol.*, **7**(4), pp. 584–599, 1989.

[95] T. Okoshi, K. Emura, K. Kikuchi and R. Th. Kersten, 'Computation of bit-error rate of various heterodyne and coherent-type optical communication schemes', *J. of Optical Commun.*, **2**(3), pp. 89–96, 1981.

[96] T. Okoshi and K. Kikuchi, *Coherent Optical Fiber Communications*, KTK Scientific Publishers (Tokyo)/Kluwer Academic Publishers (Dordrecht), 1988.

[97] L. G. Kazovsky, 'Optical heterodyning versus optical homodyning: A comparison', *J. of Optical Commun.*, **6**(1), pp. 18–24, 1985.

[98] E. Basch and T. Brown, 'Introduction to coherent optical fiber transmission', *IEEE Commun. Mag.*, **23**(5), pp. 23–30, 1985.

[99] P. S. Henry, R. A. Linke and A. H. Gnauck, 'Introduction to lightwave systems', in S. E. Miller and I. P. Kaminow (Eds.) *Optical Fiber Telecommunications II*, Academic Press, pp. 781–831, 1988.

[100] S. Yamazaki, T. Fujta and K. Emura, 'Feasibility study on optical QPSK heterodyne systems', *Opt. Fiber Commun. Conf. (OFC'88)*, New Orleans, USA, paper WC3, January 1988.

[101] R. A. Linke, 'Optical heterodyne communication systems' *IEEE Commun. Mag.*, pp. 36–41, October 1989.

[102] M. J. Creaner, R. C. Steele, I. Marshall, G. R. Walker, N. G. Walker, J. Mellis, S. Al-Chalabi, I. Sturgess, M. Rutherford, J. Davidson and M. Brain, 'Field demonstration of 565 Mbit/s DPSK coherent transmission system over 176 km of installed fiber', *Electron. Lett.*, **24**(22), pp. 1354–1356, 1988.

[103] J. Mellis, S. Al-Chalabi and L. N. Barker, 'Characteristics of fiber coupled optical isolator at 1.5μm', *Electron. Lett.*, **24**(22), pp. 1353–1354, 1988.

[104] M. C. Brain, M. J. Creaner, R. C. Steele, N. G. Walker, G. R. Walker, J. Mellis, S. Al-Chalabi, J. Davidson, M. Rutherford and I. C. Sturgess, 'Progress towards the field deployment of coherent optical fiber systems', *J. of Lightwave Technol.*, **8**(3), pp. 423–437, 1990.

[105] E. J. Bachus, R. P. Braun, C. Casper, H. M. Foisel, E. Grobmann, B. Strebel and F. J. Westphal, 'Coherent optical multicarrier systems', *J. of Lightwave Technol.*, **7**(2), pp. 375–384, 1989.

[106] R. A. Linke, 'Frequency division multiplexed optical networks using heterodyne detection', *IEEE Network*, pp. 13–20, March 1989.

[107] B. Glance, T. L. Koch, O. Scaramucci, K. C. Reichmann, U. Koren and C. A. Burrus, 'Densely spaced FDM coherent optical star network using monolithic widely frequency-tunable lasers', *Electron. Lett.*, **25**(10), pp. 672–673, 1989.

[108] S. Yamazaki, M. Shibutani, N. Shimoska, S. Murata, T. Ono, M. Kitamura, K. Emura and M. Shikada, 'A coherent optical FDM CATV distribution system', *J. of Lightwave Technol.*, **8**(3), pp. 396–405, 1990.

[109] P. Cochrane, 'Future directions in long haul fibre optic systems', *Br. Telecom Technol. J.*, **8**(2), pp. 5–17, 1990.

[110] N. Shimosaka, K. Kaede and S. Murata, 'Frequency locking of FDM optical sources using widely tunable DBR LDs', *Opt. Fiber Commun. Conf. (OFC'88)*, New Orleans, USA, paper THG3, January 1988.

[111] M. Fujiwara, N. Shimosaka, M. Nishio, S. Suzuki, S. Yamazaki, S. Murata and K. Kaede, 'A coherent photonic wavelength-division switching system for broad-band networks', *J. of Lightwave Technol.*, **8**(3), pp. 416–422, 1990.

[112] N. A. Olsson, M. G. Oberg, L. A. Koszi and G. Przybylek, '400 Mbit/s, 372 km coherent transmission experiment using in-line optical amplifier', *Electron. Lett.*, **24**(1), pp. 36–38, 1988.

[113] D. J. Maylon, R. C. Steele, M. J. Creaner, M. C. Brain and W. A. Stallard, 'Coherent optical transmission at 565 Mbit/s, through five cascaded photonic amplifiers', *Electron. Lett.*, **25**(5), pp. 354–356, 1989.

[114] M. J. Creaner, T. J. Whitley, R. C. Steele, R. A. Garnham, C. A. Millar and M. C. Brain, 'Diode-pumped erbium-doped fibre amplifier repeater in a 565 Mbit/s DPSK coherent optical transmission system', *Proc. European Conf. in Opt. Commun., ECOC*, Gothenburg (Sweden), pp. 82–85, September 1989.

[115] N. H. Taylor and A. Hadjifotiou, 'Optical amplification and its applications,' *Proc. SPIE., Int. Soc. Opt. Eng. (USA)*, **1314**, 'Fibre Optics' 90, pp. 64–67, 1990.

[116] M. J. Creaner, D. Spirit, G. R. Walker, N. G. Walker, J. Mellis, S. A. Chalabi, W. Hale, I. Sturgess, M. Rutherford, D. Trivett, M. C. Brain and R. C. Steele, 'Field demonstration of two channel coherent transmission with a diode-pumped fibre amplifier repeater,' *IEEE Opt. Fib. Commun. Conf., OFC'90*, San Francisco, USA, postdealine paper, January 1990.

13

Optical fiber measurements

13.1 Introduction

In this chapter we are primarily concerned with measurements on optical fibers which characterize the fiber. These may be split into three main areas:

(a) transmission characteristics;
(b) geometrical and optical characteristics;
(c) mechanical characteristics.

Data in these three areas are usually provided by the optical fiber manufacturer with regard to specific fibers. Hence fiber measurements are generally performed in the laboratory and techniques have been developed accordingly. This information is essential for the optical communication system designer in order that suitable choices of fibers, materials and devices may be made with regard to the system application. However, although the system designer and system user do not usually need to take fundamental measurements of the fiber characteristics there is a requirement for field measurements in order to evaluate overall system performance, and for functions such as fault location. Therefore, we also include some discussion of field measurements which take into account the effects of cabled fiber, splice and connector losses, etc.

Several organizations have become involved in standardization issues relating to optical fiber measurements. The International Telephone and Telegraph Consultative Committee, the CCITT (the acronym for its name in French) has made a few recommendations, particularly regarding single-mode fiber measurements [Ref. 1], and in the the United States the Electronics Industries Association (EIA) has published over 200 Fiber Optic Test Procedures (FOTPs). Hence there now exists a body of standardized measurement techniques. Such test methods are divided into reference test metnods (RTMs) and alternative test methods (ATMs). An RTM provides a measurement of a particular characteristic, strictly according to the definition which usually gives the highest degree of accuracy and reproducibility, whereas an ATM may be more suitable for practical use but can deviate from the strict definition; however, there must be a way to relate such results to those obtained from the reference test method.

The fiber transmission characteristics of greatest interest are those of attenuation and dispersion. For multimode fibers the latter parameter enables the bandwidth to be determined, whereas with single-mode fibers it is the intramodal or chromatic dispersion which is generally provided by manufacturers. Furthermore, the important geometrical and optical characteristics for multimode fibers are size (core and cladding diameters), numerical aperture (see Section 2.2.3) and refractive index profile, but for single-mode fibers they are the effective cutoff wavelength of the second order mode (see Section 2.5.1) and the mode-field diameter (see Section 2.5.2). Measurements of the mechanical characteristics such as tensile strength and durability were outlined in Section 4.7.1 and are therefore pursued no further in this chapter.

When attention is focused on the measurement of the transmission properties of multimode fibers, problems emerge regarding the large number of modes propagating in the fiber. The various modes show individual differences with regard to attenuation and dispersion within the fiber. Moreover, mode coupling occurs giving transfer of energy from one mode to another (see Section 2.4.2). The mode coupling which is associated with perturbations in the fiber composition or geometry, and external factors such as microbends or splices, is for instance responsible for the increased attenuation (due to radiation) of the higher order modes. These multimode propagation effects mean that both the fiber loss and

bandwidth are not uniquely defined parameters but depend upon the fiber excitation conditions and environmental factors such as cabling, bending, etc. Also, these transmission parameters may vary along the fiber length (i.e. they are not necessarily linear functions) due to the multimode propagation effects, making extrapolation of measured data to different fiber lengths less than meaningful.

It is therefore important that transmission measurements on multimode fibers are performed in order to minimize these uncertainties. In the laboratory, measurements are usually taken on continuous lengths of uncabled fiber in order to reduce the influence of external factors on the readings (this applies to both multimode and single-mode fibers). However, this does mean that the system designer must be aware of the possible deterioration in the fiber transmission characteristics within the installed system. The multimode propagation effects associated with fiber perturbations may be accounted for by allowing or encouraging the mode distribution to reach a steady state (equilibrium) distribution. This distribution occurs automatically after propagation has taken place over a certain fiber length (coupling length) depending upon the strength of the mode coupling within the particular fiber. At equilibrium the mode distribution propagates unchanged and hence the fiber attenuation and dispersion assume well defined values. These values of the transmission characteristics are considered especially appropriate for the interpretation of measurements to long-haul links and do not depend on particular launch conditions.

The equilibrium mode distribution may be achieved by launching the optical signal through a long (dummy) fiber to the fiber under test. This technique has been used to good effect [Ref. 2] but may require a kilometre of dummy fiber and is therefore not suitable for dispersion measurements. Alternatively there are a number of methods of simulating the equilibrium mode distribution with a much shorter length of fiber. Mode equilibrium may be achieved using an optical source with a mode output which corresponds to the steady state mode distribution of the fiber under test. This technique may be realized experimentally using an optical arrangement which allows the numerical aperture of the launched beam to be varied (using diaphragms) as well as the spot size of the source (using pinholes). In this case the input light beam is given an angular width which is equal to the equilibrium distribution numerical aperture of the fiber and the source spot size on the fiber input face is matched to the optical power distribution in a cross section of the fiber at equilibrium.

Other techniques involve the application of strong mechanical perturbations on a short section of the fiber in order quickly to induce mode coupling and hence equilibrium mode distribution within 1 m. These devices which simulate mode equilibrium over a short length of fiber are known as mode scramblers or mode filters.

A mode scrambler increases the power in the higher order modes relative to the lower order ones, whereas a mode filter typically reduces the power in the higher order modes without seriously affecting the power in the lower order modes. Mode filters are usually required with LED sources because more higher order mode

excitation than the equilibrium mode distribution is obtained in most multimode fibers. By contrast, a mode scrambler may be necessary for lens-less excitation with laser sources, as this technique produces more lower order modes than are contained in the equilibrium mode distribution in most multimode fibers. Hence both strategies are employed to achieve equilibrium mode power distributions in multimode fibers.

A simple mode scrambling method [Ref. 3] is to sandwich the fiber between two sheets of abrasive paper (i.e. sandpaper) placed on wooden blocks in order to provide a suitable pressure. Two slightly more sophisticated techniques are illustrated in Figure 13.1 [Refs. 4 and 5]. Figure 13.1(a) shows mechanical perturbations induced by enclosing the fiber with metal wires and applying pressure by use of a surrounding heat shrinkable tube. A method which allows adjustment and therefore an improved probability of repeatable results is shown in Figure 13.1(b). This technique involves inserting the fiber between a row of equally spaced pins, subjecting it to sinusoidal bends. Hence the variables are the number of pins giving the number of periods, the pin diameter d and the pin spacing s.

A common mode filtering technique uses a mandrel wrap applied before the test fiber as illustrated in Figure 13.2(a). In this method four or five turns of fiber are wrapped around a 20 to 30 mm diameter mandrel in order to simulate the equilibrium mode power distribution [Ref. 6]. The other popular mode filtering technique which was mentioned earlier is shown in Figure 13.2(b). This method employs a dummy fiber of length 0.5 to 1 km which is of a similar type to the test fiber. The dummy fiber is spliced before the test fiber such that an equilibrium mode distribution is established after the optical launch.

In order to test that a particular mode scrambler or filter gives an equilibrium mode distribution within the test fiber, it is necessary to check the insensitivity of the far field radiation pattern (this is related to the mode distribution, see Section 2.4.1) from the fiber with regard to changes in the launch conditions. It is also useful to compare the far field patterns from the device and a separate long length

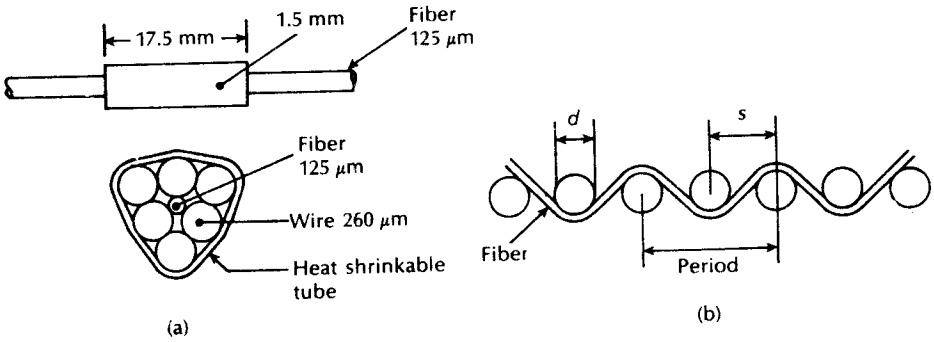

Figure 13.1 Mode scramblers: (a) heat shrinking technique [Ref. 4]; (b) bending technique [Ref. 5].

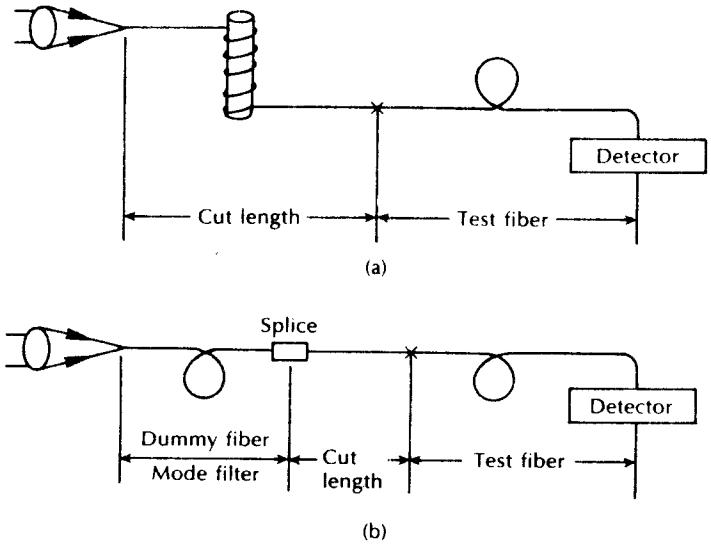

Figure 13.2 Equilibrium mode simulation by mode filtering: (a) mandrel wrap; (b) dummy fiber.

at the test fiber for coincidence [Ref. 2]. However, it must be noted that, at present, mode scramblers or filters tend to give only an approximate equilibrium mode distribution and their effects vary with different fiber types. Hence measurements involving the use of different mode scrambling methods can be subject to discrepancies. Nevertheless, the majority of laboratory measurement techniques to ascertain the transmission characteristics of multimode optical fibers use some form of equilibrium mode simulation in order to give values representative of long transmission lines. Moreover, the current standards agreements regarding equilibrium mode simulation are outlined in FOTP-50 [Ref. 7].

We commence the discussion of optical fiber measurements in Section 13.2 by dealing with the major techniques employed in the measurement of fiber attenuation. These techniques include measurement of both total fiber attenuation and the attenuation resulting from individual mechanisms within the fiber (e.g. material absorption, scattering). In Section 13.3 fiber dispersion measurements in both the time and frequency domains are discussed. Various techniques for the measurement of the fiber refractive index profile are then considered in Section 13.4. The measurement of the fiber cutoff wavelength which has particular relevance to single-mode fibers is then dealt with in Section 13.5. In Section 13.6 we discuss simple methods for measuring fiber numerical aperture. Measurement of the fiber outer and core diameters are then described in Section 13.7.

A far more important parameter than the fiber numerical aperture and core diameter for single-mode fibers is the mode-field diameter. Hence the measurement

of this single-mode fiber characteristic is discussed in Section 13.8. This is followed in Section 13.9 with a description of a measurement procedure for reflectance and optical return loss for either a fiber component or an optical link. Finally, field measurements which may be performed on optical fiber links, together with examples of measurement instruments, are discussed in Section 13.10. Particular attention is paid in this concluding section to optical time domain reflectometry (OTDR).

13.2 Fiber attenuation measurements

Fiber attenuation measurement techniques have been developed in order to determine the total fiber attenuation of the relative contributions to this total from both absorption losses and scattering losses. The overall fiber attenuation is of greatest interest to the system designer, but the relative magnitude of the different loss mechanisms is important in the development and fabrication of low loss fibers. Measurement techniques to obtain the total fiber attenuation give either the spectral loss characteristic (see Figure 3.3) or the loss at a single wavelength (spot measurement).

13.2.1 Total fiber attenuation

A commonly used technique for determining the total fiber attenuation per unit length is the cut-back or differential method. Figure 13.3 shows a schematic diagram of the typical experimental set-up for measurement of the spectral loss to obtain the overall attenuation spectrum for the fiber. It consists of a 'white' light source, usually a tungsten halogen or xenon arc lamp. The focused light is mechanically chopped at a low frequency of a few hundred hertz. This enables the lock-in amplifier at the receiver to perform phase-sensitive detection. The chopped light is then fed through a monochromator which utilizes a prism or diffraction grating arrangement to select the required wavelength at which the attenuation is to be measured. Hence the light is filtered before being focused on to the fiber by means of a microscope objective lens. A beam splitter may be incorporated before the fiber to provide light for viewing optics and a reference signal used to compensate for output power fluctuations. As indicated in Section 5.1, when the measurement is performed on multimode fibers it is very dependent on the optical launch conditions. Therefore unless the launch optics are arranged to give the steady state mode distribution at the fiber input, or a dummy fiber is used, then a mode scrambling device is attached to the fiber within the first metre. The fiber is also usually put through a cladding mode stripper, which may consist of an S-shaped groove cut in the Teflon and filled with glycerine. This device removes light launched into the fiber cladding through radiation into the index matched (or slightly higher refractive index) glycerine. A mode stripper can also be included at the fiber output end to remove any optical power which is scattered from the core

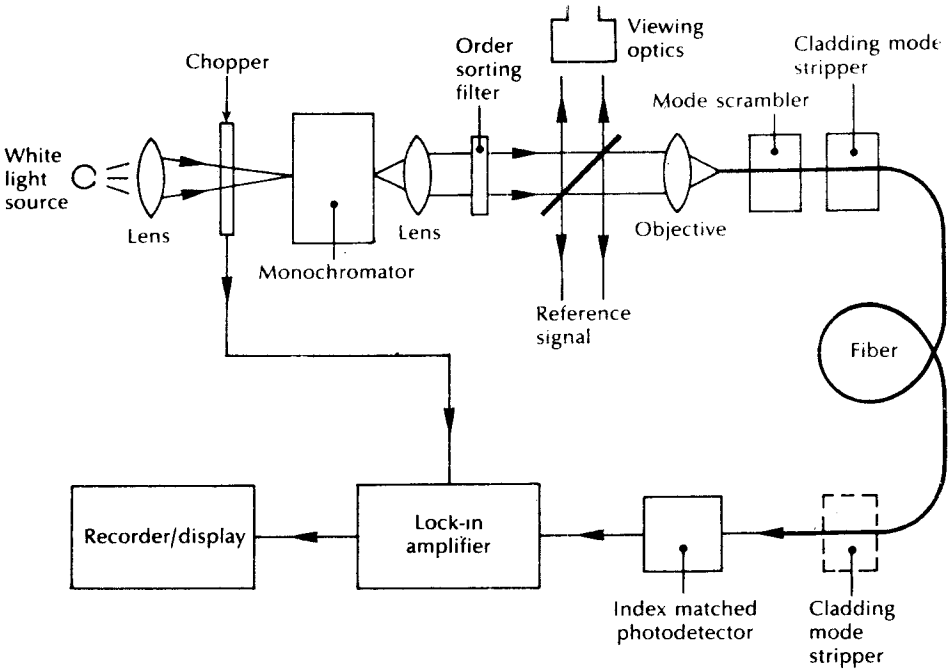

Figure 13.3 A typical experimental arrangement for the measurement of spectral loss in optical fibers using the cut-back technique.

into the cladding down the fiber length. This tends to be pronounced when the fiber cladding consists of a low refractive index silicone resin.

The optical power at the receiving end of the fiber is detected using a *p–i–n* or avalanche photodiode. In order to obtain reproducible results the photodetector surface is usually index matched to the fiber output end face using epoxy resin or an index matching cell [Ref. 8]. Finally, the electrical output from the photodetector is fed to a lock-in amplifier, the output of which is recorded.

The cut-back method* involves taking a set of optical output power measurements over the required spectrum using a long length of fiber (usually at least a kilometre). This fiber is generally uncabled having only a primary protective coating. Increased losses due to cabling (see Section 4.8.1) do not tend to change the shape of the attenuation spectrum as they are entirely radiative, and for multimode fibers are almost wavelength independent. The fiber is then cut back to a point two metres from the input end and, maintaining the same launch

* The cut-back method is outlined in FOTP-46 and FOTP-78 for multimode and single-mode fibers respectively [Refs. 9, 10]. In addition, it is the CCITT reference test method for fiber attenuation [Ref. 1].

conditions, another set of power output measurements are taken. The following relationship for the optical attenuation per unit length α_{dB} for the fiber may be obtained from Eq. (3.3):

$$\alpha_{dB} = \frac{10}{L_1 - L_2} \log_{10} \frac{P_{02}}{P_{01}} \tag{13.1}$$

L_1 and L_2 are the original and cut-back fiber lengths respectively, and P_{01} and P_{02} are the corresponding output optical powers at a specific wavelength from the original and cut-back fiber lengths. Hence when L_1 and L_2 are measured in kilometres, α_{dB} has units of dB km^{-1}

Furthermore Eq. (13.1) may be written in the form:

$$\alpha_{dB} = \frac{10}{L_1 - L_2} \log_{10} \frac{V_2}{V_1} \tag{13.2}$$

where V_1 and V_2 correspond to output voltage readings from the original fiber length and the cut-back fiber length respectively. The electrical voltages V_1 and V_2 may be directly substituted for the optical powers P_{01} and P_{02} of Eq. (13.1) as they are directly proportional to these optical powers (see Section 7.4.3). The accuracy of the results obtained for α_{dB} using this method is largely dependent on constant optical launch conditions and the achievement of the equilibrium mode distribution within the fiber. In this case only the fiber to detector power coupling changes between measurements and this variation can be made less than 0.01 dB [Ref. 6]. Hence the cut-back technique is regarded as the reference test method (RTM) for attenuation measurements by the EIA as well as the CCITT.

Example 13.1

A 2 km length of multimode fiber is attached to apparatus for spectral loss measurement. The measured output voltage from the photoreceiver using the full 2 km fiber length is 2.1 V at a wavelength of 0.85 μm. When the fiber is then cut back to leave a 2 m length the output voltage increases to 10.7 V. Determine the attenuation per kilometre for the fiber at a wavelength of 0.85 μm and estimate the accuracy of the result.

Solution: The attenuation per kilometre may be obtained from Eq. (13.2) where:

$$\alpha_{dB} = \frac{10}{L_1 - L_2} \log_{10} \frac{V_2}{V_1} = \frac{10}{1.998} \log_{10} \frac{10.7}{2.1}$$

$$= 3.5 \text{ dB km}^{-1}$$

The dynamic range of the measurements that may be taken depends upon the exact configuration of the apparatus utilized, the optical wavelength and the fiber core

diameter. However, a typical dynamic range is in the region 30 to 40 dB when using a white light source at a wavelength of 0.85 μm and multimode fiber with a core diameter around 50 μm. This may be increased to around 60 dB by use of a laser source operating at the same wavelength. It must be noted that a laser source is only suitable for making a single wavelength (spot) measurement as it does not emit across a broad band of spectral wavelengths.

Spot measurements may be performed on an experimental set-up similar to that shown in Figure 13.3. However, interference filters are frequently used instead of the monochromator in order to obtain a measurement at a particular optical wavelength. These provide greater dynamic range (10 to 15 dB improvement) than the monochromator but are of limited use for spectral measurements due to the reduced number of wavelengths that are generally available for measurement. A typical optical configuration for spot attenuation measurements is shown in Figure 13.4. The interference filters are located on a wheel to allow measurement at a selection of different wavelengths. In the experimental arrangement shown in Figure 13.4 the source spot size is defined by a pinhole and the beam angular width is varied by using different diaphragms. However, the electronic equipment utilized with this set-up is similar to that used for the spectral loss measurements illustrated

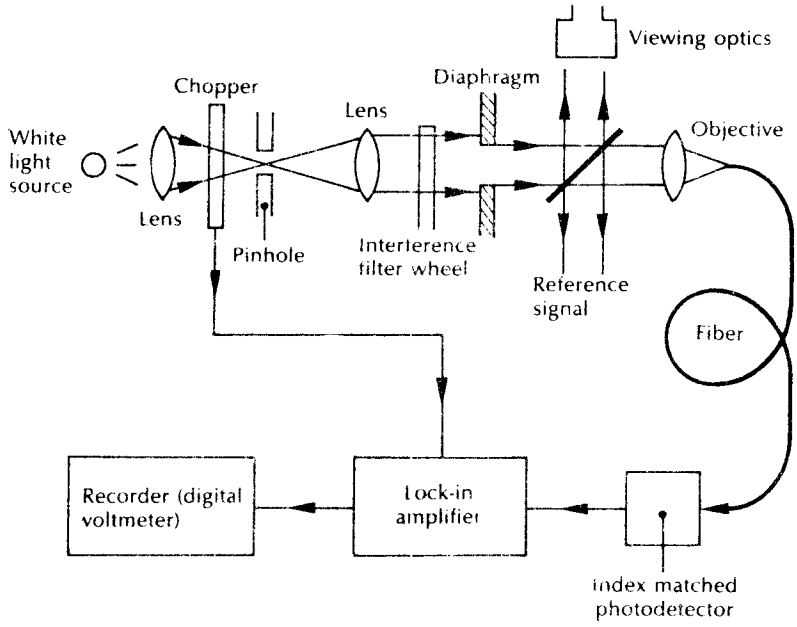

Figure 13.4 An experimental arrangement for making spot (single wavelength) attenuation measurements using interference filters and employing the cut-back technique.

in Figure 13.3. Therefore determination of the optical loss per unit length for the fiber at a particular wavelength is performed in exactly the same manner, using the cut-back method. Spot attenuation measurements are sometimes utilized after fiber cabling in order to obtain information on any degradation in the fiber attenuation resulting from the cabling process.

Although widely used, the cut-back measurement method has the major drawback of being a destructive technique. Therefore, although suitable for laboratory measurement it is far from ideal for attenuation measurements in the field. Several nondestructive techniques exist which allow the fiber losses to be calculated through a single reading of the optical output power at the far end of the fiber after determination of the near end power level. The simplest is the insertion or substitution* technique which utilizes the same experimental configuration as the cut-back method. However, the fiber to be tested is spliced, or connected by means of a demountable connector to a fiber with a known optical output at the wavelength of interest. When all the optical power is completely coupled between the two fibers, or when the insertion loss of the splice or connector is known, then the measurement of the optical output power from the second fiber gives the loss resulting from the insertion of this second fiber into the system. Hence the insertion loss due to the second fiber provides measurement of its attenuation per unit length. Unfortunately, the accuracy of this measurement method is dependent on the coupling between the two fibers and is therefore somewhat uncertain

The most popular nondestructive attenuation measurement technique for both laboratory and field use only requires access to one end of the fiber. It is the back-scatter measurement method which uses optical time domain reflectometry and also provides measurement of splice and connector losses as well as fault location. Optical time domain reflectometry finds major use in field measurements and is therefore discussed in detail in Section 13.10.1.

13.2.2 Fiber absorption loss measurement

It was indicated in the preceding section that there is a requirement for the optical fiber manufacturer to be able to separate the total fiber attenuation into the contributions from the major loss mechanisms. Material absorption loss measurements allow the level of impurity content within the fiber material to be checked in the manufacturing process. The measurements are based on calorimetric methods which determine the temperature rise in the fiber or bulk material resulting from the absorbed optical energy within the structure.

The apparatus shown in Figure 13.5 [Ref. 12] which is used to measure the absorption loss in optical fibers was modified from an earlier version which measured the absorption losses in bulk glasses [Ref. 13]. This temperature measurement technique, illustrated diagrammatically in Figure 13.5(b), has been

* Description of the substitution method is provided in FOTP-53 [Ref. 11].

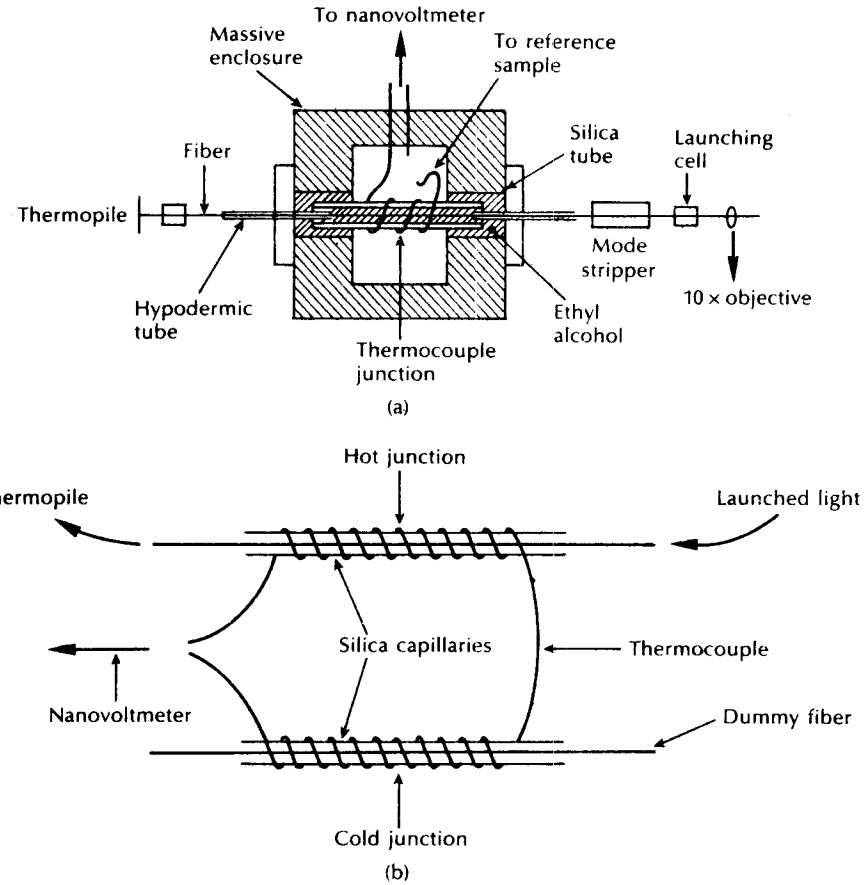

Figure 13.5 Calorimetric measurement of fiber absorption losses: (a) schematic diagram of a version of the apparatus [Ref. 12]; (b) the temperature measurement technique using a thermocouple.

widely adopted for absorption loss measurements. The two fiber samples shown in Figure 13.5(b) are mounted in capillary tubes surrounded by a low refractive index liquid (e.g. methanol) for good electrical contact, within the same enclosure of the apparatus shown in Figure 13.5(a). A thermocouple is wound around the fiber containing capillary tubes using one of them as a reference junction (dummy fiber). Light is launched from a laser source (Nd : YAG or krypton ion depending on the wavelength of interest) through the main fiber (not the dummy), and the temperature rise due to absorption is measured by the thermocouple and indicated on a nanovoltmeter. Electrical calibration may be achieved by replacing the optical fibers with thin resistance wires and by passing known electrical power through one.

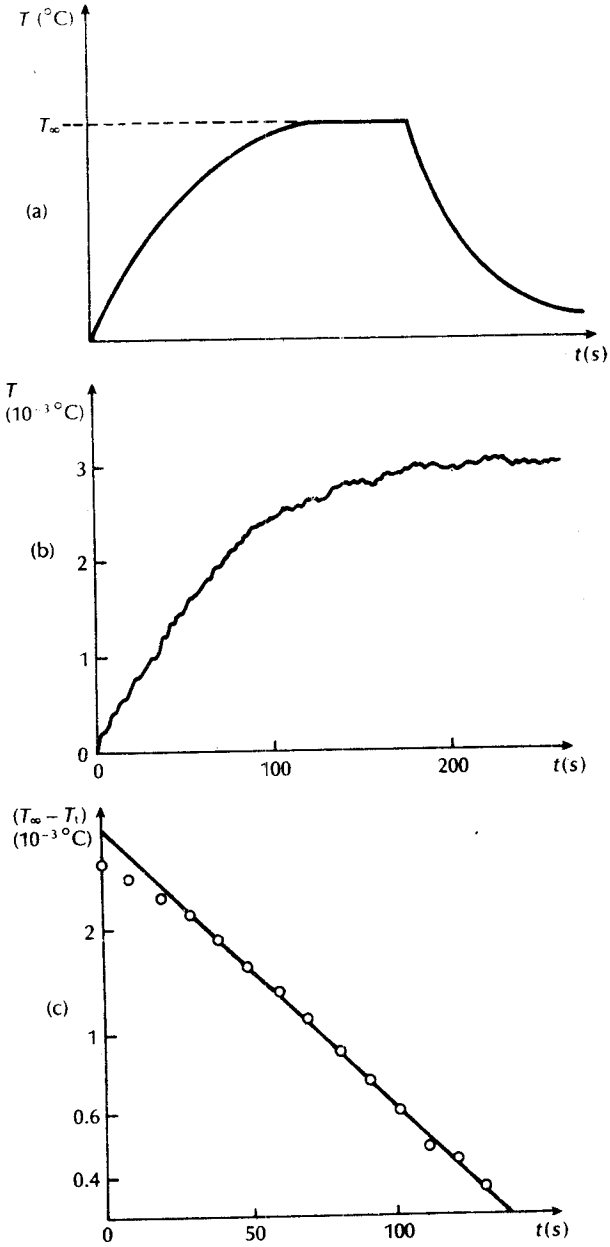

Figure 13.6 (a) A typical heating and cooling curve for a glass fiber sample. (b) A heating curve. (c) The corresponding plot of $(T_\infty - T_t)$ against time for a sample glass rod (bulk material measurement). Reproduced with permission from K. I. White and J. E. Midwinter. *Opto-electronics*, 5, p. 323, 1973.

Independent measurements can then be made using the calorimetric technique and with electrical measurement instruments.

The calorimetric measurements provide the heating and cooling curve for the fiber sample used. A typical example of this curve is illustrated in Figure 13.6(a). The attenuation of the fiber due to absorption α_{abs} may be determined from this heating and cooling characteristic. A time constant t_c can be obtained from a plot of $(T_\infty - T_t)$ on a logarithmic scale against the time t, an example of which shown in Figure 13.6(c) was obtained from the heating characteristic displayed in Figure 13.6(b) [Ref. 13]. T_∞ corresponds to the maximum temperature rise of the fiber under test and T_t is the temperature rise at a time t. It may be observed from Figure 13.6(a) that T_∞ corresponds to a steady state temperature for the fiber when the heat loss to the surroundings balances the heat generated in the fiber resulting from absorption at a particular optical power level. The time constant t_c may be obtained from the slope of the straight line plotted in Figure 13.6(c) as:

$$t_c = \frac{t_2 - t_1}{\ln (T_\infty - T_{t_1}) - \ln (T_\infty - T_{t_2})} \tag{13.3}$$

where t_1 and t_2 indicate two points in time and t_c is a constant for the calorimeter which is inversely proportional to the rate of heat loss from the device.

From detailed theory it may be shown [Ref. 13] that the fiber attenuation due to absorption is given by:

$$\alpha_{abs} = \frac{CT_\infty}{P_{opt} t_c} \text{ dB km}^{-1} \tag{13.4}$$

where C is proportional to the thermal capacity per unit length of the silica capillary and the low refractive index liquid surrounding the fiber, and P_{opt} is the optical power propagating in the fiber under test. The thermal capacity per unit length may be calculated, or determined by the electrical calibration utilizing the thin resistance wire. Usually the time constant for the calorimeter t_c is obtained using a high absorption fiber which gives large temperature differences and greater accuracy. Once t_c is determined, the absorption losses of low loss test fibers may be calculated from their maximum temperature rise T_∞, using Eq. (13.4). The temperatures are measured directly in terms of the thermocouple output (microvolts), and the optical input to the test fiber is obtained by use of a thermocouple or an optical power meter.

Example 13.2

Measurements are made using a calorimeter and thermocouple experimental arrangement as shown in Figure 13.5 in order to determine the absorption loss of an optical fiber sample. Initially a high absorption fiber is utilized to obtain a plot of $(T_\infty - T_t)$ on a logarithmic scale against t. It is found from the plot that the readings of $(T_\infty - T_t)$ after 10 and 100 seconds are 0.525 and 0.021 μV respectively.

The test fiber is then inserted in the calorimeter and gives a maximum temperature rise of $4.3 \times 10^{-4}\,^{\circ}\mathrm{C}$ with a constant measured optical power of 98 mW at a wavelength of 0.75 μm. The thermal capacity per kilometre of the silica capillary and fluid is calculated to be $1.64 \times 10^{4}\ \mathrm{J\,^{\circ}C^{-1}}$

Determine the absorption loss in $\mathrm{dB\ km^{-1}}$, at a wavelength of 0.75 μm, for the fiber under test.

Solution: Initially, the time constant for the calorimeter is determined from the measurements taken on the high absorption fiber using Eq. (13.3) where:

$$t_c = \frac{t_2 - t_1}{\ln (T_\infty - T_{t_1}) - \ln (T_\infty - T_{t_2})}$$

$$= \frac{100 - 10}{\ln (T_\infty - T_{10}) - \ln (T_\infty - T_{100})}$$

$$= \frac{90}{\ln (0.525) - \ln (0.021)}$$

$$= 28.0\ \mathrm{s}$$

Then the absorption loss of the test fiber may be obtained using Eq. (13.4) where:

$$\alpha_{abs} = \frac{CT_\infty}{P_{opt} t_c} = \frac{1.64 \times 10^{4} \times 4.3 \times 10^{-4}}{98 \times 10^{-3} \times 28.0}$$

$$= 2.6\ \mathrm{dB\,km^{-1}}$$

Hence direct measurement of the contribution of absorption losses to the total fiber attenuation may be achieved. However, fiber absorption losses are often obtained indirectly from measurement of the fiber scattering losses (see the next section) by subtraction from the total fiber attenuation, measured by one of the techniques discussed in Section 13.2.1.

13.2.3 Fiber scattering loss measurement

The usual method of measuring the contribution of the losses due to scattering within the total fiber attenuation is to collect the light scattered from a short length of fiber and compare it with the total optical power propagating within the fiber. Light scattered from the fiber may be detected in a scattering cell as illustrated in the experimental arrangement shown in Figure 13.7. This may consist of a cube of six square solar cells (Tynes cell [Ref. 14]) or an integrating sphere and detector [Ref. 15]. The solar cell cube which contains index matching fluid surrounding the fiber gives measurement of the scattered light, but careful balancing of the detectors is required in order to achieve a uniform response. This problem is overcome in the integrating sphere which again usually contains index matching fluid but responds

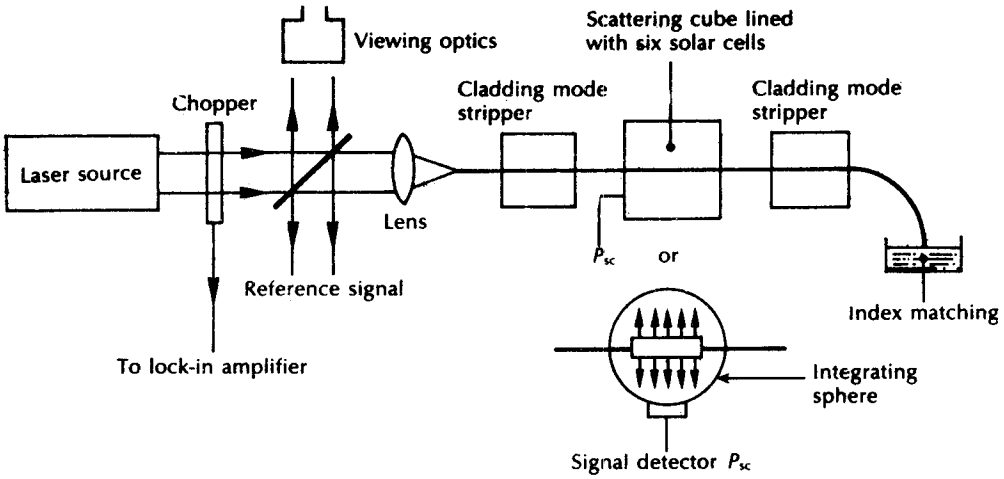

Figure 13.7 An experimental setup for measurement of fiber scattering loss illustrating both the solar cell cube and integrating sphere scattering cells.

uniformly to different distributions of scattered light. However, the integrating sphere does exhibit high losses from internal reflections. Other variations of the scattering cell include the internally reflecting cell [Ref. 16] and the sandwiching of the fiber between two solar cells [Ref. 17].

A laser source (i.e. He–Ne, Nd:YAG, krypton ion) is utilized to provide sufficient optical power at a single wavelength together with a suitable instrument to measure the response from the detector. In order to avoid inaccuracies in the measurement resulting from scattered light which may be trapped in the fiber, cladding mode strippers (see Section 13.2.1) are placed before and after the scattering cell. These devices remove the light propagating in the cladding so that the measurements are taken only using the light guided by the fiber core. Also to avoid reflections contributing to the optical signal within the cell, the output fiber end is index matched using either a fluid or suitable surface.

The loss due to scattering α_{sc} following Eq. (3.3) is given by:

$$\alpha_{sc} = \frac{10}{l(\text{km})} \log_{10}\left(\frac{P_{opt}}{P_{opt} - P_{sc}}\right) \text{ dB km}^{-1} \tag{13.5}$$

where l(km) is the length of the fiber contained within the scattering cell, P_{opt} is the optical power propagating within the fiber at the cell and P_{sc} is the optical power scattered from the short length of fiber l within the cell. As $P_{opt} \gg P_{sc}$, then the logarithm in Eq. (13.5) may be expanded to give:

$$\alpha_{sc} = \frac{4.343}{l(\text{km})} \left(\frac{P_{sc}}{P_{opt}}\right) \text{ dB km}^{-1} \tag{13.6}$$

Since the measurements of length are generally in centimetres and the optical power is normally registered in volts, Eq. (13.6) can be written as:

$$\alpha_{sc} = \frac{4.343 \times 10^5}{l(\text{cm})}\left(\frac{V_{sc}}{V_{opt}}\right) \text{ dB km}^{-1} \tag{13.7}$$

where V_{sc} and V_{opt} are the voltage readings corresponding to the scattered optical power and the total optical power within the fiber at the cell. The relative experimental accuracy (i.e. repeatability) for scatter loss measurements are in the range ± 0.2 dB using the solar cell cube and around 5% with the integrating sphere. However, it must be noted that the absolute accuracy of the measurements is somewhat poorer, being dependent on the calibration of the scattering cell and the mode distribution within a multimode fiber.

Example 13.3

A He–Ne laser operating at a wavelength of 0.63 μm was used with a solar cell cube to measure the scattering loss in a multimode fiber sample. With a constant optical output power the reading from the solar cell cube was 6.14 nV. The optical power measurement at the cube without scattering was 153.38 μV. The length of the fiber in the cube was 2.92 cm. Determine the loss due to scattering in dB km^{-1} for the fiber at a wavelength of 0.63 μm.

Solution: The scattering loss in the fiber at a wavelength of 0.63 μm may be obtained directly using Eq. (13.7) where.

$$\alpha_{sc} = \frac{4.343 \times 10^5}{l(\text{cm})}\left(\frac{V_{sc}}{V_{opt}}\right)$$

$$= \frac{4.343 \times 10^5}{2.92}\left(\frac{6.14 \times 10^{-9}}{153.38 \times 10^{-6}}\right)$$

$$= 6.0 \text{ dB km}^{-1}$$

13.3 Fiber dispersion measurements

Dispersion measurements give an indication of the distortion to optical signals as they propagate down optical fibers. The delay distortion which, for example, leads to the broadening of transmitted light pulses, limits the information-carrying capacity of the fiber. Hence as shown in Section 3.8 the measurement of dispersion allows the bandwidth of the fiber to be determined. Therefore, besides attenuation, dispersion is the most important transmission characteristic of an optical fiber. As discussed in Section 3.8 there are three major mechanisms which produce dispersion in optical fibers (material dispersion, waveguide dispersion and intermodal

dispersion). The importance of these different mechanisms to the total fiber dispersion is dictated by the fiber type.

For instance, in multimode fibers (especially step index), intermodal dispersion tends to be the dominant mechanism, whereas in single-mode fibers intermodal dispersion is nonexistent as only a single mode is allowed to propagate. In the single-mode case the dominant dispersion mechanism is intramodal (i.e. chromatic dispersion). The dominance of intermodal dispersion in multimode fibers makes it essential that dispersion measurements on these fibers are performed only when the equilibrium mode distribution has been established within the fiber, otherwise inconsistent results will be obtained. Therefore devices such as mode scramblers or filters must be utilized in order to simulate the steady state mode distribution.

Dispersion effects may be characterized by taking measurements of the impulse response of the fiber in the time domain, or by measuring the baseband frequency response in the frequency domain. If it is assumed that the fiber response is linear with regard to power [Ref. 19], a mathematical description in the time domain for the optical output power $P_o(t)$ from the fiber may be obtained by convoluting the power impulse response $h(t)$ with the optical input power $P_i(t)$ as:

$$P_o(t) = h(t) * P_i(t) \tag{13.8}$$

where the asterisk * denotes convolution. The convolution of $h(t)$ with $P_i(t)$ shown in Eq. (13.8) may be evaluated using the convolution integral where:

$$P_o(t) = \int_{-\infty}^{\infty} P_i(t - x)h(x)\,dx \tag{13.9}$$

In the frequency domain the power transfer function $H(\omega)$ is the Fourier transform of $h(t)$ and therefore by taking the Fourier transforms of all the functions in Eq. (13.8) we obtain,

$$\mathscr{P}_o(\omega) = H(\omega)\mathscr{P}_i(\omega) \tag{13.10}$$

where ω is the baseband angular frequency. The frequency domain representation given in Eq. (13.10) is the least mathematically complex, and by performing the Fourier transformation (or the inverse Fourier transformation) it is possible to switch between the time and frequency domains (or vice versa) by mathematical means. Hence, independent measurement of either $h(t)$ or $H(\omega)$ allows determination of the overall dispersive properties of the optical fiber. Thus fiber dispersion measurements can be made in either the time or frequency domains.

13.3.1 Time domain measurement

The most common method for time domain measurement of pulse dispersion in multimode optical fibers is illustrated in Figure 13.8 [Ref. 20]. Short optical pulses (100 to 400 ps) are launched into the fiber from a suitable source (e.g. AlGaAs injection laser) using fast driving electronics. The pulses travel down the length of fiber under test (around 1 km) and are broadened due to the various dispersion

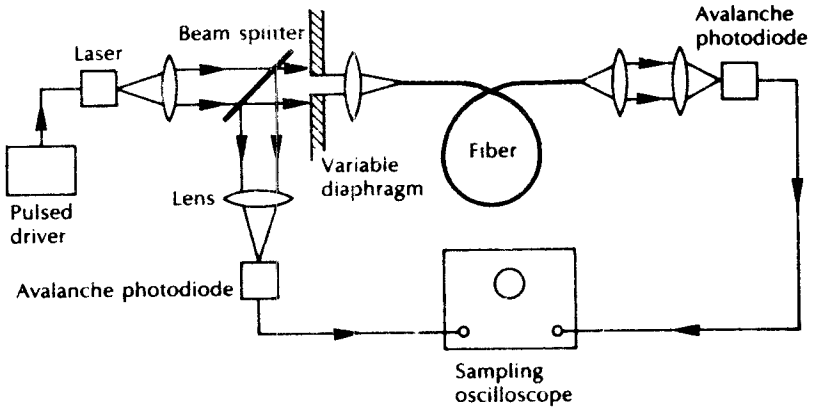

Figure 13.8 Experimental arrangement for making multimode fiber dispersion measurements in the time domain [Ref. 20].

mechanisms. However, it is possible to take measurements of an isolated dispersion mechanism by, for example, using a laser with a narrow spectral width when testing a multimode fiber. In this case the intramodal dispersion is negligible and the measurement thus reflects only intermodal dispersion. The pulses are received by a high speed photodetector (i.e. avalanche photodiode) and are displayed on a fast sampling oscilloscope. A beam splitter is utilized for triggering the oscilloscope and for input pulse measurement.

After the initial measurement of output pulse width, the long fiber length may be cut back to a short length and the measurement repeated in order to obtain the effective input pulse width. The fiber is generally cut back to the lesser of 10 m or 1% of its original length [Ref. 6]. As an alternative to this cut-back technique, the insertion or substitution method similar to that used in fiber loss measurement (see Section 13.2.1) can be employed. This method has the benefit of being nondestructive and only slightly less accurate than the cut-back technique. These time domain measurement methods for multimode fiber are covered in FOTP-51 [Ref. 21].

The fiber dispersion is obtained from the two pulse width measurements which are taken at any convenient fraction of their amplitude. However, unlike the considerations of dispersion in Sections 3.8 to 3.11 where rms pulse widths are used, dispersion measurements are normally made on pulses using the half maximum amplitude or 3 dB points. If $P_i(t)$ and $P_o(t)$ of Eq. (13.8) are assumed to have a Gaussian shape then Eq. (13.8) may be written in the form:

$$\tau_o^2(3\text{ dB}) = \tau^2(3\text{ dB}) + \tau_i^2(3\text{ dB}) \tag{13.11}$$

where $\tau_i(3\text{ dB})$ and $\tau_o(3\text{ dB})$ are the 3 dB pulse widths at the fiber input and output, respectively, and $\tau(3\text{ dB})$ is the width of the fiber impulse response again measured at half the maximum amplitude. Hence the pulse dispersion in the fiber (commonly

referred to as the pulse broadening when considering the 3 dB pulse width) in ns km^{-1} is given by:

$$\tau(3\text{ dB}) = \frac{(\tau_o^2(3\text{ dB}) - \tau_i^2(3\text{ dB}))^{\frac{1}{2}}}{L}\text{ ns km}^{-1} \tag{13.12}$$

where $\tau(3\text{ dB})$, $\tau_i(3\text{ dB})$ and $\tau_o(3\text{ dB})$ are measured in ns and L is the fiber length in km. It must be noted that if a long length of fiber is cut back to a short length in order to take the input pulse width measurement then L corresponds to the difference between the two fiber lengths in km. When the launched optical pulses and the fiber impulse response are Gaussian then the 3 dB optical bandwidth for the fiber B_{opt} may be calculated using [Ref. 22]:

$$\begin{aligned} B_{opt} \times \tau(3\text{ dB}) &= 0.44\text{ GHz ns} \\ &= 0.44\text{ MHz ps} \end{aligned} \tag{13.13}$$

Hence estimates of the optical bandwidth for the fiber may be obtained from the measurements of pulse broadening without resorting to rigorous mathematical analysis.

Example 13.4

Pulse dispersion measurements are taken over a 1.2 km length of partially graded multimode fiber. The 3 dB widths of the optical input pulses are 300 ps, and the corresponding 3 dB widths for the output pulses are found to be 12.6 ns. Assuming the pulse shapes and fiber impulse response are Gaussian calculate:

(a) the 3 dB pulse broadening for the fiber in ns km^{-1}:
(b) the fiber bandwidth–length product.

Solution: (a) The 3 dB pulse broadening may be obtained using Eq. (13.12) where:

$$\tau(3\text{ dB}) = \frac{(12.6^2 - 0.3^2)^{\frac{1}{2}}}{1.2} = \frac{(158.76 - 0.09)^{\frac{1}{2}}}{1.2}$$

$$= 10.5\text{ ns km}^{-1}$$

(b) The optical bandwidth for the fiber is given by Eq. (13.13) as:

$$B_{opt} = \frac{0.44}{\tau(3\text{ dB})} = \frac{0.44}{10.5}\text{ GHz km}$$

$$= 41.9\text{ MHz km}$$

The value obtained for B_{opt} corresponds to the bandwidth–length product for the fiber because the pulse broadening in part (a) was calculated over a 1 km fiber length. Also it may be noted that in this case the narrow input pulse width makes little difference to the calculation of the pulse broadening. The input pulse width

becomes significant when measurements are taken on low dispersion fibers (e.g. single-mode).

The above dispersion measurement techniques allow the total dispersion for multimode fibers to be determined. It is clear, however, that intramodal or chromatic dispersion is an important transmission parameter, particularly for single-mode fibers. Moreover, it can also be a significant distortion effect in multimode fibers even though intermodal dispersion is normally dominant. The time domain measurement of chromatic dispersion is outlined in FOTP-168 [Ref. 23]. A typical experimental arrangement is shown in Figure 13.9. The pulse delay versus optical wavelength is measured for both long and short fiber lengths. The source usually comprises multiple injection lasers possibly including wavelength tunable devices (see Section 6.10). When $\Delta T(\lambda)$ is the delay difference for the length difference $L_1 - L_2$, then the specific group delay per unit length $\tau_g(\lambda)$ is given by [Ref. 6]:

$$\tau_g(\lambda) = \frac{\Delta T(\lambda)}{L_1 - L_2} \tag{13.14}$$

Differentiation of Eq. (13.14) provides the chromatic dispersion D_T following Eq. (3.46) where:

$$D_T(\lambda) = \frac{d\tau_g}{d\lambda} \text{ ps nm}^{-1}\text{ km}^{-1} \tag{13.15}$$

and the dispersion slope S from Eq. (3.52):

$$S(\lambda) = \frac{dD_T}{d\lambda} \text{ ps nm}^{-2}\text{ km}^{-1} \tag{13.16}$$

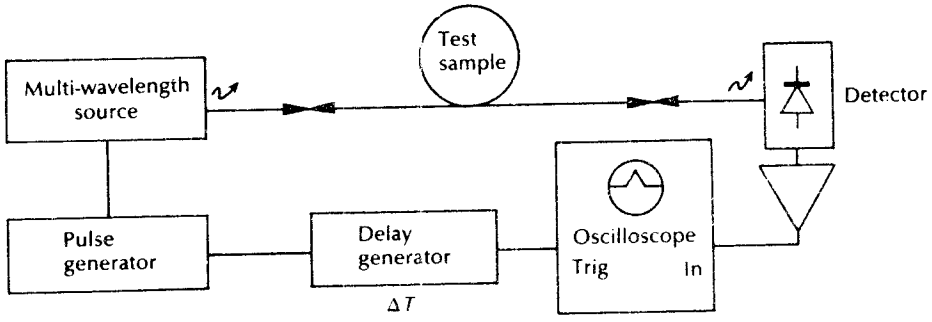

Figure 13.9 Experimental arrangement for the measurement of intramodal or chromatic dispersion by time delay.

This pulse delay method is also one of the two reference test methods to obtain chromatic dispersion in single-mode fibers which are recommended by the CCITT [Ref. 25].

13.3.2 Frequency domain measurement

Frequency domain measurement is the preferred method for acquiring the bandwidth of multimode optical fibers. This is because the baseband frequency response $H(\omega)$ of the fiber may be obtained directly from these measurements using Eq. (13.10) without the need for any assumptions of Gaussian shape, or alternatively, the mathematically complex deconvolution of Eq. (13.8) which is necessary with measurements in the time domain. Thus the optical bandwidth of a multimode fiber is best obtained from frequency domain measurements.

One of two frequency domain measurement techniques is generally used. The first utilizes a similar pulsed source to that employed for the time domain measurements shown in Figure 13.8. However, the sampling oscilloscope is replaced by a spectrum analyser which takes the Fourier transform of the pulse in the time domain and hence displays its constituent frequency components. The experimental arrangement is illustrated in Figure 13.10.

Comparison of the spectrum at the fiber output $\mathscr{P}_o(\omega)$ with the spectrum at the fiber input $\mathscr{P}_i(\omega)$ provides the baseband frequency response for the fiber under test following Eq. (5.10) where:

$$H(\omega) = \frac{\mathscr{P}_o(\omega)}{\mathscr{P}_i(\omega)} \tag{13.17}$$

The second technique involves launching a sinusoidally modulated optical signal at different selected frequencies using a sweep oscillator. Therefore the signal

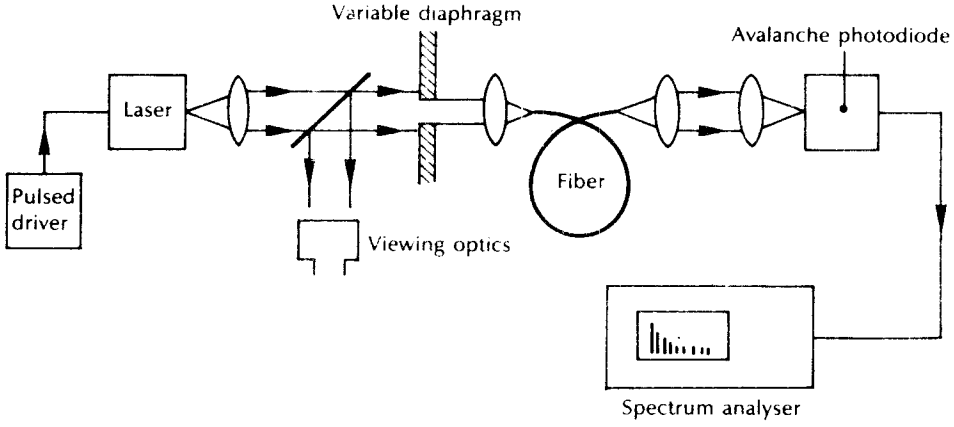

Figure 13.10 Experimental setup for making fiber dispersion measurements in the frequency domain using a pulsed laser source.

energy is concentrated in a very narrow frequency band in the baseband region, unlike the pulse measurement method where the signal energy is spread over the entire baseband region. A possible experimental arrangement for this swept frequency measurement method is shown in Figure 13.11 [Ref. 24]. The optical source is usually an injection laser, which may be directly modulated (see Section 7.5) from the sweep oscillator. A spectrum analyser may be used in order to obtain a continuous display of the swept frequency signal. Again, Eq. (13.17) is utilized to obtain the baseband frequency response, employing either the cut-back or substitution procedure in a similar manner to the time domain measurement (see Section 13.3.1). However, the spectrum analyser provides no information on the phase of the received signal Therefore a vector voltmeter or ideally a network analyser can be employed to give both the frequency and phase information. This multimode fiber frequency domain measurement method is described in FOTP-30 [Ref. 25].

The intramodal or chromatic dispersion for single-mode fibers may also be obtained using frequency domain measurement techniques. The second reference test method recommended by the CCITT [Ref. 1] falls into this category and is known as the phase shift method. This technique is also covered in FOTP-169 [Ref. 26]. To obtain the phase shift $\phi(\lambda)$ versus wavelength, the pulse generator in Figure 13.9 (corresponding to the time domain measurement) is replaced by a high frequency oscillator operating at a constant frequency and the delay generator and oscilloscope are replaced by a phase meter or vector voltmeter. Finally, an electrical or optical reference channel is connected between the oscillator and the meter.

When an optical signal, which is sinusoidally modulated in power with frequency f_m, is transmitted through a single-mode fiber of length L, then the modulation

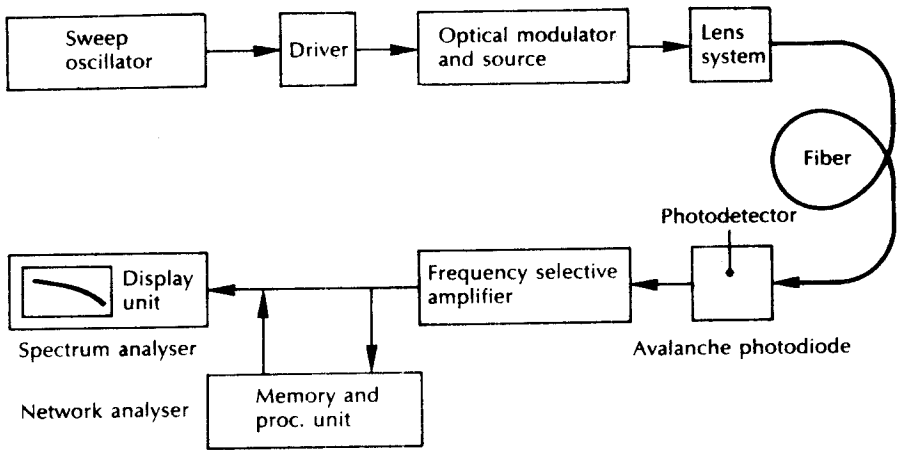

Figure 13.11 Block schematic showing an experimental arrangement for the swept frequency measurement method to provide fiber dispersion measurements in the frequency domain [Ref. 24].

envelope is delayed in time by:

$$\frac{L}{v_g} = \tau_g L \tag{13.18}$$

where v_g is the group velocity which corresponds to the signal velocity. Since a delay of one modulation period T_m or $1/f_m$ corresponds to a phase shift of 2π, then the sinusoidal modulation is phase shifted in the fiber by an angle ϕ_m where:

$$\phi_m = \frac{2\pi\tau_g L}{T_m} = 2\pi f_m \tau_g L \tag{13.19}$$

Hence the specific group delay is given by:

$$\tau_g = \frac{\phi_m}{2\pi f_m L} \tag{13.20}$$

Again the chromatic dispersion and the dispersion slope can be obtained by differentiation following Eqs. (13.15) and (13.16) respectively. Finally, alternative direct measurement techniques using a differential phase shift method are described in FOTP-175.

13.4 Fiber refractive index profile measurements

The refractive index profile of the fiber core plays an important role in characterizing the properties of optical fibers. It allows determination of the fiber's numerical aperture and the number of modes propagating within the fiber core, whilst largely defining any intermodal and/or profile dispersion caused by the fiber. Hence a detailed knowledge of the refractive index profile enables the impulse response of the fiber to be predicted. Also as the impulse response and consequently the information-carrying capacity of the fiber is strongly dependent on the refractive index profile, it is essential that the fiber manufacturer is able to produce particular profiles with great accuracy, especially in the case of graded index fibers (i.e. optimum profile). There is therefore a requirement for accurate measurement of the refractive index profile. These measurements may be performed using a number of different techniques each of which exhibit certain advantages and drawbacks. In this section we will discuss some of the more popular methods which may be relatively easily interpreted theoretically, without attempting to review all the possible techniques which have been developed.

13.4.1 Interferometric methods

Interference microscopes (e.g. Mach–Zehnder, Michelson) have been widely used to determine the refractive index profiles of optical fibers. The technique usually involves the preparation of a thin slice of fiber (slab method) which has both ends accurately polished to obtain square (to the fiber axes) and optically flat surfaces

The slab is often immersed in an index matching fluid, and the assembly is examined with an interference microscope. Two major methods are then employed, using either a transmitted light interferometer (Mach–Zehnder [Ref. 27]) or a reflected light interferometer (Michelson [Ref. 28]). In both cases light from the microscope travels normal to the prepared fiber slice faces (parallel to the fiber axis), and differences in refractive index result in different optical path lengths. This situation is illustrated in the case of the Mach–Zehnder interferometer in Figure 13.12(a). When the phase of the incident light is compared with the phase of the emerging light, a field of parallel interference fringes is observed. A photograph of the fringe pattern may then be taken, an example of which is shown in Figure 13.12(b) [Ref. 30].

The fringe displacements for the points within the fiber core are then measured using as reference the parallel fringes outside the fiber core (in the fiber cladding). The refractive index difference between a point in the fiber core (e.g. the core axis) and the cladding can be obtained from the fringe shift q, which corresponds to a number of fringe displacements. This difference in refractive index δn is given by [Ref. 6]:

$$\delta n = \frac{q\lambda}{x} \tag{13.21}$$

where x is the thickness of the fiber slab and λ is the incident optical wavelength. The slab method gives an accurate measurement of the refractive index profile, although computation of the individual points, is somewhat tedious unless an

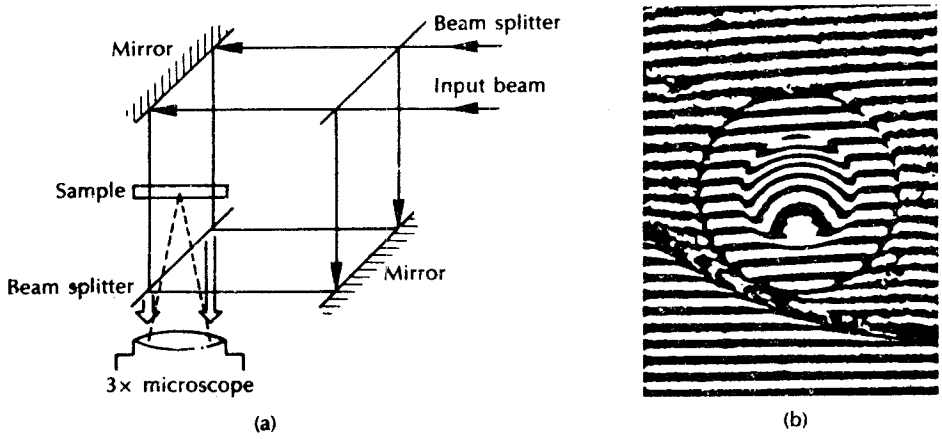

Figure 13.12 (a) The principle of the Mach–Zehnder interferometer [Ref. 27]. (b) The interference fringe pattern obtained with an interference microscope from a graded index fiber. Reproduced with permission from L. G. Cohen, P. Kaiser J. M. MacChesney, P. N. O'Connor and H. M. Presby. *Appl. Phys. Lett.*, **26**, p. 472, 1975.

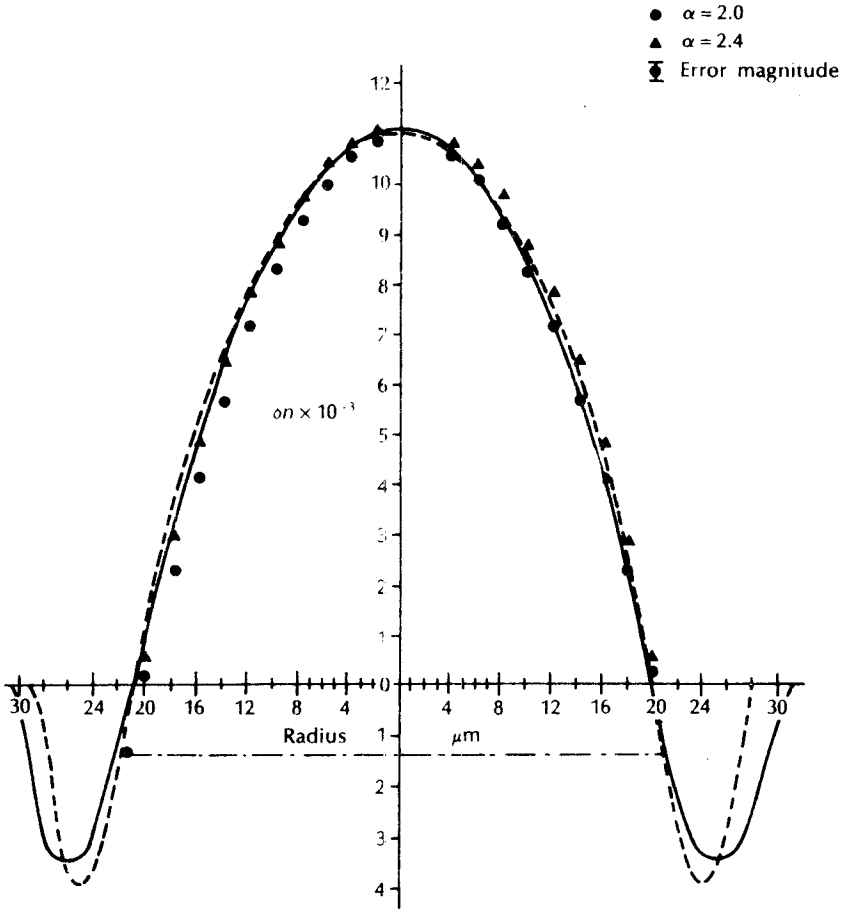

Figure 13.13 The fiber refractive index profile computed from the interference pattern shown in Figure 13.12(b). Reproduced with permission from L. G. Cohen, P. Kaiser, J. M. MacChesney, P. N. O'Connor and H. M. Presby. *Appl. Phys. Lett.*, **26**, p. 472, 1975.

automated technique is used. Figure 13.13 [Ref. 30] shows the refractive index profile obtained from the fringe pattern indicated in Figure 13.12(b).

A limitation of this method is the time required to prepare the fiber slab. However, another interferometric technique has been developed [Ref. 32] which requires no sample preparation. In this method the light beam is incident to the fiber perpendicular to its axis; this is known as transverse shearing interferometry. Again fringes are observed from which the fiber refractive index profile may be

$$N(t) = x(t) \cos \omega_{IF} t + y(t) \sin \omega_{IF} t \tag{12.26}$$

13.4.2 Near field scanning method

The near field scanning or transmitted near field method utilizes the close resemblance that exists between the near field intensity distribution and the refractive index profile, for a fiber with all the guided modes equally illuminated. It provides a reasonably straightforward and rapid method fo acquiring the refractive index profile. When a diffuse Lambertian source (e.g. tungsten filament lamp or LED) is used to excite all the guided modes then the near field optical power density at a radius r from the core axis $P_D(r)$ may be expressed as a fraction of the core axis near field optical power density $P_D(0)$ following [Ref. 33]:

$$\frac{P_D(r)}{P_D(0)} = C(r,z)\left[\frac{n_1^2(r) - n_2^2}{n_1^2(0) - n_2^2}\right] \tag{13.22}$$

where $n_1(0)$ and $n_1(r)$ are the refractive indices at the core axis and at a distance r from the core axis respectively, n_2 is cladding refractive index and $C(r,z)$ is a correction factor. The correction factor which is incorporated to compensate for any leaky modes present in the short test fiber may be determined analytically. A set of normalized correction curves is, for example, given in Ref. 34. For multimode fiber such a transmitted near field method is described in FOTP-43 [Ref. 35]. However, at present there is no transmitted near field FOTP for single-mode fiber.

An experimental configuration is shown in Figure 13.14. The output from a Lambertian source is focused on to the end of the fiber using a microscope objective lens. A magnified image of the fiber output end is displayed in the plane of a small active area photodetector (e.g. silicon p–i–n photodiode). The photodetector which scans the field transversely receives amplification from the phase sensitive

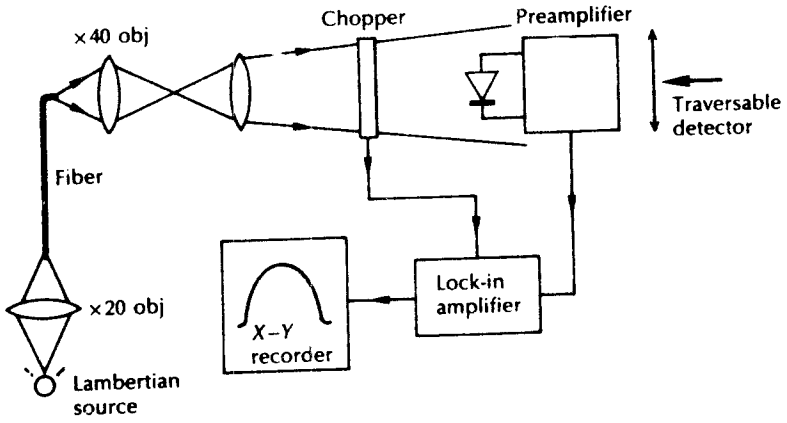

Figure 13.14 Experimental setup for the near field scanning measurement of the refractive index profile [Ref. 37].

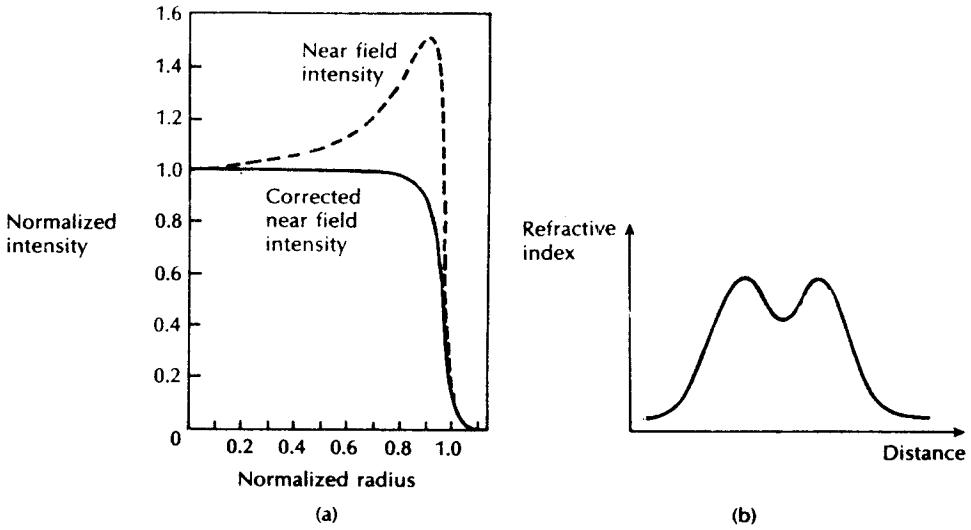

Figure 13.15 (a) The refractive index profile of a step index fiber measured using the near field scanning method, showing the near field intensity and the corrected near field intensity. Reproduced with permission from F. E. M. Sladen, D. N. Payne and M. J. Adams, *Appl. Phys. Lett.*, **28**, p. 225, 1976. (b) The refractive index profile of a practical step index fiber measured by the near field scanning method [Ref. 33].

combination of the optical chopper and lock-in amplifier. Hence the profile may be plotted directly on an $X-Y$ recorder. However, the profile must be corrected with regard to $C(r, z)$ as illustrated in Figure 13.15(a) which is very time consuming. Both the scanning and data acquisition can be automated with the inclusion of a minicomputer [Ref. 34].

The test fiber is generally 2 m in length to eliminate any differential mode attenuation and mode coupling. A typical refractive index profile for a practical step index fiber measured by the near field scanning method is shown in Figure 13.15(b). It may be observed that the profile dips in the centre at the fiber core axis. This dip was originally thought to result from the collapse of the fiber preform before the fiber is drawn in the manufacturing process but has been recently shown to be due to the layer structure inherent at the deposition stage [Ref. 36].

13.4.3 Refracted near field method

The refracted near field (RNF) or refracted ray method is complementary to the transmitted near field technique (see Section 13.4.2) but has the advantage that it does not require a leaky mode correction factor or equal mode excitation. Moreover, it provides the relative refractive index differences directly without recourse to external calibration or reference samples. The RNF method is the most

commonly used technique for the determination of the fiber refractive index profile [Ref. 38] and is the EIA reference test method for both multimode and single-mode fibers. Details of the test procedure are provided in FOTP-44 [Ref. 39].

A schematic of an experimental set-up for the RNF method is shown in Figure 13.16. A short length of fiber is immersed in a cell containing a fluid of slightly higher refractive index. A small spot of light typically emitted from a 633 nm helium neon laser for best resolution is scanned across the cross sectional diameter of the fiber. The measurement technique utilizes that light which is not guided by the fiber but escapes from the core into the cladding. However, light escaping from the fiber core partly results from the power leakage from the leaky modes which is an unknown quantity. The effect of this radiated power reaching the detector is undesirable and therefore it is blocked using an opaque circular screen, as shown in Figure 13.16(a). The refracted ray trajectories are illustrated in Figure 13.16(b) where θ' is the angle of incidence in the fiber core, θ is the angle of refraction in the fiber core and θ'' constitutes the angle of the refracted inbound rays external to the fiber core. Any light leaving the fiber core below a minimum angle θ''_{min} is prevented from reaching the detector by the opaque screen (Figure 13.16(a)). Moreover, it may be observed from Figure 13.16(b) that this minimum angle corresponds to a minimum angle of incidence θ'_{min}. However, all light at an angle

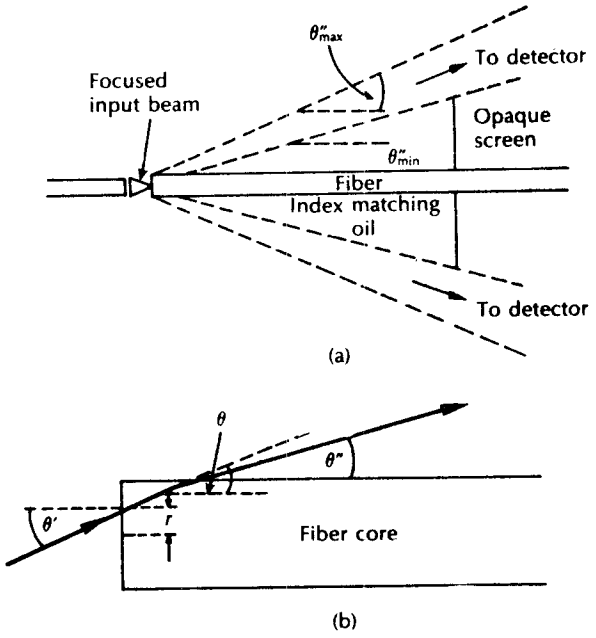

Figure 13.16 Refracted near field method for the measurement of refractive index profile: (a) experimental arrangement; (b) illustration of the ray trajectories [Ref. 40].

of incidence $\theta' > \theta'_{\min}$ must be allowed to reach the detector. To ensure that this process occurs it is advisable that input apertures are used to limit the convergence angle of the input beam to a suitable maximum angle $\theta'_{\max}$ corresponding to a refracted angle $\theta''_{\max}$. In addition, the immersion of the fiber in an index matching fluid prevents reflection at the outer cladding boundary. Hence all the refracted light emitted from the fiber at angles over the range $\theta''_{\min}$ to $\theta''_{\max}$ may be detected.

The detected optical power as a function of the radial position of the input beam $P(r)$ is measured and a value $P(a)$ corresponding to the input beam being focused into the cladding is also obtained. The refractive index profile $n(r)$ for the fiber core is then given by [Ref. 40]:

$$n(r) = n_2 + n_2 \cos \theta''_{\min}(\cos \theta''_{\min} - \cos \theta'_{\max}) \frac{P(a) - P(r)}{P(a)} \tag{13.23}$$

where n_2 is the cladding refractive index. Furthermore, Eq. (13.23) can be written as:

$$n(r) = k_1 - k_2 P(r) \tag{13.24}$$

It is clear that $n(r)$ is proportional to $P(r)$ and hence the measurement system can be calibrated to obtain the constants k_1 and k_2. For example, a calibration scheme in which the power that passes the opaque screen is monitored as it is translated along the optical axis provided an early strategy [Refs. 41, 42]. Alternative calibration techniques which allow accurate RNF measurements are described in Ref. 38.

13.5 Fiber cutoff wavelength measurements

A multimode fiber has many cutoff wavelengths because the number of bound propagating modes is usually large. For example, considering a parabolic refractive index graded fiber, following Eq. (2.95) the number of guided modes M_g is:

$$M_g = \left(\frac{\pi a}{\lambda}\right)^2 (n_1^2 - n_2^2) \tag{13.25}$$

where a is the core radius and n_1 and n_2 are the core peak and cladding indices respectively. It may be observed from Eq. (13.25) that operation at longer wavelengths yields fewer guided modes. Therefore it is clear that as the wavelength is increased, a growing number of modes are cutoff where the cutoff wavelength of a LP_{lm} mode is the maximum wavelength for which the mode is guided by the fiber.

Usually the cutoff wavelength refers to the operation of single-mode fiber in that it is the cutoff wavelength of the LP_{11} mode (which has the longest cutoff wavelength) which makes the fiber single moded when the fiber diameter is reduced to 8 or 9 μm. Hence the cutoff wavelength of the LP_{11} is the shortest wavelength above which the fiber exhibits single-mode operation and it is therefore an

important parameter to measure (see Section 2.5.1). The theoretical value of the cutoff wavelength can be determined from the fiber refractive index profile following Eq. (2.98). Because of the large attenuation of the LP_{11} mode near cutoff, however, the parameter which is experimentally determined is called the effective cutoff wavelength which is always smaller than the theoretical cutoff wavelength by as much as 100 to 200 nm [Ref. 43]. It is this effective cutoff wavelength which limits the wavelength region for which the fiber is 'effectively' single-mode.

The effective cutoff wavelength is normally measured by increasing the signal wavelength in a fixed length of fiber until the LP_{11} mode is undetectable. Since the attenuation of the LP_{11} mode is dependent on the fiber length and its radius of curvature, the effective cutoff wavelength tends to vary with the method of measurement. Moreover, numerous methods of measurement have been investigated [Refs. 6, 43] and because these techniques can give significantly different results, the measurement has caused some problems [Ref. 44]. Nevertheless, three methods were recommended by the CCITT in 1986 [Ref. 1]; two of which, being transmitted power techniques, were recommended as reference test methods. In addition, these two techniques correspond to the EIA standard test method FOTP-80 [Ref. 45].

The effective cutoff wavelength has been defined by the CCITT as the wavelength greater than which the ratio between the total power, including the launched higher order modes, and the fundamental mode power has decreased to less than 0.1 dB in a quasi-straight 2 m fiber length with one single loop of 140 mm radius.* Measurement configurations which enable the determination of fiber cutoff wavelength by the RTMs are shown in Figure 13.17. A single turn configuration is illustrated in Figure 13.17(a), whilst the split mandrel configuration of Figure 13.17(b) proves convenient for fiber handling. The other test apparatus is the same as that employed for the measurement of fiber attenuation by the cut-back method (Figure 13.2). However, the launch conditions used must be sufficient to excite both the fundamental and the LP_{11} modes, and it is important that cladding modes are stripped from the fiber.

In the bending-reference technique the power $P_s(\lambda)$ transmitted through the fiber sample in the configurations shown in Figure 13.17 is measured as a function of wavelength. Thus the quantity $P_s(\lambda)$ corresponds to the total power, including launched higher order modes, of the CCITT definition for cutoff wavelength. Then keeping the launch conditions fixed, at least one additional loop of sufficiently small radius (60 mm or less) is introduced into the test sample to act as a mode filter to suppress the secondary LP_{11} mode without attenuating the fundamental mode at the effective cutoff wavelength. In this case the smaller transmitted spectral power $P_b(\lambda)$ is measured which corresponds to the fundamental mode power referred to in the definition. The bend attenuation $a_b(\lambda)$ comprising the level difference

* It should be noted that the 2 m fiber length corresponds to the length specified in the cut-back attenuation measurements (Section 13.2.1).

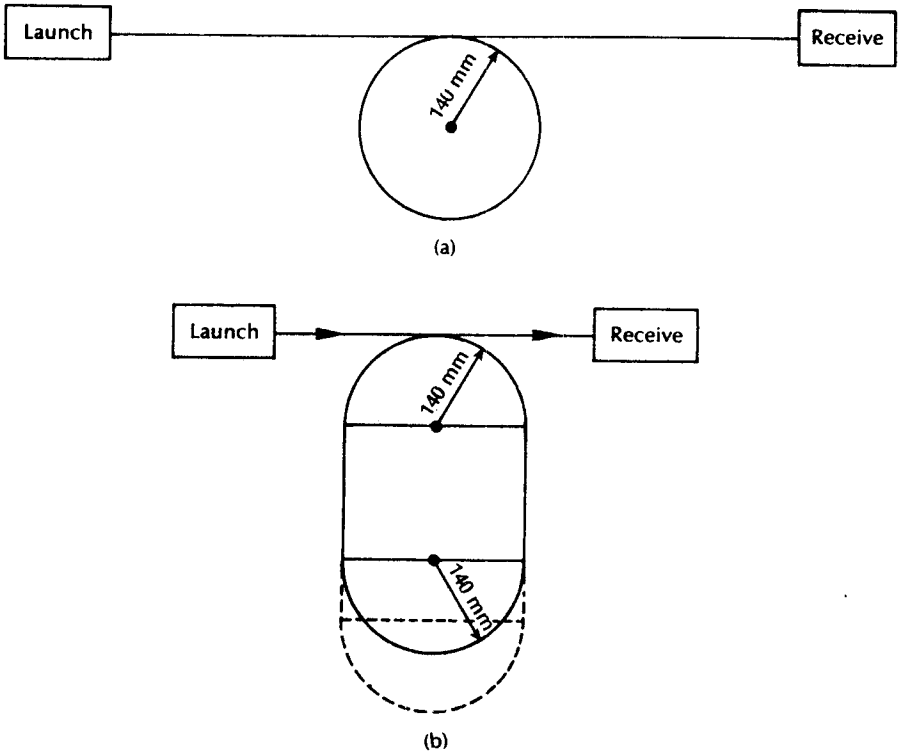

Figure 13.17 Configurations for the measurement of uncabled fiber cutoff wavelength: (a) single turn; (b) split mandrell [Refs. 1, 45].

between the total power and the fundamental power is calculated as:

$$a_b(\lambda) = 10 \log_{10} \frac{P_s(\lambda)}{P_b(\lambda)} \tag{13.26}$$

The bend attenuation characteristic exhibits a peak in the wavelength region where the radiation losses resulting from the small loop are much higher for the LP_{11} mode than for the LP_{01} fundamental mode, as illustrated in Figure 13.18. It should be noted that the shorter wavelength side of the attenuation maximum corresponds to the LP_{11} mode, being well confined in the fiber core, and hence negligible loss is induced by the 60 mm diameter loop, whereas on the longer wavelength side the LP_{11} mode is not guided in the fiber and therefore, assuming that the loop diameter is large enough to avoid any curvature loss to the fundamental mode, there is also no increase in loss. Using the CCITT and EIA definition for the effective cutoff wavelength λ_{ce} it may be determined as the longest wavelength at which the bend attenuation or level difference $a_b(\lambda)$ equals 0.1 dB, as shown in Figure 13.18.

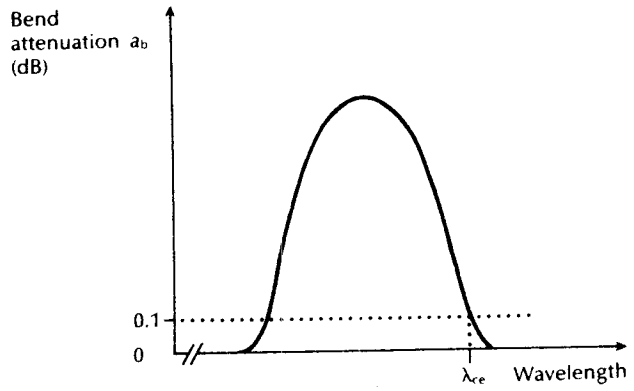

Figure 13.18 Bend attenuation against wavelength in the bending method for the measurement of cutoff wavelength λ_{ce}.

The other RTM is called the power step method [Ref. 46] or the multimode reference technique [Ref. 6]. Again, the fiber configurations shown in Figure 13.17 are employed with the test apparatus the same as that to measure fiber attenuation by the cut-back method. Furthermore, the launch conditions must again be sufficient to excite both the fundamental and LP_{11} modes and, as in the bending method, the transmitted power $P_s(\lambda)$ is measured as a function of wavelength. Next, however, the 2 m length of single-mode fiber is replaced by a short (1 to 2 m) length of multimode fiber and the spectral power $P_m(\lambda)$ emerging from the end of the multimode fiber is measured.

The relative attenuation $a_m(\lambda)$ or level difference between the powers launched into the multimode and single-mode fibers may be computed as:

$$a_m(\lambda) = 10 \log_{10} \frac{P_s(\lambda)}{P_m(\lambda)} \tag{13.27}$$

A typical characteristic showing the level difference as a function of wavelength is provided in Figure 13.19 in which the step reduction of level difference around cutoff may be observed. This results from the increase in power obtained at the output of the single-mode fiber from propagation of the LP_{11} mode, as well as the fundamental LP_{01} mode when going through the cutoff wavelength. To obtain the effective cutoff wavelength, the longest wavelength portion of the characteristic is fitted to a straight line and the intersection of the $a_m(\lambda)$ curve with another parallel straight line displaced by 0.1 dB produces the result. It should be noted, however, that accurate measurement requires an attenuation difference of not less than 2 dB [Ref. 6]. Such a difference may be readily obtained as there are two modes in the primary LP_{01} mode group and four in the secondary LP_{11} mode group. Hence with equal excitation of both groups the maximum attenuation difference is $10 \log_{10} (2 + 4)/2$, or 4.8 dB, when going through cutoff [Ref. 46]. Finally, this method and

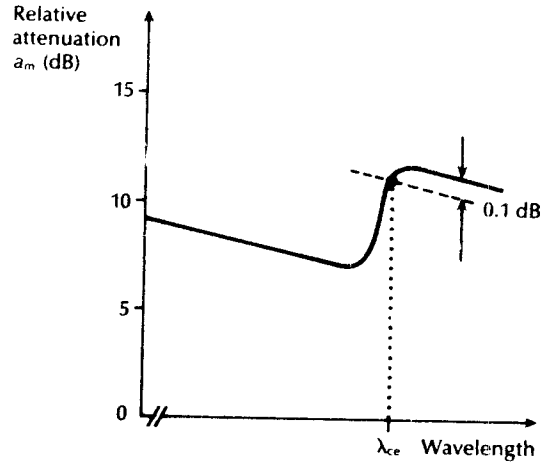

Figure 13.19 Relative attenuation against wavelength in the power step technique for the measurement of cutoff wavelength λ_{ce}.

the bending reference technique have been shown to yield approximately the same values for the effective cutoff wavelength in a round robin test [Ref. 47].

A third method for determination of the effective cutoff wavelength which is recommended by the CCITT as an alternative test method [Ref. 1] is the measurement of the change in spot size with wavelength [Ref. 48]. In this case the spot size is measured as a function of wavelength by the transverse offset method (see Section 13.8) using a 2 m length of fiber on each side of the joint with a single loop of radius 140 mm formed in each 2 m length. When the fiber is operating in

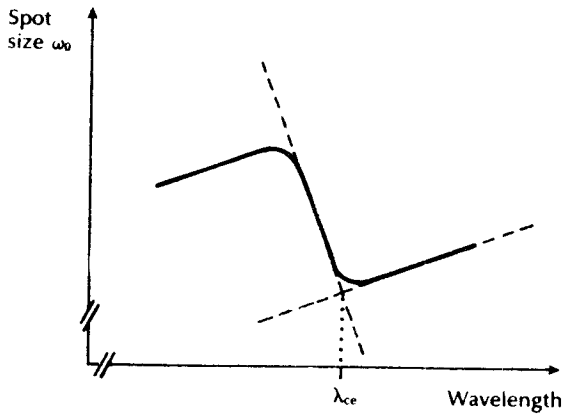

Figure 13.20 Wavelength dependence of the spot size in the spot size technique for the measu ement of cutoff wavelength λ_{ce}.

the single-mode region, the spot size increases almost linearly with increasing wavelength [Ref. 43], as may be observed in Figure 13.20. However, as the cutoff wavelength is approached, the contribution from the second order mode creates a significant change in the spot size from the expected single-mode values. At this point two straight lines with a positive and negative slope can be fitted through the measured points, as illustrated in Figure 13.20, and the intersection point corresponds to the effective cutoff wavelength.

The effective cutoff wavelength for a cabled single-mode fiber will generally be smaller than that of the uncabled fiber because of bend effects (both micro- and macrobending). A procedure for this measurement is outlined in FOTP-170 [Ref. 49] which is similar to the transmitted power methods of FOTP-80.

13.6 Fiber numerical aperture measurements

The numerical aperture is an important optical fiber parameter as it affects characteristics such as the light-gathering efficiency and the normalized frequency of the fiber (V). This in turn dictates the number of modes propagating within the fiber (also defining the single-mode region) which has consequent effects on both the fiber dispersion (i.e. intermodal) and, possibly, the fiber attenuation (i.e. differential attenuation of modes). The numerical aperture (NA) is defined for a step index fiber in air by Eq. (2.8) as:

$$NA = \sin \theta_a = (n_1^2 - n_2^2)^{\frac{1}{2}} \tag{13.28}$$

where θ_a is the maximum acceptance angle, n_1 is the core refractive index and n_2 is the cladding refractive index. It is assumed in Eq. (13.28) that the light is incident on the fiber end face from air with a refractive index (n_0) of unity. Although Eq. (13.28) may be employed with graded index fibers, the numerical aperture thus defined represents only the local NA of the fiber on its core axis (the numerical aperture for light incident at the fiber core axis). The graded profile creates a multitude of local NAs as the refractive index changes radially from the core axis. For the general case of a graded index fiber these local numerical apertures $NA(r)$ at different radial distances r from the core axis may be defined by:

$$NA(r) = \sin \theta_a(r) = (n_1^2(r) - n_2^2)^{\frac{1}{2}} \tag{13.29}$$

Therefore, calculations of numerical aperture from refractive index data are likely to be less accurate for graded index fibers than for step index fibers unless the complete refractive index profile is considered. However, if refractive index data is available on either fiber type from the measurements described in Section 13.4, the numerical aperture may be determined by calculation.

Alternatively, a simple commonly used technique for the determination of the fiber numerical aperture is now described by FOTP-177 [Ref. 50] and involves measurement of the far field radiation pattern from the fiber. This measurement may be performed by directly measuring the far field angle from the fiber using a

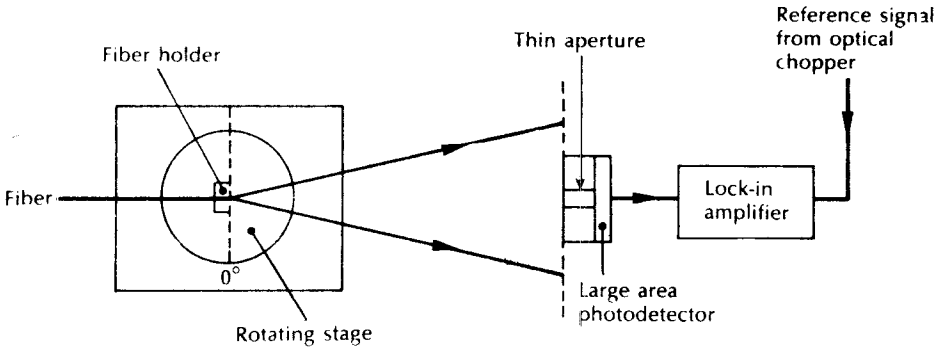

Figure 13.21 Fiber numerical aperture measurement using a scanning photodetector and a rotating stage.

rotating stage, or by calculating the far field angle using trigonometry. An example of an experimental arrangement with a rotating stage is shown in Figure 13.21. A 2 m length of the graded index fiber has its faces prepared in order to ensure square smooth terminations. The fiber output end is then positioned on the rotating stage with its end face parallel to the plane of the photodetector input, and so that its output is perpendicular to the axis of rotation. Light at a wavelength of 0.85 μm is launched into the fiber at all possible angles (overfilling the fiber) using an optical system similar to that used in the spot attenuation measurements (Figure 13.4).

The photodetector, which may be either a small area device or an apertured large area device, is placed 10 to 20 cm from the fiber and positioned in order to obtain a maximum signal with no rotation (0°). Hence when the rotating stage is turned the limits of the far field pattern may be recorded. The output power is monitored and plotted as a function of angle; the maximum acceptance angle being obtained when the power drops to 5% of the maximum intensity [Ref. 51]. Thus the numerical aperture of the fiber can be obtained from Eq. (13.28). This far field scanning measurement may also be performed with the photodetector located on a rotational stage and the fiber positioned at the centre of rotation. Moreover FOTP-177 also outlines a technique to obtain the numerical aperture from the refractive index profile of the fiber.

A less precise measurement of the numerical aperture can be obtained from the far field pattern by trigonometric means. The experimental apparatus is shown in Figure 13.22 where the end prepared fiber is located on an optical base plate or slab. Again light is launched into the fiber under test over the full range of its numerical aperture, and the far field pattern from the fiber is displayed on a screen which is positioned a known distance D from the fiber output end face. The test fiber is then aligned so that the optical intensity on the screen is maximized. Finally, the pattern size on the screen A is measured using a calibrated vernier caliper. The numerical

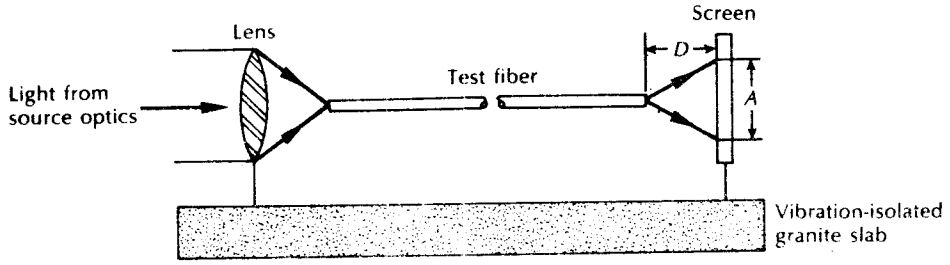

Figure 13.22 Apparatus for trigonometric fiber numerical aperture measurement.

aperture can be obtained from simple trigonometrical relationships where:

$$NA = \sin \theta_a = \frac{A/2}{[(A/2)^2 + D^2]^{\frac{1}{2}}} = \frac{A}{(A^2 + 4D^2)^{\frac{1}{2}}} \tag{13.30}$$

Example 13.5

A trigonometrical measurement is performed in order to determine the numerical aperture of a step index fiber. The screen is positioned 10.0 cm from the fiber end face. When illuminated from a wide angled visible source the measured output pattern size is 6.2 cm. Calculate the approximate numerical aperture of the fiber.

Solution: The numerical aperture may be determined directly, using Eq. (13.30) where:

$$NA = \frac{A}{(A^2 + 4D^2)^{\frac{1}{2}}} = \frac{6.2}{(38.44 + 400)^{\frac{1}{2}}} = 0.30$$

It must be noted that the accuracy of this measurement technique is dependent upon the visual assessment of the far field pattern from the fiber.

The above measurement techniques are generally employed with multimode fibers only, as the far field patterns from single-mode fibers are affected by diffraction phenomena. These are caused by the small core diameters of single-mode fibers which tend to invalidate simple geometric optics measurements. However, more detailed analysis of the far field pattern allows determination of the normalized frequency and core radius for single-mode fibers, from which the numerical aperture may be calculated using Eq. (2.69) [Ref. 52].

Far field pattern measurements with regard to multimode fibers are dependent on the length of the fiber tested. When the measurements are performed on short fiber lengths (around 1 m) the numerical aperture thus obtained corresponds to that defined by Eq. (13.28) or (13.29) However, when a long fiber length is utilized

which gives mode coupling and the selective attenuation of the higher order modes, the measurement yields a lower value for the numerical aperture. It must also be noted that the far field measurement techniques give an average (over the local NAs) value for the numerical aperture of graded index fibers. Hence alternative methods must be employed if accurate determination of the fiber's NA is required [Ref. 53].

13.7 Fiber diameter measurements

13.7.1 Outer diameter

It is essential during the fiber manufacturing process (at the fiber drawing stage) that the fiber outer diameter (cladding diameter) is maintained constant to within 1%. Any diameter variations may cause excessive radiation losses and make accurate fiber–fiber connection difficult. Hence on-line diameter measurement systems are required which provide accuracy better than 0.3% at a measurement rate greater than 100 Hz (i.e. a typical fiber drawing velocity is 1 $m s^{-1}$). Use is therefore made of noncontacting optical methods such as fiber image projection and scattering pattern analysis.

The most common on-line measurement technique uses fiber image projection (shadow method) and is illustrated in Figure 13.23 [Ref. 54]. In this method a laser beam is swept at a constant velocity transversely across the fiber and a measurement

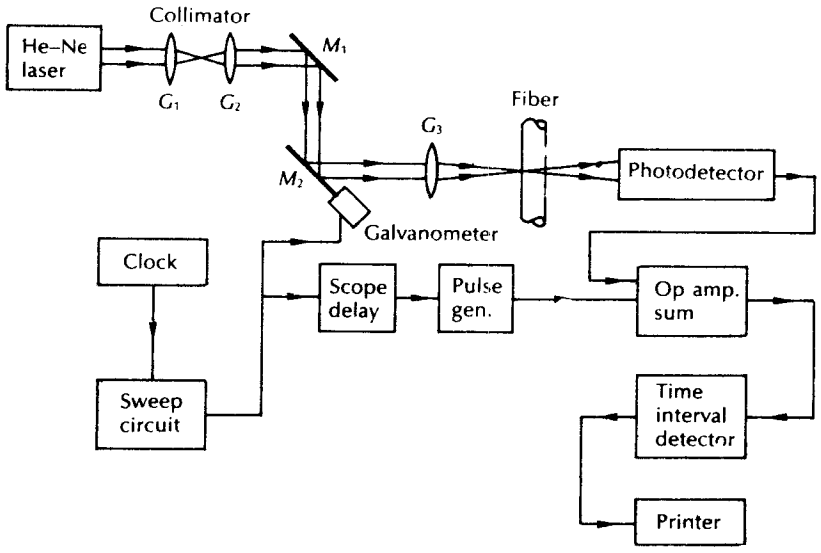

Figure 13.23 The shadow method for the on-line measurement of the fiber outer diameter [Ref. 54].

is made of the time interval during which the fiber intercepts the beam and casts a shadow on a photodetector. In the apparatus shown in Figure 13.23 the beam from a laser operating at a wavelength of 0.6328 μm is collimated using two lenses (G_1 and G_2). It is then reflected off two mirrors (M_1 and M_2), the second of which (M_2) is driven by a galvanometer which makes it rotate through a small angle at a constant angular velocity before returning to its original starting position. Therefore, the laser beam which is focused in the plane of the fiber by a lens (G_3) is swept across the fiber by the oscillating mirror, and is incident on the photodetector unless it is blocked by the fiber. The velocity ds/dt of the fiber shadow thus created at the photodetector is directly proportional to the mirror velocity $d\phi/dt$ following:

$$\frac{ds}{dt} = l\frac{d\phi}{dt} \tag{13.31}$$

where l is the distance between the mirror and the photodetector.

Furthermore, the shadow is registered by the photodetector as an electrical pulse of width W_e which is related to the fiber outer diameter d_o as:

$$d_o = W_e\frac{ds}{dt} \tag{13.32}$$

Thus the fiber outer diameter may be quickly determined and recorded on the printer. The measurement speed is largely dictated by the inertia of the mirror rotation and its accuracy by the rise time of the shadow pulse.

Example 13.6

The shadow method is used for the on-line measurement of the outer diameter of an optical fiber. The apparatus employs a rotating mirror with an angular velocity of 4 rad s^{-1} which is located 10 cm from the photodetector. At a particular instant in time a shadow pulse of width 300 μs is registered by the photodetector Determine the outer diameter of the optical fiber in μm at this instant in time.

Solution: The shadow velocity may be obtained from Eq. (13.31) where:

$$\frac{ds}{dt} = l\frac{d\phi}{dt} = 0.1 \times 4 = 0.4 \text{ m s}^{-1}$$

$$= 0.4\ \mu\text{m}\,\mu\text{s}^{-1}$$

Hence the fiber outer diameter d_o in μm is given by Eq. (5.24):

$$d_o = W_e\frac{ds}{dt} = 300\ \mu\text{s} \times 0.4\ \mu\text{m}\,\mu\text{s}^{-1}$$

$$= 120\ \mu\text{m}$$

Other on-line measurement methods, enabling faster diameter measurements, involve the analysis of forward or backward far field patterns which are produced when a plane wave is incident transversely on the fiber. These techniques generally require measurement of the maxima in the centre portion of the scattered pattern from which the diameter can be calculated after detailed mathematical analysis [Refs. 55 to 58]. They tend to give good accuracy (e.g. ± 0.25 μm [Ref. 58]) even though the theory assumes a perfectly circular fiber cross section. Also for step index fibers the analysis allows determination of the core diameter, and core and cladding refractive indices.

Measurements of the fiber outer diameter after manufacture (off-line) may be performed using a micrometer or dial gage. These devices can give accuracies of the order of ± 0.5 μm. Alternatively, off-line diameter measurements can be made with a microscope incorporating a suitable calibrated micrometer eyepiece.

13.7.2 Core diameter

The core diameter for step index fibers is defined by the step change in the refractive index profile at the core–cladding interface. Therefore the techniques employed for determining the refractive index profile (interferometric, near field scanning, refracted ray, etc.) may be utilized to measure the core diameter. Graded index fibers present a more difficult problem as, in general, there is a continuous transition between the core and the cladding. In this case it is necessary to define the core as an area with a refractive index above a certain predetermined value if refractive index profile measurements are used to obtain the core diameter.

Core diameter measurement is also possible from the near field pattern of a suitably illuminated (all guided modes excited) fiber. The measurements may be taken using a microscope equipped with a micrometer eyepiece similar to that employed for off-line outer diameter measurements. However, the core–cladding interface for graded index fibers is again difficult to identify due to fading of the light distribution towards the cladding, rather than the sharp boundary which is exhibited in the step index case. Nevertheless, details of the above measurement procedures are provided in FOTP-58 [Ref. 59].

13.8 Mode-field diameter for single-mode fiber

It was indicated in Section 2.5.2 that for single-mode fiber the geometric distribution of light in the propagating mode rather than the core diameter or numerical aperture is what is important in predicting the operational properties such as waveguide dispersion, launching and jointing losses, and microbending loss. In particular, the mode-field diameter (MFD) which is a measure of the width of the distribution of the electric field intensity is used to predict many of these properties. Alternatively, the spot size which is simply equal to half the MFD, or the mode-field radius, is utilized.

Since the field of the fundamental mode of a circularly symmetric fiber is bell shaped and exhibits circular symmetry (see Figure 2.31), not only is its extent readily described by the MFD, but it can be expressed in terms of both the near field (i.e. the optical field distribution on the output face of the fiber) and the far field (i.e. the radiation pattern at larger distances, typically a few millimetres, from the fiber end face) distributions [Ref. 60]. Hence direct measurement of the MFD may be obtained using either near field or far field scanning techniques. These basic methods are covered for standardization purposes in FOTP-165 [Ref. 61] and FOTP-164 [Ref. 62] respectively

A typical experimental arrangement for measurement of the near field intensity distribution using a scanning fiber is illustrated in Figure 13.24 [Ref. 60]. As would be expected it has distinct similarities to the experimental setup for the near field scanning of the refractive index profile shown in Figure 13.14. The arrangement utilizes a relatively intense light source (an LED or injection laser) operating at the desired wavelength to inject optical power into the fiber under test. A lens system is required to magnify the fiber output end, the image of which is scanned across a diameter using another fiber on a motor driven translation stage pigtailed to a small area photodiode. The near field MFD, d_n may be obtained using [Ref. 60]:

$$d_n = 2\sqrt{2}\left\{\frac{\int_0^\infty E^2(r)r^3\,dr}{\int_0^\infty E^2(r)r\,dr}\right\}^{\frac{1}{2}} \tag{13.33}$$

where $|E(r)|^2$ is the local near field intensity at radius r. Equation (13.33) assumes a non-Gaussian field distribution in which the near field MFD is proportional to the rms width of the near field distribution. The numerical integration of the local

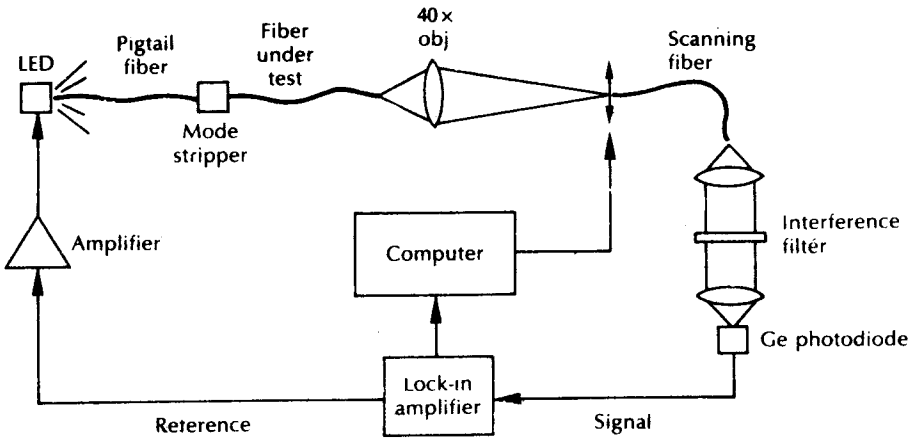

Figure 13.24 Experimental setup for near field intensity distribution measurements (near field scanning) to obtain mode-field diameter.

measured near field intensities at intervals determined by the dynamic range of the setup thus allows d_n to be calculated. Although the near field scanning technique provides a direct way to measure the MFD, the method suffers from inaccuracies resulting from lens distortion, difficulties in locating and stably holding the image plane at the detector, and a limited dynamic range with only a small portion of the optical power reaching the photodetector.

Another direct MFD measurement technique is obtained by scanning the far field intensity distribution. This method is very straightforward to implement, as shown in Figure 13.25. The experimental arrangement required comprises a high intensity light source (an injection laser is normally needed) and a photodetector mounted on a motor driven rotational stage. It is necessary that the far field intensity pattern be detected at a sufficiently large distance from the centre of the fiber output end such that good angular resolution is achieved in detection. When using a pigtailed injection laser source, however, this distance may be as low as a few millimetres. Furthermore, the angular sector scanned in front of the fiber must be sufficiently wide (between ± 20 and 25°) to completely include the main lobe of the radiation pattern. In particular, this aspect is critical when dispersion modified fibers are scanned because they exhibit broad far field distributions.

The far field MFD d_f can be obtained directly by inserting the measured far field intensities into [Ref. 6]:

$$d_f = \frac{\sqrt{2}}{\pi} \left\{ \frac{F(\theta) \sin \theta \cos \theta \, d\theta}{F(\theta) \sin^3 \theta \cos \theta \, d\theta} \right\}^{\frac{1}{2}} \tag{13.34}$$

where $F(\theta)$ corresponds to the measured data. Again, the integration can be performed numerically. It should be noted, however, that in this case the rms far field, or Petermann II [Ref. 63] definition has been adopted by the EIA in FOTP-164. This definition applies to non-Gaussian measurements and is particularly appropriate for dispersion modified fiber operating at a wavelength of 1.55 μm. Other integrative far field methods also include various aperture techniques, two of which are reported in standards, namely; the variable aperture method in FOTP-167 [Ref. 64]; and the knife-edge method in FOTP-174 [Ref. 65].

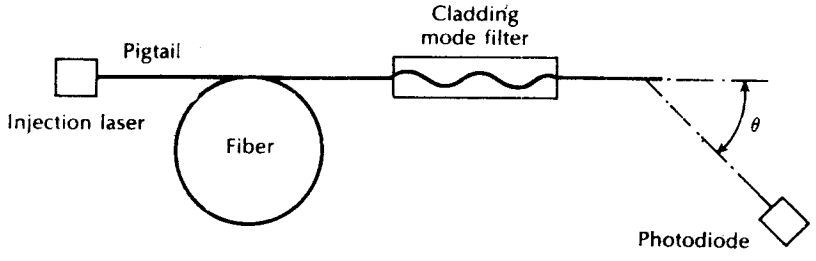

Figure 13.25 Experimental arrangement for far field intensity distribution measurements (far field scanning) to obtain mode-field diameter.

Finally, an indirect method for the measurement of the MFD which has proved popular is the transverse offset technique [Refs. 43, 60, 66, 67]. It overcomes some of the drawbacks associated with the near and far field methods by measurement of the power transmitted through a mechanical butt splice as one of the fibers is swept transversely through the alignment position. The experimental apparatus is shown in Figure 13.26 which employs the same single-mode fiber on either side of the joint. This technique makes use of the dependence of splice loss on spot size for Gaussian modes. Hence the variation of transmitted power with offset, $P(u)$, which is measured on a high precision translation stage, can be fitted to the expected Gaussian dependence. For the case of identical fibers with an MFD of $2\omega_o$ this is given by [Ref. 67]:

$$P(u) = P_o \exp\left(\frac{-u^2}{2\omega_o^2}\right) \tag{13.35}$$

where u is the offset and P_o is the maximum transmitted power. The means of fit to Eq. (13.35) is very important as the pattern departs from the Gaussian distribution. Moreover, it has been found that an unweighted truncated fit with the truncation de-emphasizing the Gaussian tails gives good agreement with near field and far field techniques for circularly symmetric single-mode fiber [Ref. 67].

The transverse offset technique has several advantages; in particular it is efficient in its use of optical power since most of the light is intercepted and transmitted, in contrast to the near field method. Furthermore, it is possible to use a tungsten lamp and monochromatic combination to provide a tunable optical source which allows easy measurement of the MFD as a function of wavelength. The technique therefore lends itself to the determination of the cutoff wavelength as mentioned in Section 13.5. In addition, it is relatively rapid, quite accurate (with less than 2%

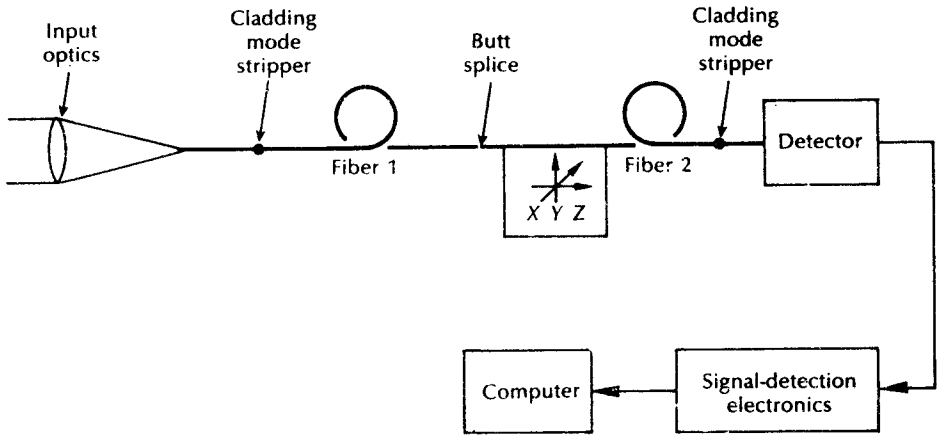

Figure 13.26 Experimental setup for the measurement of mode-field diameter by transverse offset technique.

error in spot size [Ref. 68]) and does not require complex mathematical evaluation. Finally, it is a technique which is described in CCITT G.652 [Ref. 1].

13.9 Reflectance and optical return loss

It was indicated in Section 6.7.4 that reflections along a fiber link (i.e. optical feedback) can adversely affect injection laser stability. Furthermore, multiple reflections can contribute to the noise levels at the optical detector. Fresnel reflection r occurs at a fiber–air interface, as discussed in Section 5.2, giving a reflectance of around 4% or -14 dB. The optical return loss (ORL) is therefore defined as [Ref. 6]:

$$ORL = -10 \log_{10} r \tag{13.36}$$

It should be noted that the term reflectance is sometimes utilized when referring to single components whereas the optical return loss applies to a series of components, including the fiber, along a link.

Low values of reflectance can be obtained with fusion splicing and with carefully designed mechanical joints. For example, the use of index matching gel can substantially reduce reflections. Nevertheless, certain mechanisms can cause larger values of reflectance. These include optical interference produced in the cavity between two fiber end faces as well as reflection from a high index layer formed on the end face of a highly polished fiber. Ideally, the optical return loss needs to be maintained at levels above 40 dB to avoid detrimental effects on the performance of the fiber link [Ref. 6].

Optical return loss measurements can be performed using an optical continuous wave reflectometer (OCWR), as described in FOTP-107 [Ref. 69]. In this arrangement, shown in Figure 13.27, a continuous wave LED or injection laser source is connected to the input port 1 of a four port coupler and a detector is connected to input port 2. Then a jumper cable with the reflecting components to be measured is spliced to output port 4 and output port 3 is made nonreflecting using an index matching gel or a tight fiber loop. The optical power P_r at port 2, which results from reflections caused by the components and the coupler, is thus

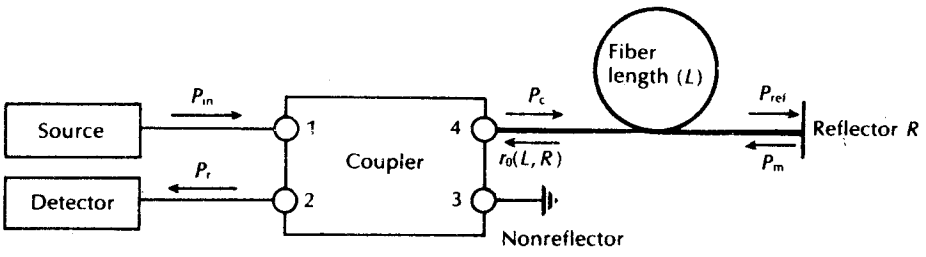

Figure 13.27 Optical return loss measurement using a four port coupler.

measured. Next the jumper cable is removed and replaced by a nonreflecting termination. This allows P_c due only to the coupler to be measured at port 2. The detector is then transferred to port 4 and the power incident upon the reflector P_{ref} is measured.

Apart from the loss in transmission between port 4 and port 2, the fraction of the reflected power from the components under test is $(P_r - P_c)/P_{ref}$. To obtain the ports 4 to 2 loss, the source and detector are connected to ports 4 and 2, respectively, providing a measurement P_{out}. Finally, a power P_{in} is measured by connecting the source directly to the detector such that P_{out}/P_{in} is the fraction of optical power transmitted between port 4 and port 2. Hence the optical return loss is given by:

$$ORL = 10 \log_{10} \left(\frac{P_{out} P_{ref}}{P_{in}(P_r - P_c)} \right) \tag{13.37}$$

The OCWR is a d.c. instrument and only provides a measurement of the overall optical return loss for a component on a link; it does not allow information on the location of a number of reflecting components to be obtained. A device which can, however, provide this information, albeit in a more complex manner, is the optical time domain reflectometer which is described in Section 13.10.1.

13.10 Field measurements

The measurements discussed in the preceding sections are primarily suited to the laboratory environment where quite sophisticated instrumentation may be used. However, there is a requirement for the measurement of the transmission characteristics of optical fibers when they are located in the field within an optical communication system. It is essential that optical fiber attenuation and dispersion measurements, connector and splice loss measurements and fault location be performed on optical fiber links in the field. Although information on fiber attenuation and dispersion is generally provided by the manufacturer, this is not directly applicable to cabled, installed fibers which are connected in series within an optical fiber system. Effects such as microbending (see Section 4.8.1) with the resultant mode coupling (see Section 2.4.2) affect both the fiber attenuation and dispersion. It is also found that the simple summation of the transmission parameters with regard to individual connected lengths of fiber cable does not accurately predict the overall characteristics of the link [Ref. 70]. Hence test equipment has been developed which allows these transmission measurements to be performed in the field.

In general, field test equipment differs from laboratory instrumentation in a number of aspects as it is required to meet the exacting demands of field measurement. Therefore the design criteria for field measurement equipment include:

1. Sturdy and compact encasement which must be portable.
2. The ready availability of electrical power must be ensured by the incorporation of batteries or by connection to a generator. Hence the equipment should maintain accuracy under conditions of varying supply voltage and/or frequency.
3. In the event of battery operation, the equipment must have a low power consumption.
4. The equipment must give reliable and accurate measurements under extreme environmental conditions of temperature, humidity and mechanical load.
5. Complicated and involved fiber connection arrangements should be avoided. The equipment must be connected to the fiber in a simple manner without the need for fine or critical adjustment.
6. The equipment cannot usually make use of external triggering or regulating circuits between the transmitter and receiver due to their wide spacing on the majority of optical links.

Even if the above design criteria are met, it is likely that a certain amount of inaccuracy will have to be accepted with field test equipment. For example, it may not be possible to include adjustable launching conditions (i.e. variation in spot size and numerical aperture) in order to create the optimum. Also, because of the large dynamic range required to provide measurements over long fiber lengths, lossy devices such as mode scramblers may be omitted. Therefore measurement accuracy may be impaired through inadequate simulation of the equilibrium mode distribution.

A number of portable, battery-operated optical power meters are commercially available. Some of these instruments are of small dimension and therefore are designed to be hand-held, whilst others, which generally provide greater accuracy and stability, are slightly larger in size. A typical example of the latter type is shown in Figure 13.28. Such devices usually measure optical power in dBm or dBμ (i.e. 0 dBm is equivalent to 1 mW and 0 dBμ is equivalent to 1 μW; see Example 13.7) over a specified range (e.g. 0.38 to 1.15 μm or 0.75 to 1.7 μm). In most cases the spectral range is altered by the incorporation of different demountable sensor heads (i.e. wide area photodiodes). For example, the optical power meter displayed in Figure 13.28 can be used with five different sensor heads (three of which are shown in the foreground of Figure 13.28) comprising either silicon, germanium or InGaAs photodiodes. The device is also specified to have a measurement range from -100 dBm (0.1 pW) to $+3$ dBm (2 mW) with an accuracy of $\pm 5\%$ when employing the latter sensor head.

It must be noted, however, that although these instruments often take measurements over a certain spectral range this simply implies that they may be adjusted to be compatible with the centre emission frequency of particular optical sources so as to obtain the most accurate reading of optical power. Therefore, the devices do not generally give spectral attenuation measurements unless the source optical output frequency is controlled or filtered to achieve single wavelength operation. Optical power meters may be used for measurement of the absolute

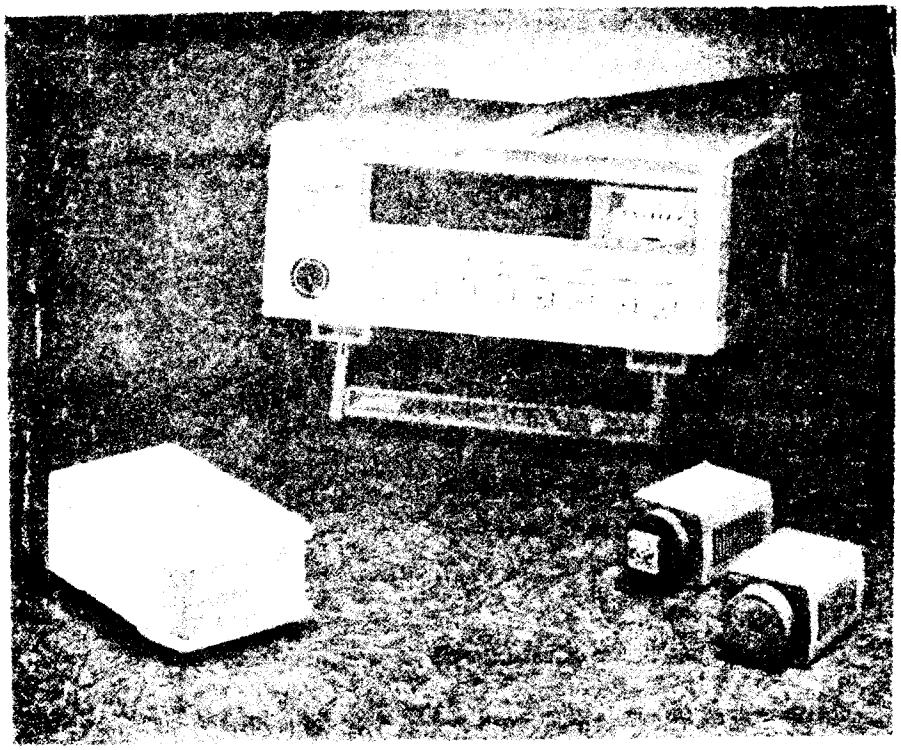

Figure 13.28 The Anritsu ML9001A optical power meter. Courtesy of Anritsu Europe Limited.

optical attenuation on a fiber link by employing the cut-back technique. Other optical system parameters which may also be obtained using such instruments are the measurement of individual splice and connector losses, the determination of the absolute optical output power emitted from the source (see Sections 6.5 and 7.4.1) and the measurement of the responsivity or the absolute photocurrent of the photodetector in response to particular levels of input optical power (see Section 8.6).

Example 13.7

An optical power meter records optical signal power in either dBm or dBμ.

(a) Convert the optical signal powers of 5 mW and 20 μW to dBm.
(b) Convert optical signal powers of 0.3 mW and 80 nW to dBμ.

Solution: The optical signal power can be expressed in decibels using:

$$\text{dB} = 10 \log_{10} \left(\frac{P_o}{P_r} \right)$$

where P_o is the received optical signal power and P_r is a reference power level.

(a) For a 1 mW reference power level:

$$\text{dBm} = 10 \log_{10} \left(\frac{P_o}{1 \text{ mW}} \right)$$

Hence an optical signal power of 5 mW is equivalent to

$$\textit{Optical signal power} = 10 \log_{10} 5 = 6.99 \text{ dBm}$$

and an optical power of 20 μW is equivalent to:

$$\begin{aligned} \textit{Optical signal power} &= 10 \log_{10} 0.02 \\ &= -16.99 \text{ dBm} \end{aligned}$$

(b) For a 1 μW reference power level:

$$\text{dB}\mu = 10 \log_{10} \left(\frac{P_o}{1 \ \mu\text{W}} \right)$$

Therefore an optical signal power of 0.3 mW is equivalent to:

$$\begin{aligned} \textit{Optical signal power} = 10 \log_{10} \left(\frac{P_o}{1 \ \mu\text{W}} \right) &= 10 \log_{10} 30 \\ &= 14.77 \text{ dB}\mu \end{aligned}$$

and an optical signal power of 800 nW is equivalent to:

$$\begin{aligned} \textit{Optical signal power} &= 10 \log_{10} 0.8 \\ &= -0.97 \text{ dB}\mu \end{aligned}$$

There are a number of portable measurement test sets specifically designed for fiber attenuation measurements which require access to both ends of the optical link. These devices tend to use the cut-back measurement technique unless correction is made for any difference in connector losses between the link and a short length of similar reference cable. A block schematic of an optical attenuation meter consisting of a transmitter and receiver unit is shown in Figure 13.29 [Ref. 70]. Reproducible readings may be obtained by keeping the launched optical power from the light source absolutely constant. A constant optical output power is achieved with the equipment illustrated in Figure 13.29 using an injection laser and a regulating circuit which is driven from a reference output of the source derived from a photodiode. Hence any variations in the laser output power are rectified by automatic adjustment of the modulating voltage, and therefore current, from the

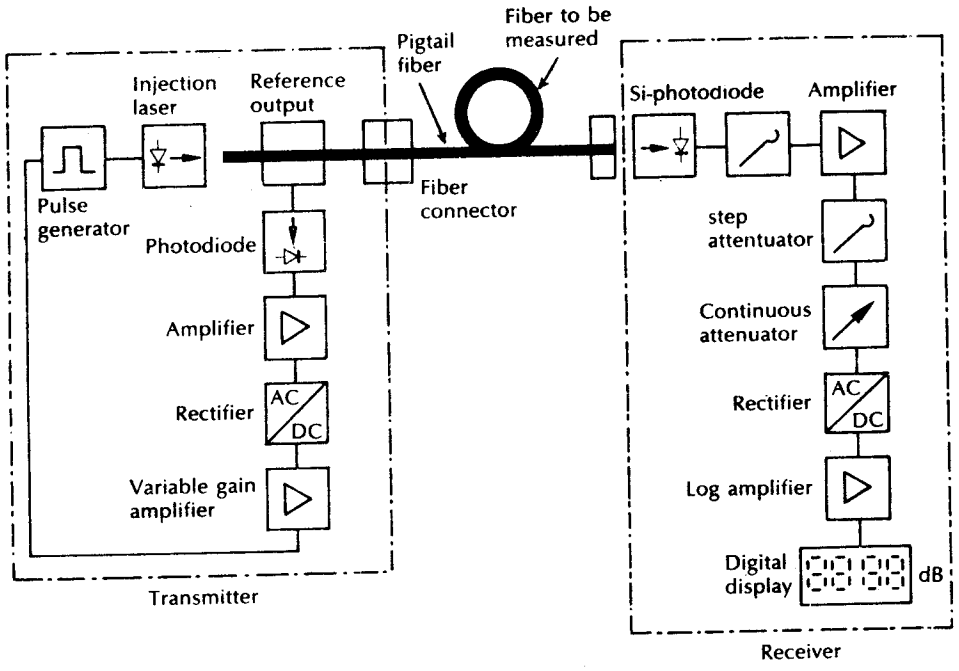

Figure 13.29 An optical attenuation meter [Ref. 70].

pulse generator. A large area photodiode is utilized in the receiver to eliminate any effects from differing fiber end faces. It is generally found that when a measurement is made on multimode fiber a short cut-back reference length of a few metres is insufficient to obtain an equilibrium mode distribution. Hence unless a mode scrambling device together with a mode stripper are used, it is likely that a reference length of around 500 m or more will be required if reasonably accurate measurements are to be made. When measurements are made without a steady state mode distribution in the reference fiber a significantly higher loss value is obtained which may be as much as 1 dB km^{-1} above the steady state attenuation [Refs. 22 and 71].

Several field test sets are available for making dispersion measurements on optical fiber links. These devices generally consist of transmitter and receiver units which take measurements in the time domain. Short light pulses ($\simeq 200$ ns) are generated from an injection laser and are broadened by transmission down the optical link before being received by a fast response photodetector (i.e. avalanche photodiode) and displayed on a sampling oscilloscope. This is similar to the dispersion measurements in the time domain discussed in Section 13.3. If it is assumed that the pulses have a near Gaussian shape, Eq. (13.13) may be utilized to determine the pulse broadening on the link, and hence the 3 dB optical bandwidth may be obtained.

13.10.1 Optical time domain reflectometry (OTDR)

A measurement technique which is far more sophisticated and which finds wide application in both the laboratory and the field is the use of optical time domain reflectometry (OTDR). This technique is often called the backscatter measurement method. It provides measurement of the attenuation on an optical link down its entire length giving information on the length dependence of the link loss. In this sense it is superior to the optical attenuation measurement methods discussed previously (Section 13.2) which only tend to provide an averaged loss over the whole length measured in dB km^{-1}. When the attenuation on the link varies with length, the averaged loss information is inadequate. OTDR also allows splice and connector losses to be evaluated as well as the rotation of any faults on the link. It relies upon the measurement and analysis of the fraction of light which is reflected back within the fiber's numerical aperture due to Rayleigh scattering (see Section 3.4.1). Hence the backscattering method which was first described by Barnoski and Jensen [Ref. 72] has the advantages of being nondestructive (i.e. does not require the cutting back of the fiber) and of requiring access to one end of the optical link only.

The backscattered optical power as a function of time $P_{Ra}(t)$ may be obtained from the following relationship [Ref. 73]:

$$P_{Ra}(t) = \tfrac{1}{2} P_i S \gamma_R W_o v_g \exp(-\gamma v_g t) \tag{13.38}$$

where P_i is the optical power launched into the fiber, S is the fraction of captured optical power, γ_R is the Rayleigh scattering coefficient (backscatter loss per unit length), W_o is the input optical pulse width, v_g is the group velocity in the fiber and γ is the attenuation coefficient per unit length for the fiber. The fraction of captured optical power S is given by the ratio of the solid acceptance angle for the fiber to the total solid angle as:

$$S \simeq \frac{\pi (NA)^2}{4\pi n_1^2} = \frac{(NA)^2}{4n_1^2} \tag{13.39}$$

It must be noted that the relationship given in Eq. (13.39) applies to step index fibers and the parameter S for a graded index fiber is generally a factor of 2/3 lower than for a step index fiber with the same numerical aperture [Ref. 74]. Hence using Eqs. (13.38) and (13.39) it is possible to determine the backscattered optical power from a point along the link length in relation to the forward optical power at that point.

Example 13.8

An optical fiber link consists of multimode step index fiber which has a numerical aperture of 0.2 and a core refractive index of 1.5. The Rayleigh scattering coefficient for the fiber is 0.7 km^{-1}. When light pulses of 50 ns duration are

launched into the fiber, calculate the ratio in decibels of the backscattered optical power to the forward optical power at the fiber input. The velocity of light in a vacuum is 2.998×10^8 ms^{-1}.

Solution: The backscattered optical power $P_{Ra}(t)$ is given by Eq. (13.38) where:

$$P_{Ra}(t) = \tfrac{1}{2} P_o S \gamma_R W_o v_g \exp(-\gamma v_g t)$$

At the fiber input $t = 0$; hence the power ratio is:

$$\frac{P_{Ra}(0)}{P_i} = \tfrac{1}{2} S \gamma_R W_o v_g$$

Substituting for S from Eq. 5.26) gives:

$$\frac{P_{Ra}(0)}{P_i} = \frac{1}{2}\left[\frac{(NA)^2 \gamma_R W_o v_g}{4n_1^2}\right]$$

The group velocity in the fiber v_g is defined by Eq. (2.40) as:

$$v_g = \frac{c}{N_g} \simeq \frac{c}{n_1}$$

Therefore

$$\frac{P_{Ra}(0)}{P_i} = \frac{1}{2}\left[\frac{NA^2 \gamma_R W_o c}{4n_1^3}\right]$$

$$= \frac{1}{2}\left[\frac{(0.02)^2 0.7 \times 10^{-3} \times 50 \times 10^{-9} \times 2.998 \times 10^8}{4(1.5)^3}\right)$$

$$= 1.555 \times 10^{-5}$$

In decibels

$$\frac{P_{Ra}(0)}{P_i} = 10 \log_{10} 1.555 \times 10^{-5}$$

$$= 48.1 \text{ dB}$$

Hence in Example 13.9 the backscattered optical power at the fiber input is 48.1 dB down on the forward optical power. The backscattered optical power should not be confused with any Fresnel reflection at the fiber input end face resulting from a refractive index mismatch. This could be considerably greater than the backscattered light from the fiber, presenting measurement problems with OTDR if it is allowed to fall on to the receiving photodetector of the equipment described below.

A block schematic of the backscatter measurement method is shown in Figure 13.30 [Ref. 75]. A light pulse is launched into the fiber in the forward direction from an injection laser using either a directional coupler or a system of external

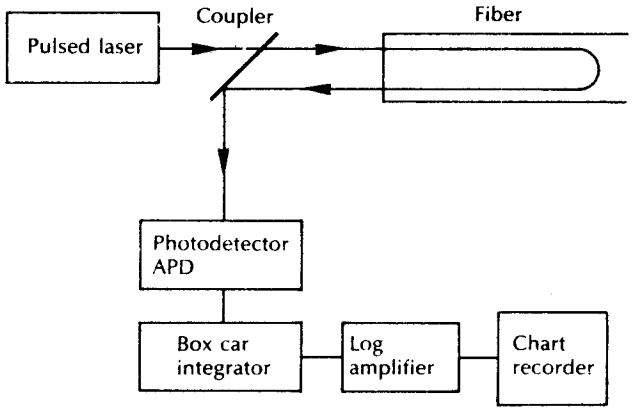

Figure 13.30 Optical time domain reflectometry or the backscatter measurement method.

lenses with a beam splitter (usually only in the laboratory). The backscattered light is detected using an avalanche photodiode receiver which drives an integrator in order to improve the received signal to noise ratio by giving an arithmetic average over a number of measurements taken at one point within the fiber. This is necessary as the received optical signal power from a particular point along the fiber length is at a very low level compared with the forward power at that point by some 45 to 60 dB (see Example 13.9), and is also swamped with noise. The signal from the integrator is fed through a logarithmic amplifier and averaged measurements for successive points within the fiber are plotted on a chart recorder. This provides location-dependent attenuation values which give an overall picture of the optical loss down the link. A possible backscatter plot is illustrated in Figure 13.31 [Ref. 76] which shows the initial pulse caused by reflection and backscatter from the input coupler followed by a long tail caused by the distributed Rayleigh scattering from the input pulse as it travels down the link. Also shown in the plot is a pulse corresponding to the discrete reflection from a fiber joint, as well as a discontinuity due to excessive loss at a fiber imperfection or fault. The end of the fiber link is indicated by a pulse corresponding to the Fresnel reflection incurred at the output end face of the fiber. Such a plot yields the attenuation per unit length for the fiber by simply computing the slope of the curve over the length required. Also the location and insertion losses of joints and/or faults can be obtained from the power drop at their respective positions on the link. Finally the overall link length can be determined from the time difference between reflections from the fiber input and output end faces. Standard methods for these measurements are covered in FOTP-59 to 61 [Refs. 77 to 79] and they provide very powerful techniques for field measurements on optical fiber links. In addition, FOTPs are in process for the measurement of splice or connector loss and the measurement of splice or connector return loss utilizing an OTDR [Ref. 6].